Frequency Diverse Array Radars: Beampattern Design and Target Parameter Estimation

By

Shaiza

00000330239

Supervisor

Asst. Prof. Hussain Ali, PhD

Department of Electrical Engineering

A thesis submitted to the faculty of Electrical Engineering Department, Military College of Signals , National University of Sciences and Technology, Islamabad, Pakistan, in partial fulfillment of the requirements for the degree of MS in Electrical (Signal Processing) Engineering.

January 2023

Thesis Acceptance Certificate

Certified that final copy of MS/MPhil thesis written by **Shaiza**, Registration No. **00000330239**, of **Military College of Signals** has been vetted by the undersigned, found complete in all respects as per NUST Statutes/Regulations, is free of plagiarism, errors and mistakes and is accepted as partial fulfillment for award of MS/M Phil degree. It is further certified that necessary amendments as pointed out by GEC members of the scholar have also been incorporated in the said thesis.

Signature: _____

Name of Advisor: **Asst. Prof. Hussain Ali, PhD**

Date: _____

Signature (HoD): _____

Date: _____

Signature (Dean): _____

Date: _____

Abstract

The frequency diverse array (FDA) radar beampattern depends on the angle, time and range whereas phased array radar has angle-dependent beampattern only. Therefore, the FDA is more attractive and flexible than phased-array radars. The beampattern design is important for effective target localization. In this thesis, transmit array weights optimization is performed using the IFFT algorithm to design a transmit beampattern to illuminate the desired angular direction and range. The designed beampattern has a high dwell time, and therefore, it can accurately detect even weak targets with a high probability. Each target is characterized by its range and angle. Thus, estimation of both the angle and range for the proposed FDA radar is performed to accurately locate the target using the double-pulse method. The double-pulse method first transmits a pulse with zero frequency offset to determine the angle of the target independently, and then another pulse is transmitted at a non-zero frequency offset to determine the range of the target by using the estimated angle. The proposed scheme can also minimize noise effects using the minimum power distortionless response (MPDR) beamformer at the receiver. Therefore, the target parameter estimation method is used to determine the exact 2D spatial location of the target. In addition, the Cramer-Rao lower bound (CRLB) for the FDA radar is derived. The root-mean-squared error (RMSE) for both the angle and range is plotted to compare the existing FDA radar performance with the proposed FDA radar and simulations are performed to verify the results.

Index Terms: Frequency diverse array radar, beampattern, inverse-fast-fourier transform (IFFT).

Dedication

This thesis is dedicated to MY BELOVED PARENTS, BROTHER, SISTERS, HONORABLE TEACHERS AND FRIENDS for their love, endless support and encouragement.

Acknowledgments

Glory be to Allah (S.W.A), the Creator, the Sustainer of the Universe. Who only has the power to honour whom He please, and to abase whom He please. Verily no one can do anything without His will. From the day, I came to NUST till the day of my departure, He was the only one Who blessed me and opened ways for me, and showed me the path of success. Their is nothing which can payback for His bounties throughout my research period to complete it successfully.

Shaiza

Contents

List of Figures

List of Tables

ACRONYMS

Frequency Diverse Array	FDA
Radio Frequency	RF
High Frequency	HF
Intermediate Frequency	IF
Phased Array	PA
Uniform Linear Array	ULA
Discrete prolate spheroidal sequences	DPSS
Discrete-Fourier-transform	DFT
Inverse-fast-Fourier-transform	IFFT
Multi-carrier frequency diverse array	MCFDA
Direction of arrival	DOA
Transmit-subaperturing	TS
Multiple-input multiple-output	MIMO
Signal-to-interference-plus-noise ratio	SINR
Continuous Wave	CW
Pulsed Wave	PW
Signal to noise ratio	SNR
Root-mean-squared error	RMSE
Minimum Power distortionless response	MPDR
Semi-definite-programming	SDP
Quadratic programming	QP
Cramer-Rao Lower Bound	CRLB

NOTATION

Vector	$\mathbf{x}$
Matrix	$\mathbf{X}$
m-th row and n-th column of $\mathbf{X}$	$x_m(n)$
Transpose of $\mathbf{X}$	$\mathbf{X}^{\mathsf{T}}$
Conjugate transposition of $\mathbf{X}$	$\mathbf{X}^{\mathsf{H}}$
Kronecker product	$\otimes$
Fast-Fourier-transform (FFT)	$\mathscr{F}\{\cdot\}$
Real part of $\mathbf{x}$	$\mathcal{R}\{\cdot\}$
Identity matrix	$\mathbf{I}$
Diagonal matrix	$\mathrm{diag}(\cdot)$

Chapter 1

Introduction and Motivation

1.1 Radar

Radar is an acronym for "radio detection and ranging." Radar is used for the detection of objects through the reflection of radio waves. The radar operates in the frequency range f_c from 2 MHz to 220 GHz corresponding to a wavelength of $\lambda = \frac{c}{f_c}$, 150 m to 1.37 mm. Therefore, the radar system operates in the high frequency (HF) band to the millimeter band according to its operating frequency. The frequency band of radar is chosen according to the application of radar; for example, for small-range applications, high-frequency radars are used, whereas for long-range applications, low-frequency radars are used.

A basic radar system is shown in Fig. 1.1. The main element of the radar is the antenna element that transmits the desired modulated waveform towards the target. The desired waveform is first generated by the waveform generator, which is modulated to the desired radio frequency (RF) by the transmitter. The receiver receives the received echoes of the target, which is passed through low-noise RF amplifier, mixer and intermediate frequency (IF) amplifier to demodulate the received bandpass signal to the baseband signal. Finally, signal-processing techniques are applied to the demodulated signal, which involves pulse compression, matched filtering, integration and Doppler filtering. The output data is displayed based on the radar objective.

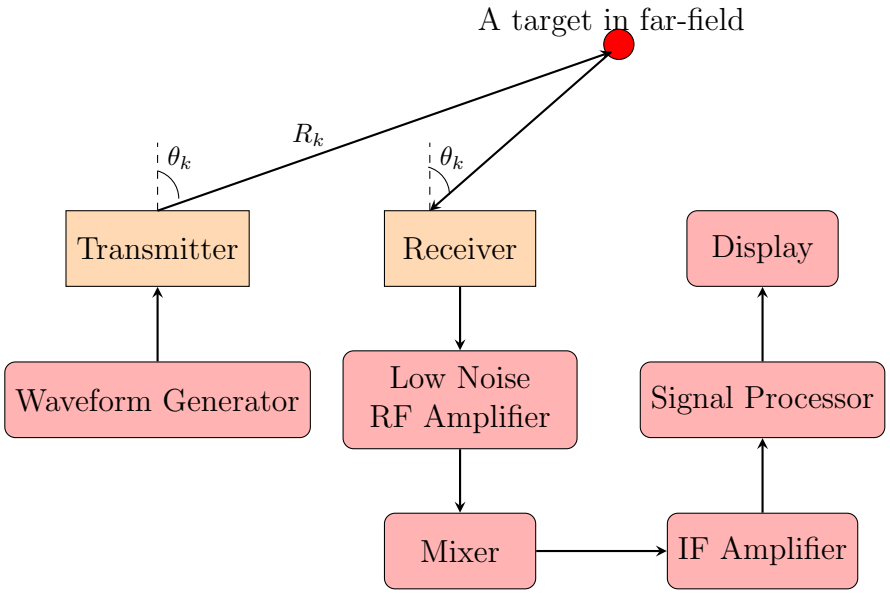

Figure 1.1: Block diagram of a radar system.

Radars are broadly used for object detection, imaging and tracking. Besides, surveillance applications, radar is also used for air traffic control, weather monitoring, enforcing speed limits, collision avoidance in ships. Based upon its application, there are various types of radar, that is, air borne, space borne, police traffic radar and weather radar etc.

The antenna arrays are used in radars with different configurations to have desired beampatterns. These different configurations include:

- Array with uniform spacing.
- Array with non-uniform spacing.
- Array with uniform weighting.
- Array with non-uniform weighting.
- Array operating at same carrier frequency.
- Sub-arrays operating at different carrier frequencies.

The most commonly discussed array configuration include isotropic radiators with a linear array having uniform spacing called uniform linear array (ULA) opearting at same carrier frequency with uniform weights.

1.2 FDA Radar

The main idea of FDA radar is application of small frequency increment f_o in addition to carrier frequency f_c which results in angle, time and range dependent beampattern of FDA radar. Consider a linear array of M transmit antenna elements as shown in Fig. 1.2. The electric field radiated from all antenna elements would be superposition of electric field radiated from each element towards a target located at R_k and θ_k. The magnitude and phase of current excitation is denoted by a_m and ψ_m respectively.

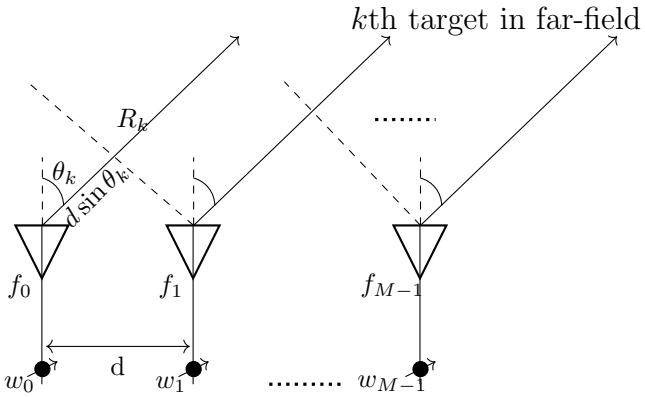

Figure 1.2: FDA transmitter.

$$E = \sum_{m=0}^{M-1} a_m e^{-j\psi_m} \frac{e^{j(\omega_m t - k_m R_m)}}{R_m} f_e(\theta_k, \phi_k) \tag{1.2.1}$$

where the element pattern $f_e(\theta_k, \phi_k)$ considers the electric field directional dependence. The distance of the target from the mth antenna element incorporating the path length effects $R_m = R_k - md\sin(\theta_k)$.

$$E = \sum_{m=0}^{M-1} a_m e^{-j\psi_m} \frac{e^{j(\omega_m t - k_m (R_k - md\sin(\theta_k)))}}{R_k - md\sin(\theta_k)} f_e(\theta_k, \phi_k) \tag{1.2.2}$$

In case of FDA radar the element factor $f_e(\theta, \phi)$ is a function of frequency $\omega_m = \omega_c + m\omega_o$.

$$\begin{aligned} E &= \sum_{m=0}^{M-1} a_m e^{-j\psi_m} \frac{e^{j((\omega_c + m\omega_o)t - k_m(R_k - md\sin(\theta_k)))}}{R_k - md\sin(\theta_k)} f_e(\omega_c + m\omega_o) \\ &= \sum_{m=0}^{M-1} a_m e^{-j\psi_m} e^{j(\omega_c + m\omega_o)t} \frac{e^{-jk_m(R_o - md\sin(\theta_k))}}{R_k - md\sin(\theta_k)} f_e(\omega_c + m\omega_o) \end{aligned} \tag{1.2.3}$$

where $k_m = k_c + mk_o = \frac{2\pi f_c}{c} + \frac{2\pi m f_o}{c}$.

$$E = \sum_{m=0}^{M-1} a_m e^{-j\psi_m} e^{j(\omega_c + m\omega_o)t} \frac{e^{-j(k_c + mk_o)(R_k - md\sin(\theta_k))}}{R_k - md\sin(\theta_k)} f_e(\omega_c + m\omega_o) \tag{1.2.4}$$

At far-field, the term $R_k - md\sin(\theta_k) \approx R_k$. Since, this is only the fall off factor of electric field due to range. But this approximation could not be done with phase of electric field. Since the current applied across all antennas is phase coherent. So $e^{-j\psi_m}$ is dropped. For uniform excitation $a_m = 1$, the electric field equation modifies to

$$\begin{aligned} E &= \frac{1}{R_k} \sum_{m=0}^{M-1} e^{j(\omega_c + m\omega_o)t} e^{-j(k_c + mk_o)(R_k - md\sin(\theta_k))} f_e(\omega_c + m\omega_o) \\ &= \frac{1}{R_k} e^{j(\omega_c t - k_c R_k)} \sum_{m=0}^{M-1} e^{jm(\omega_o t + k_c d\sin(\theta_k) - k_o R_k + mk_o d\sin(\theta_k))} f_e(\omega_c + m\omega_o) \end{aligned} \tag{1.2.5}$$

Applying the FDA fundamental constraint $f_c \gg f_o$. Therefore,

$$m\omega_c \gg \omega_o \tag{1.2.6}$$

$$k_c d\sin(\theta_k) \gg mk_o d\sin(\theta_k) \tag{1.2.7}$$

The electric field equation becomes

$$E = \frac{1}{R_k} e^{j(\omega_c t - k_c R_k)} \sum_{m=0}^{M-1} e^{jm(\omega_o t + k_c d\sin(\theta_k) - k_o R_k)} f_e(\omega_c) \tag{1.2.8}$$

From (1.2.8), the Array Factor is obtained as given by

$$\begin{aligned}\mathrm{AF}(t, R_k, \theta_k) &= \sum_{m=0}^{M-1} e^{jm(\omega_o t + k_c d \sin(\theta_k) - k_o R_k)} \\ &= \frac{1 - e^{jM(\omega_o t + k_c d \sin(\theta_k) - k_o R_k)}}{1 - e^{j(\omega_o t + k_c d \sin(\theta_k) - k_o R_k)}} \\ &= e^{j\frac{(M-1)}{2}(\omega_o t + k_c d \sin(\theta_k) - k_o R_k)} \frac{\sin\left(\frac{M(\omega_o t + k_c d \sin(\theta_k) - k_o R_k)}{2}\right)}{\sin\left(\frac{(\omega_o t + k_c d \sin(\theta_k) - k_o R_k)}{2}\right)} \end{aligned} \quad (1.2.9)$$

If no frequency offset is applied, $f_o = 0$ Hz and only carrier frequency frequency is used then, the FDA radar transmits an angle-dependent beampattern similar to that of a phased array (PA) radar. The transmit beampattern of FDA radar for $M = 40$, $f_c = 5$ GHz, $f_o = 0$ Hz and $d = \frac{\lambda}{2}$ is shown in Fig. 1.3. For any non-zero f_o , the FDA radar transmits a range, angle and time-dependent beampattern. For a time instance $t = 0$ s, the angle and range-dependent transmit beampattern of the FDA radar for $f_o = 5$ kHz is shown in Fig. 1.4.

1.2.1 Continuous Wave (CW) FDA Radar

Standard FDA radar transmits a continuous wave from the transmit FDA antenna elements, which results in a periodic range, angle and time dependent beampattern. The standard FDA radars excited with CWs are referred as CW FDA radars. FDA transmit beampattern scans in range and angle as a function of time. Standard FDA transmits continuous and periodic **S**-shaped beampattern, which scans the whole two-dimensional (2D) observation spatial section. For positive frequency increment, the transmit beampattern scans in clockwise direction and for negative frequency increment, the transmit beampattern scans in anticlockwise direction.

To investigate the periodicity of FDA transmit beampattern from the array factor equation (1.2.9). The maximum value of array factor is obtained when argument

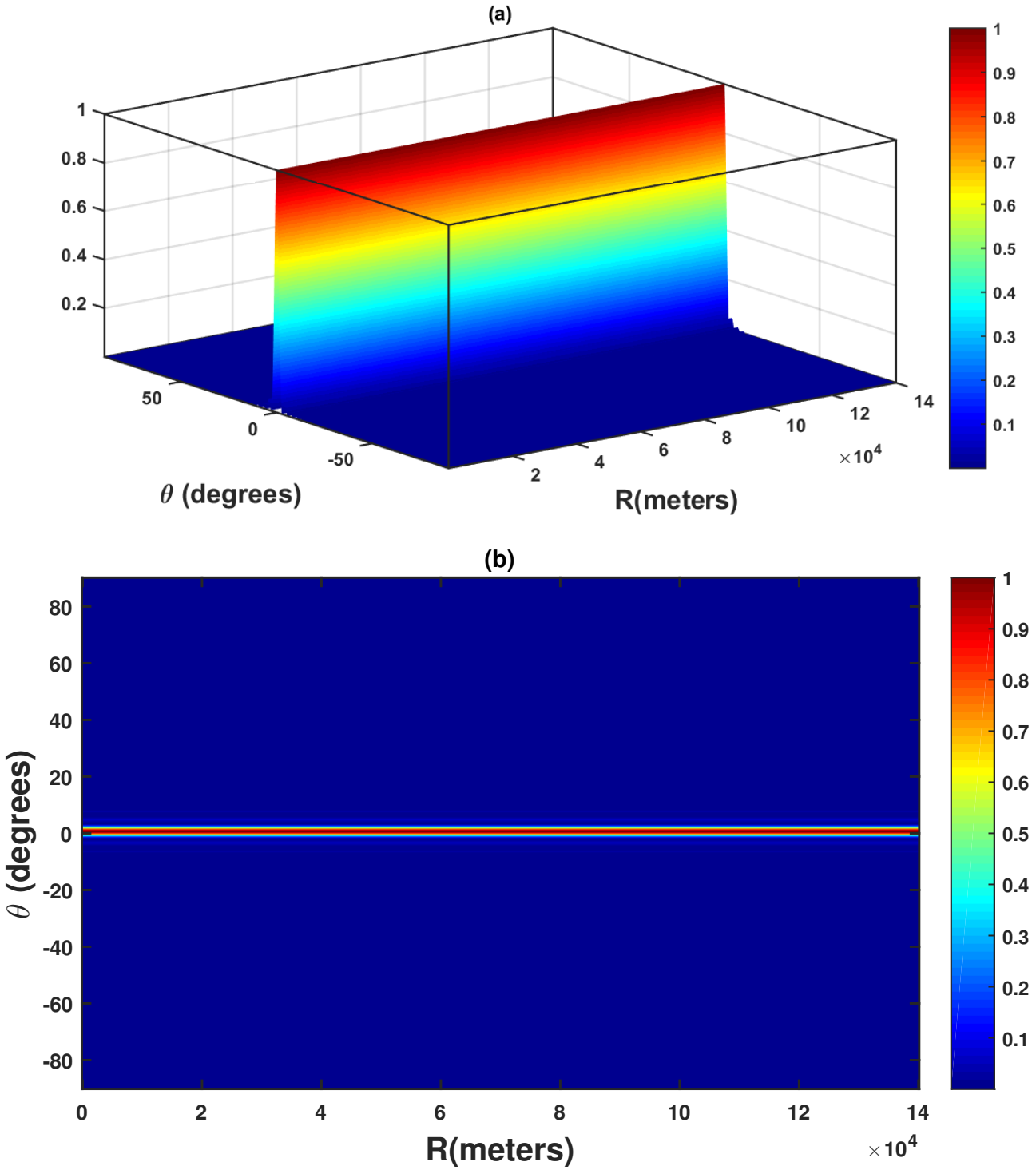

Figure 1.3: FDA range and angle-dependent beampattern for $f_o = 0$ Hz (a) 3D view (b) 2D view

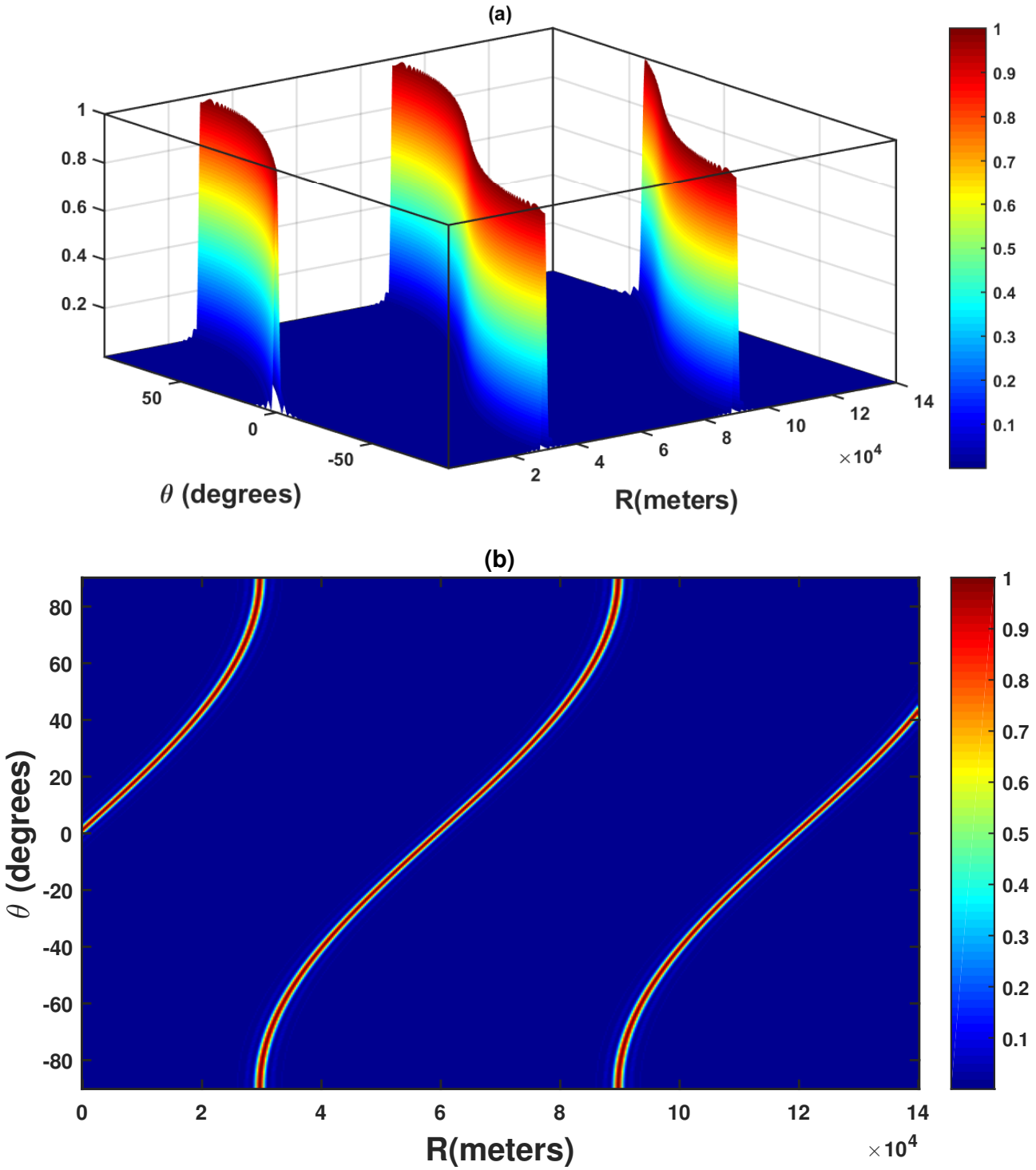

Figure 1.4: FDA range and angle-dependent beampattern for $f_o = 5$ kHz (a) 3D view (b) 2D view

of sin is a multiple of 2π.

$$\begin{aligned} \omega_o t + k_c d \sin(\theta_k) - k_o R_k &= 2\pi \\ 2\pi f_o t + \frac{2\pi f_c d \sin(\theta_k)}{c} - \frac{2\pi f_o R_k}{c} &= 2\pi \end{aligned} \tag{1.2.10}$$

Solving (1.2.10) for t, the equation simplifies to

$$t = \frac{1}{f_o} + \frac{R_k}{c} - \frac{d \sin(\theta_k)}{\lambda f_o} \tag{1.2.11}$$

Therefore, the FDA transmit beampattern is a periodic function of time with a fundamental period of $\frac{1}{f_o}$ for a fixed range R_k and angle θ_k. FDA transmit beampattern for $M = 40$, $f_c = 5$ GHz, $f_o = 5$ kHz, $d = \frac{\lambda}{2}$, $\theta_k = 10^o$ and $R_k = 30$ km is shown as a function of t in Fig. 1.5. The beampattern is periodic in time with a period of $\frac{1}{fo} = 200\mu$s.

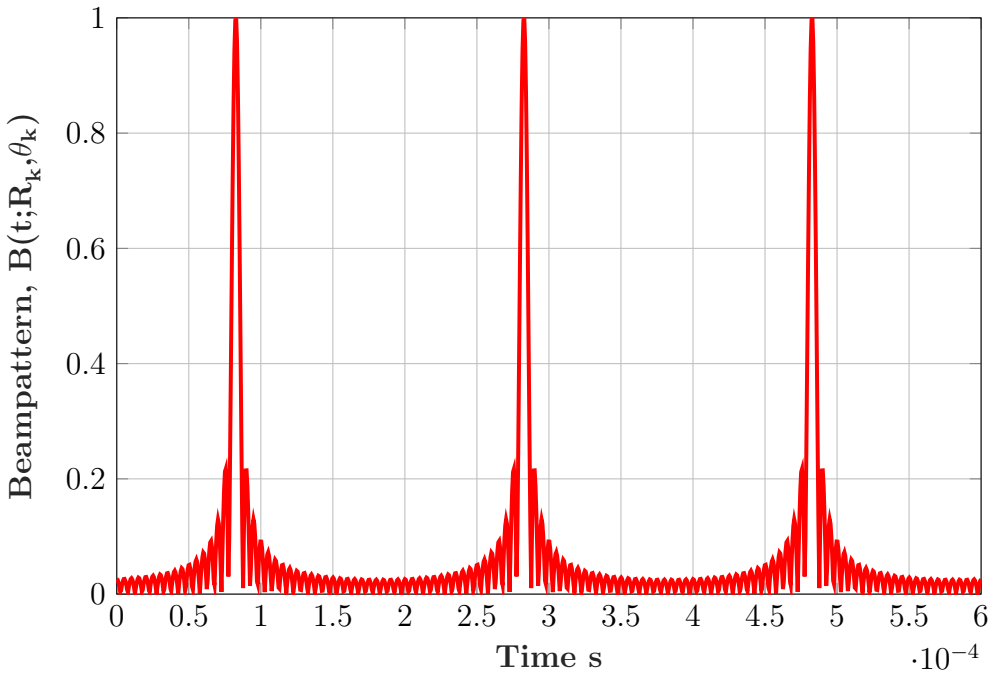

Figure 1.5: Standard FDA time-dependent beampattern for R_k and θ_k fixed.

Solving (1.2.10) for R, the equation simplifies to

$$R = ct - \frac{c}{f_o} + \frac{f_c d \sin(\theta_k)}{f_o} \tag{1.2.12}$$

Therefore, the FDA transmit beampattern is a periodic function of range with a fundamental period of $\frac{c}{f_o}$ for a fixed time t and angle θ_k. For $t = 100\mu$s and $\theta_k = 10^o$, the FDA transmit beampattern is periodic in range with a period of $\frac{c}{f_o} = 60$ km as shown in Fig. 1.6. So, the main beam would illuminate the target completely after 60 km.

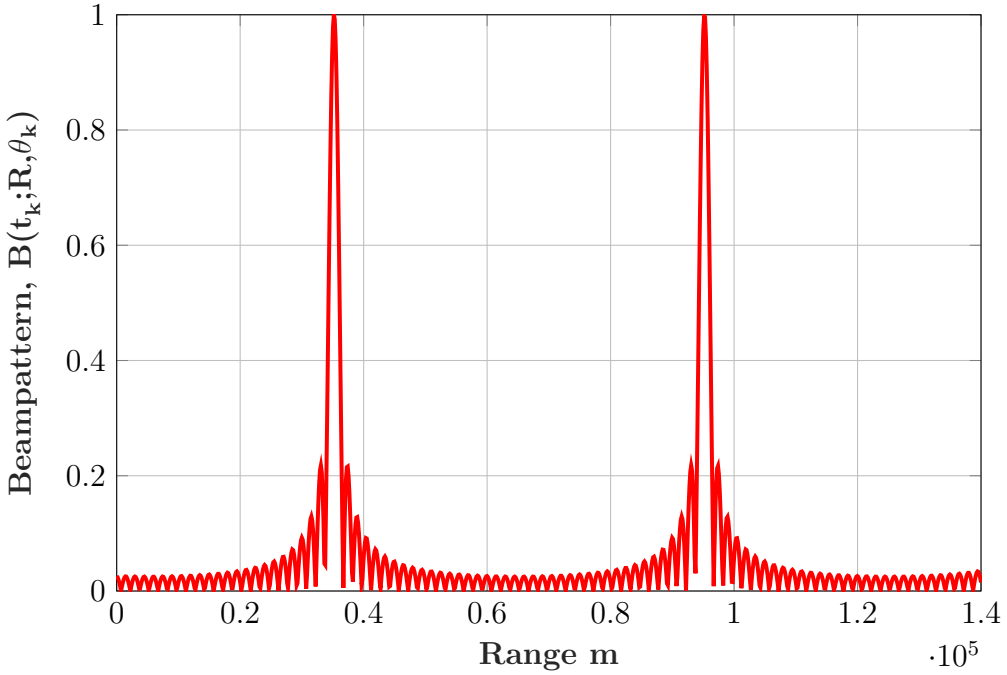

Figure 1.6: Standard FDA range-dependent beam pattern for t and θ_k fixed.

Solving (1.2.10) for $\sin(\theta)$, the equation simplifies to

$$\sin(\theta) = \frac{\lambda}{d} - \frac{cf_o t}{f_c d} + \frac{f_o R_k}{f_c d} \tag{1.2.13}$$

Therefore, the FDA transmit beampattern is a periodic function of angle with a fundamental period of $\frac{\lambda}{d}$ for a fixed time t and range R_k. For $d = \frac{\lambda}{2}$, $t = 100\mu$s and $R_k = 30$ km, the FDA transmit beampattern is periodic in angle with a period of 2 rad as shown in Fig. 1.7.

The 2D and 3D views of the FDA range and angle-dependent transmit beampattern for the 2D spatial section, $\theta_o = [-90^o, 90^o]$, $R_o = [0, 140$ km$]$ and $f_o = 1$ kHz are shown for four different time instances for $t = 0$s,$t = 400\mu$s, $t = 800\mu$s and

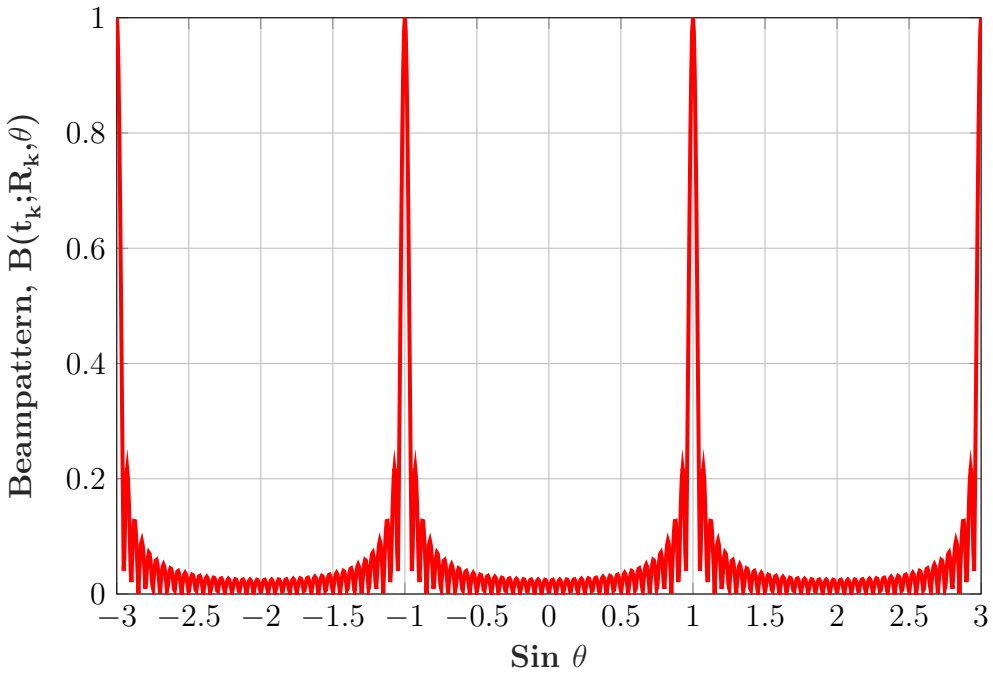

Figure 1.7: Standard FDA angle-dependent beam pattern for t and R_k fixed.

$t = 1$ms in Figs. 1.8 through Fig. 1.9 respectively.

The electromagnetic field pattern of the FDA radar propagates in time. Since, the beampattern is perodic in time therefore, for $t = 0$s and $t = 1$ms, the transmit beampattern is identical. The f_o applied across the transmit antenna elements causes the beampattern to scan in angle with time. The beam steering in FDA radar depends on choice of frequency offset. For a particular f_o, the beam steering is constant for different time instances. The beamsteering for a range R is given by [6]

$$\sin(\theta) = \frac{-Rf_o}{c(d/\lambda)}. \tag{1.2.14}$$

For $t = 0$s as shown in Fig. 1.8, the FDA beampattern steers to 69^o only for range upto 140 km. For $t = 400\mu$s, the FDA beampattern scans angle changes from -55^o to 13^o. For $t = 800\mu$s, the FDA beampattern scans the angular region from 22^o to 90^o upto a range of 90 km and -90^o to 34^o upto a range of 140 km. For $t = 1$ms, the transmit beampattern is same as that for $t = 0$s due to periodicity of beampattern with period of every 1ms.

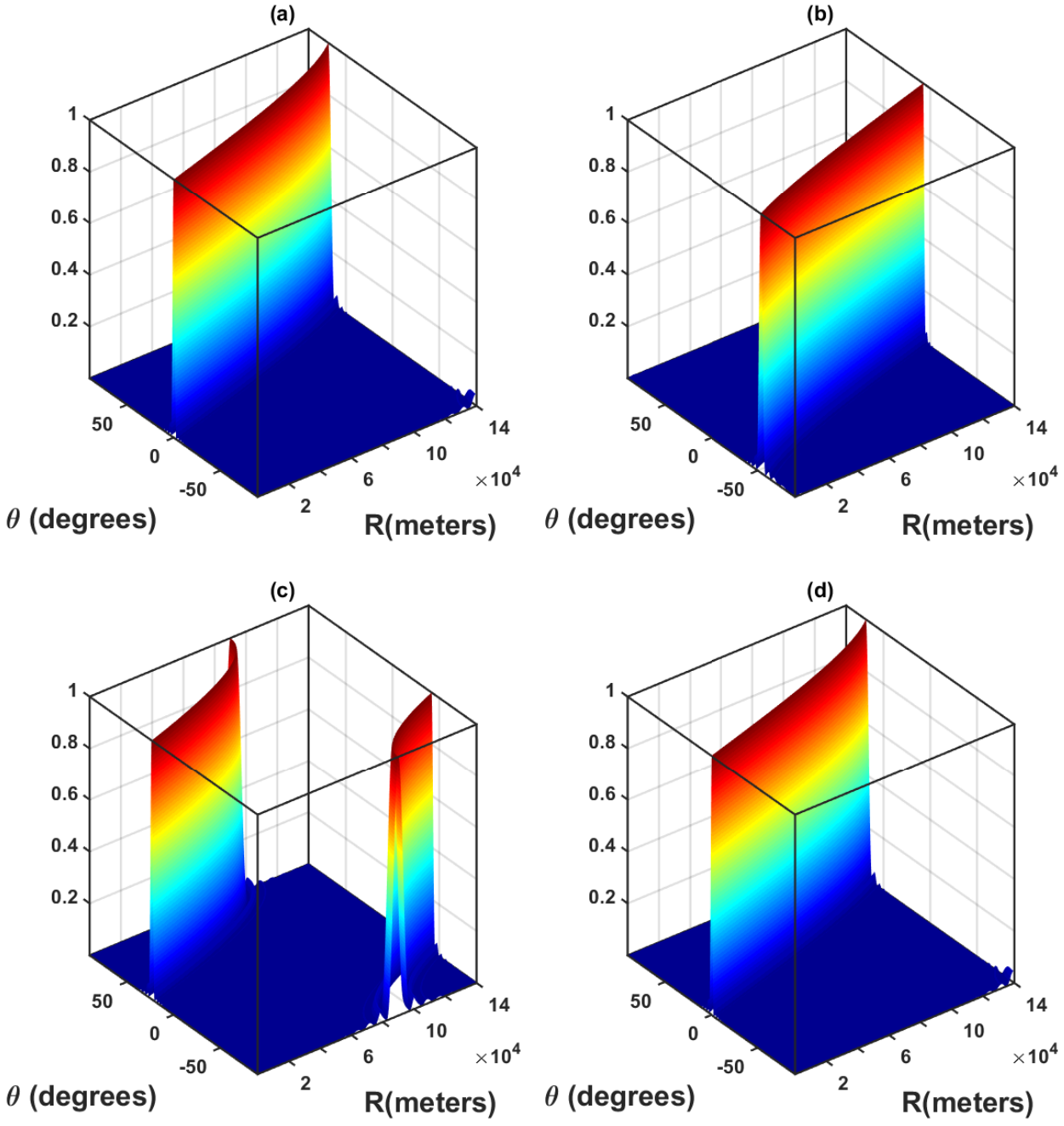

Figure 1.8: 3D view of standard FDA range and angle-dependent beampattern at different time instants
(a) at $t = 0$s (b) at $t = 400\mu$s (c) at $t = 800\mu$s (d) at $t = 1$ms

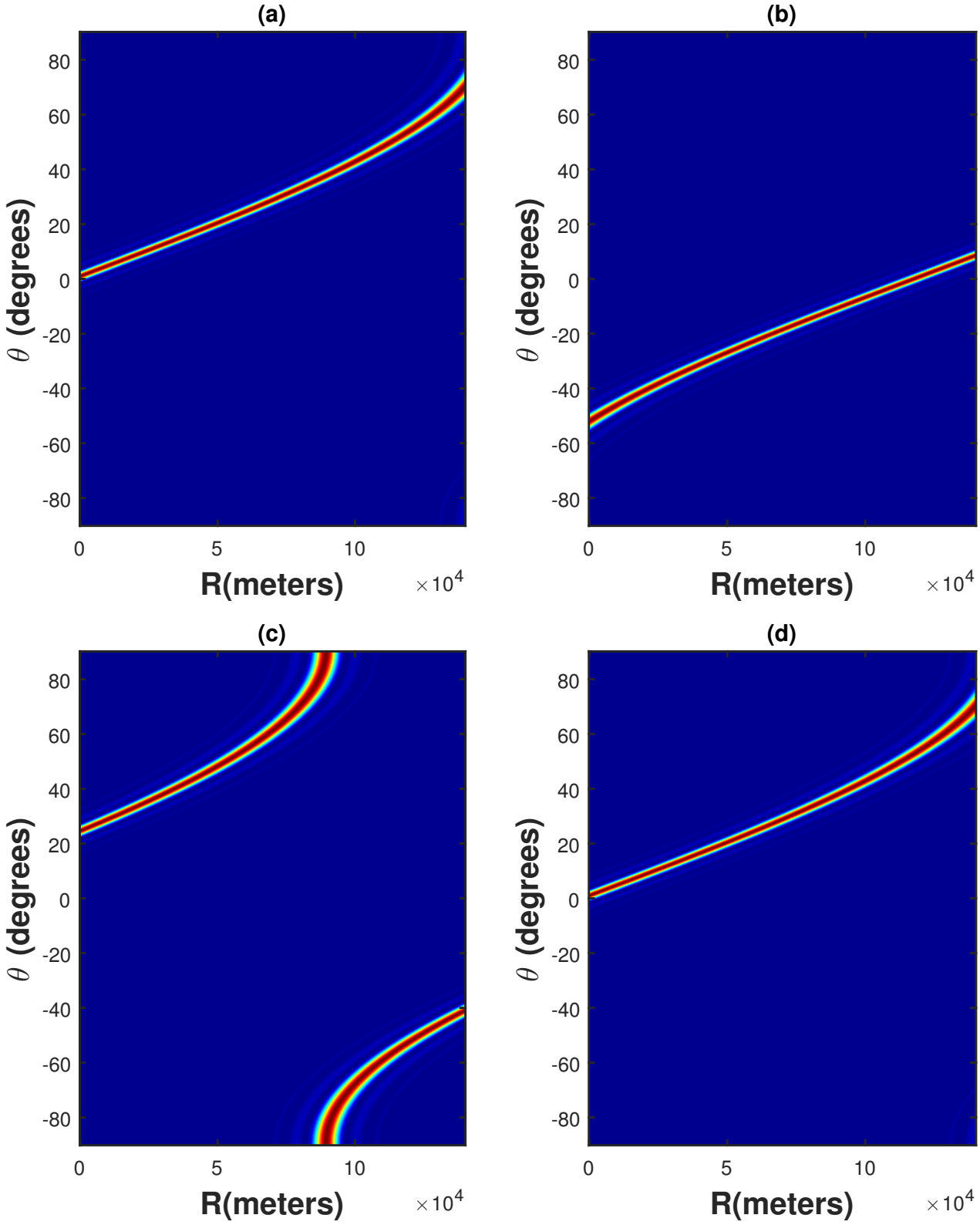

Figure 1.9: 2D view of standard FDA range and angle-dependent beampattern at different time instants
(a) at $t = 0$s (b) at $t = 400\mu$s (c) at $t = 800\mu$s (d) at $t = 1$ms

The FDA transmits beampattern scans of the entire angular and range observation region over different time instants. In CW FDA radar, the transmit beampattern is narrow. Therefore, its beampattern dwell time is very small, so there is a higher probability of missing weak targets. Beampattern dwell time is a major concern in CW FDA radars. Signal processing involves more complexity for CW FDA radars, and controlling the beampattern direction for the desired 2D spatial section is quite difficult. To overcome these issues, practical radars transmit pulse waves.

1.2.2 Pulsed Wave (PW) FDA Radar

Pulsed FDA radar transmits pulses of very small duration T from the transmit antennas over regular time intervals. The PW FDA transmits a range- and angle-dependent beampattern with a quasi-stationary beampattern. The transmitted beampattern scans the maximum range region according to the duration of the transmitted pulse.

For $M = 40$, $f_c = 5$ GHz, $f_o = 1$ kHz, $d = \frac{\lambda}{2}$ and $T = 100\mu$s, the 2D and 3D views of the PW FDA transmit beampattern are shown for four different time instances for $t = 0$s, $t = 100\mu$s, $t = 200\mu$s and $t = 300\mu$s in Figs. 1.10 through Fig. 1.11 respectively. The transmit beampattern steering for pulsed FDA is given by [18]

$$\sin(\theta) = \frac{-f_o T}{\lambda/d}. \tag{1.2.15}$$

The beampattern steers to -11.5^o, so the angular scanning region is the same from $\theta = 0^o$ to $\theta = -11.5^o$. At time $t = \frac{R_k}{c}$, the transmitted signal reaches the target. For $T = 100\mu$s the leading edge of the transmitted signal reaches the range $R = 30$ km, whereas its trailing edge is at $R = 0$. Therefore, at $t = 100\mu$s, the transmitted signal scans up to $R = 30$ km, according to the time duration of the transmitted pulse. For $t = 200\mu$s, the FDA-transmitted pulse scanning range region is from $R = 30$ km to $R = 60$ km; similarly, for $t = 300\mu$s and $t = 400\mu$s, the FDA-transmitted pulse scanning range region is from $R = 60$ km to $R = 90$

km and from $R = 90$ km to $R = 120$ km, respectively.

In pulsed-wave FDA radars, transmit beampattern optimization has been performed. The direction and dwell time of the transmit beampattern are controlled by the transmit antenna element weight design. The shape of the transmit beampattern has also controlled by frequency-offset optimization. Several techniques for antenna element weight design and frequency offset optimization have been proposed in the literature.

1.3 Literature Review

In frequency diverse array (FDA) radar, a small frequency shift is applied across each of the antenna elements along with carrier frequency [1]– [4]. Owing to this small frequency shift, the FDA radar has a range-dependent beampattern in addition to angle and time-dependent beampatterns [5]– [8]. The FDA radar has a periodic angle, range and time-dependent beampattern [9]. Hence the FDA radar is more flexible and capable of locating targets present in different directions and at different ranges [10]. The FDA radar also has the potential to suppress range-dependent interference [11].

1.3.1 Transmit Antenna Elements Weights Design

To steer the FDA radar beampattern in different spatial regions, weights are applied across the transmit antenna elements. Several weight optimization techniques are discussed in [12]– [14]. In [15], using discrete prolate spheroidal sequences (DPSS), the transmit antenna weight vector is obtained by optimizing the transmit energy. The transmit energy of the FDA is maximized within the desired two-dimensional spatial sector out of the total observation sector; hence, the beampattern within the desired region is obtained, but there is no control over the side lobes of the designed beampattern.

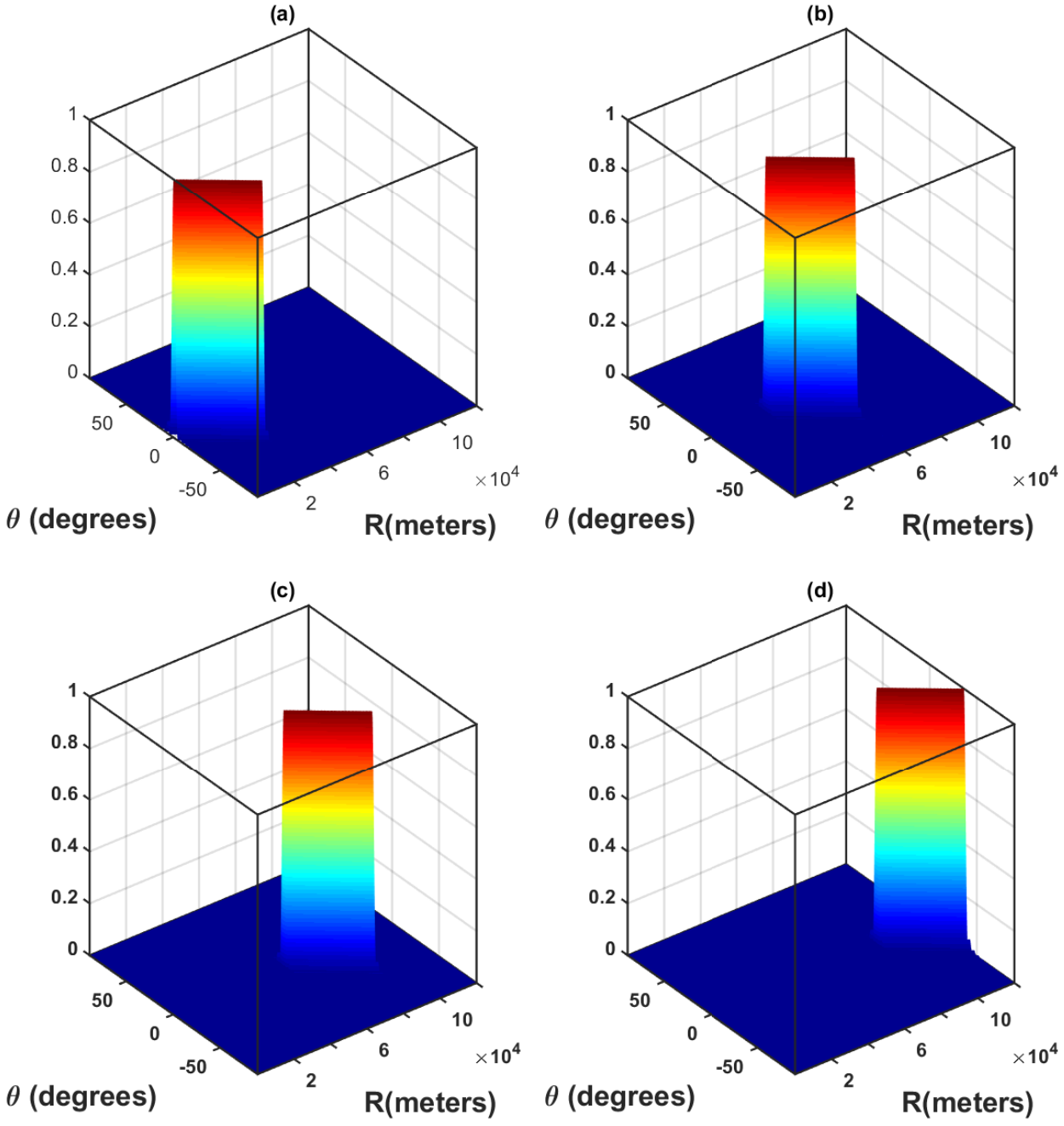

Figure 1.10: 3D view of pulsed FDA range and angle-dependent beampattern at different time instants
(a) at $t = 100\mu$s (b) at $t = 200\mu$s (c) at $t = 300\mu$s (d) at $t = 400\mu$s

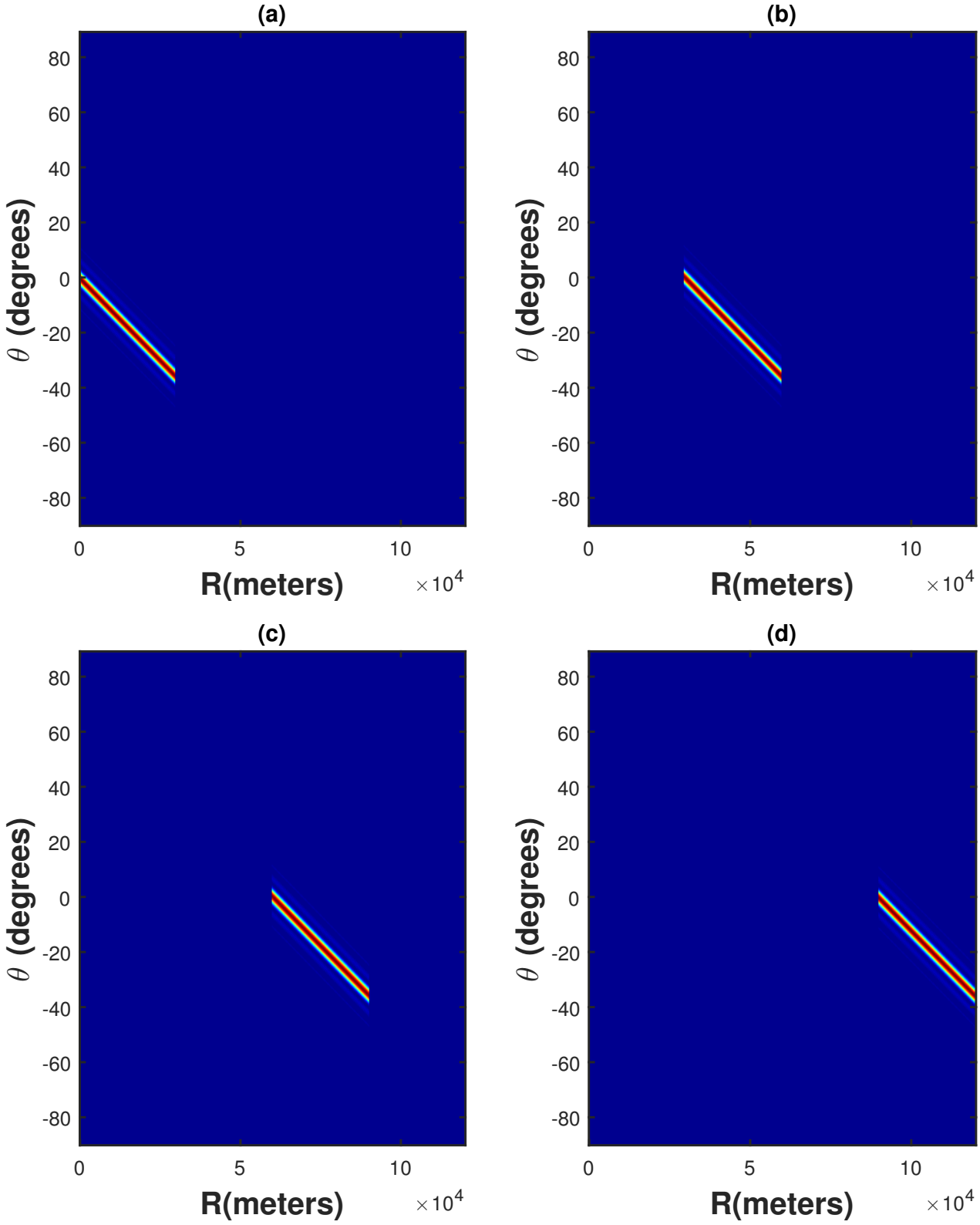

Figure 1.11: 2D view of pulsed FDA range and angle-dependent beampattern at different time instants
(a) at $t = 100\mu$s (b) at $t = 200\mu$s (c) at $t = 300\mu$s (d) at $t = 400\mu$s

In [16], the side lobes of the transmit beampattern are minimized within the specified level by second-order cone programming and thus the transmit antenna element weights are optimized using convex optimization. Another method is discussed in [17], in which the sidelobes of the beampattern are also suppressed using a Hamming window-based nonuniform frequency offset at the transmit antenna elements. The beampattern designed in [17] has a relatively sharp main lobe and shorter dwell time.

A discrete-Fourier-transform (DFT) FDA radar has been proposed in [18] for designing a beampattern within the desired angular direction for a pulsed FDA radar. The transmit antenna element weights are obtained by computing the inverse-fast-Fourier-transform (IFFT) of the desired array factor. The beampattern designed in [18] has a larger dwell time and lower computational complexity; however, the designed beampattern performance evaluation has not been performed for target localization. A time invariant transmit beampattern is designed in [19] using convex weight optimization at the transmit array.

1.3.2 Subarrays based FDA

In the standard FDA, the transmitted beampattern is coupled in angle, range and time. The multi-carrier frequency diverse array (MCFDA) transmits the signals at multiple carrier frequencies, resulting in a decoupled beampattern. In [20], an MCFDA was proposed that optimizes the transmit weights using convex optimization to design single-dot and multi-dot transmit beampatterns with decreased sidelobes. Another MCFDA designed in [21] uses three different convex optimization algorithms to decouple the transmit beampattern in angle, range and time. The transmit beampattern has a large beamwidth and large sidelobes. The use of convex optimization algorithms results in a large computational complexity in the design of the transmit weights.

The sparse MCFDA proposed in [22] uses a modified genetic algorithm to optimize

the cost function. The cost function minimizes the difference between the desired and designed responses and reduces the computational complexity of the transmit weight design. The FDA beampattern has an autoscanning feature [23] since FDA beampattern is angle, range and time-dependent. The designed beampattern has reduced sidelobes, but the beampattern is very narrow and the dwell time is small. For multiple-target detection, a conditional GLRT-based method was proposed [24] for receiver antennas for uniform-weighted FDA-transmitted beampattern.

1.3.3 Target Localization in FDA

There are various techniques for target localization discussed in [25]– [32]. Most studies on target localization use uniform weights at the transmit antenna elements. A uniformly weighted double-pulse frequency FDA radar has been proposed in [33], where the first pulse was transmitted to determine the direction of arrival (DOA) of the target and the range of the target was determined by transmitting another pulse. In [34], a uniformly weighted subarray FDA radar has been discussed. The transmit antenna elements are divided into different subarrays and each subarray transmits waveforms at distinct frequency shifts; thus the target direction and range are jointly determined.

A transmit-subaperturing (TS) FDA radar is proposed in [35], which tracks the target using optimization criteria to find out the location of the target. TS-FDA divides FDA main array into subarrays and cognitively determines the location of the target. The target tracking performance and computational complexity of the proposed TS-FDA is high. A distributed FDA-multiple-input multiple-output (MIMO) has been proposed in [36], with uniformly weighted transmit antenna elements to suppress deceptive mainlobe jammers. The method involves two steps to sustain mainlobe and suppress sidelobes via MVDR beamformer design and Wiener filter design.

The FDA-MIMO proposed in [37] adaptively determines the transmit weights by maximizing the output signal-to-interference-plus-noise ratio (SINR) to suppress deceptive mainlobe jammers. The proposed method allocates the transmit power

by assuming orthogonal waveforms at the transmitter and computes their covariance matrix which results in lower computational complexity but orthogonality limits its practical implementability. In [18], it is discussed that a beampattern designed using IFFT weights can effectively localize of targets in multiple directions.

1.4 Motivation

Standard FDA radar beampattern has a shorter dwell time and in most of the proposed literature, propagation delay has been ignored and all the weights optimization algorithms are computationally complex except the one DFT based algorithm [18] which has used the correct model for FDA radar incorporating all propagation time delays and mentioning transient and steady-state beampatterns as well and it has a high dwell time and capable of locating more than one target in multiple directions as well as its computational complexity is less than that of all techniques proposed in the literature. In [18], the beampattern is designed for desired angular direction only as well as signal model is derived from the transmit antennas till the target and the localization of the target has not been done which is really very important for locating the target and for its practical application of use. The main goal of this thesis is to design a time-invariant 2D beampattern for desired angular direction and range and the derivation of received signal model for target parameter estimation for performance evaluation of designed beampattern.

Following are the objectives of this research thesis.

- Derivation of closed-form solution of transmit antenna element weights for 2D beampattern design.
- Derivation of the received signal model.
- To estimate the location of the target using MPDR Beamformer.
- Derivation of Cramer-Rao Lower Bound for FDA Radar.

1.5 Contribution and Organization

The main contribution of this thesis is the design of a low-complexity algorithm for a 2D time-invariant beampattern design. The complete mathematical details and bounds are given, and the performance evaluation of the proposed beampattern is presented.

The rest of the thesis is organised as follows:

1. Chapter 2 first presents the mathematics and simulations of the time-variant beampattern design and then the time-invariant beampattern design.

2. Chapter 3 presents the received signal model for the FDA radar. The two variants of the received signal model are presented with both FDA zero-frequency offset and non-zero frequency offset. The idea for the selection of parameters for designing a focused beampattern is discussed in detail.

3. In Chapter 4, the target parameter estimation is performed by estimating the angle and the range of the target. The CRLB is derived, and the simulation results are shown to verify the effectiveness of the proposed beampattern.

4. Chapter 5 summarizes all chapters and concludes the thesis. Finally, the future directions of the proposed work are discussed.

5. The references have been mentioned at the end.

Chapter 2

Beampattern Design in FDA Radar

2.1 System Model

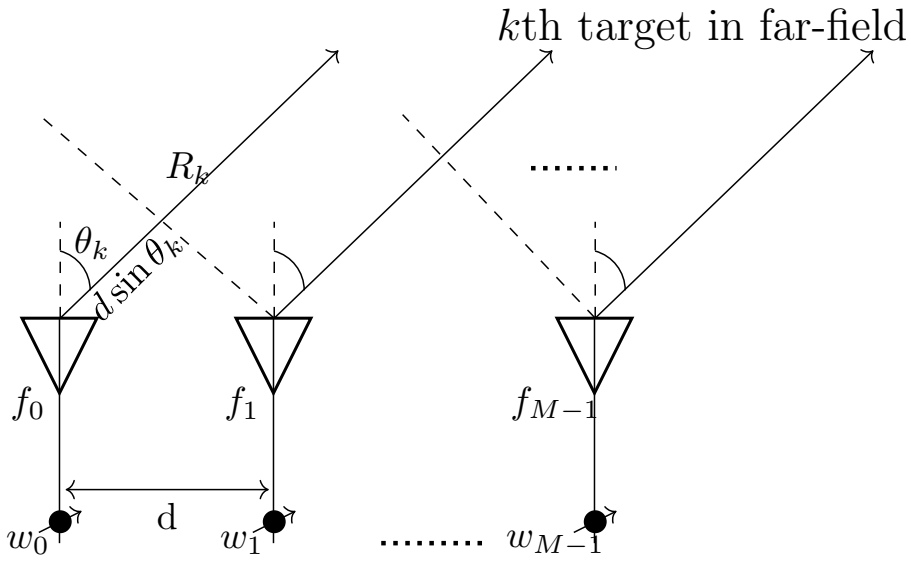

Figure 2.1: FDA Radar Transmitter.

Consider a frequency diverse array radar setup with linear arrays of antenna elements. We assume M number of antenna elements in the transmitter array and N number of antenna elements at the receiver array with uniform separation between the antenna elements denoted by d. Each antenna element transmits a signal $s_m(t)$

using a carrier frequency f_c but with small frequency shift f_m introduced at mth antenna element. The transmitted signal is given by

$$s_m(t) = w_m e^{-j2\pi(f_c+f_m)t}, \qquad m = 0, 1, \cdots, M-1 \tag{2.1.1}$$

There is a possible point target k located in far-field at an angle θ_k where θ_k is the angle of the target with the perpendicular to the array and the distance of the target from the array is R_k as shown in Fig. 1. The received signal at the target is obtained after a delay in time τ as given by

$$\begin{aligned} p(t) &= \sum_{m=0}^{M-1} w_m e^{-j2\pi(f_c+f_m)(t-\tau)}, \qquad \tau = \frac{R_k - md\sin(\theta_k)}{c} \\ &= \sum_{m=0}^{M-1} w_m e^{-j2\pi(f_c+f_m)(t-\frac{R_k-md\sin(\theta_k)}{c})} \end{aligned} \tag{2.1.2}$$

where c denotes the speed of light in space. If we choose linearly increasing frequency shifts f_o, that is, uniform inter-element frequency offset as $f_m = mf_o$, then

$$\begin{aligned} p(t) &= \sum_{m=0}^{M-1} w_m e^{-j2\pi(f_c+mf_o)(t-\frac{R_k-md\sin(\theta_k)}{c})} \\ &= e^{-j2\pi f_c(t-\frac{R_k}{c})} \sum_{m=0}^{M-1} w_m e^{-j2\pi\left[mf_o(t-\frac{R_k}{c})+\frac{mf_c d\sin(\theta_k)}{c}+\frac{m^2 f_o d\sin(\theta_k)}{c}\right]} \\ &= e^{-j2\pi f_c(t-\frac{R_k}{c})} \sum_{m=0}^{M-1} w_m e^{-j2\pi\left[mf_o(t-\frac{R_k}{c})+(f_c+mf_o)\frac{md\sin(\theta_k)}{c}\right]}. \end{aligned} \tag{2.1.3}$$

The fundamental condition for FDA radar is $f_c \gg mf_o$, therefore,

$$p(t) = e^{-j2\pi f_c(t-\frac{R_k}{c})} \sum_{m=0}^{M-1} w_m e^{-j2\pi\left[mf_o(t-\frac{R_k}{c})+\frac{mf_c d\sin(\theta_k)}{c}\right]}. \tag{2.1.4}$$

The transmit antenna elements send pulses each of duration T. The transmitted pulse from the reference antenna element 0 reaches the target at time instant $t_0 = \frac{R_k}{c}$, whereas the signal from antenna element 1 reaches the target at $t_1 = t_0 - \tau_1 = \frac{R_k}{c} - \frac{d\sin(\theta_k)}{c}$, where τ_1 is the delay incorporating the path length effects

due to antenna 1. Similarly, the signal from the $(M-1)$th antenna element reaches the target at time $t_{M-1} = t_0 - \tau_{M-1} = \frac{R_k}{c} - \frac{(M-1)d\sin(\theta_k)}{c}$, where τ_{M-1} is the delay incorporating the path length effects due to antenna $M-1$. Hence, the signal from the $(M-1)$th antenna reaches the target first, because of the maximum frequency applied across it. Suppose, L pulses are transmitted from each antenna element. The target is illuminated by the transmitted pulses for $t \geq t_0 - \tau_{M-1}$. The array factor for a given θ_k and R_k can be defined as

$$AF(t, R_k, \theta_k) = \begin{cases} \sum_{m=0}^{M-1} w_m e^{-j2\pi\left[mf_o(t-\frac{R_k}{c})+\frac{mf_c d\sin(\theta_k)}{c}\right]} & \text{for } t \geq t_{M-1}, \\ 0 & \text{for } t < t_{M-1}. \end{cases} \tag{2.1.5}$$

The beampattern as a function of θ and R can be found as

$$B(t, R, \theta) = \left|AF(t, R, \theta)\right|^2, \tag{2.1.6}$$

where θ and R are the observation angle and observation range regions, respectively, as given by

$$-90^o \leq \theta \leq 90^o \tag{2.1.7}$$

$$\text{and } R_{min} \leq R \leq R_{max}. \tag{2.1.8}$$

R_{min} and R_{max} denote the minimum and maximum values in the observation range region, respectively. For $t \geq t_0$, all the transmitted pulses completely illuminate the target and there is steady-state response of beampattern as given by

$$B_s(t, R, \theta) = \left|AF_s(t, R, \theta)\right|^2, \qquad \text{for } t \geq t_0. \tag{2.1.9}$$

2.2 Proposed Beampattern Design

As discussed in section 2.1, the array factor for $t \geq t_0$ is given by

$$\mathrm{AF}(t, R, \theta) = \sum_{m=0}^{M-1} w_m e^{-j2\pi\left[m f_o(t-\frac{R_k}{c})+\frac{m f_c d \sin(\theta_k)}{c}\right]}. \tag{2.2.1}$$

Putting $c = f_c\lambda$ and assuming that the separation between the antenna elements equal to the half of wavelength λ of the carrier frequency, i.e., $d = \frac{\lambda}{2}$, the array factor is simplified as

$$\begin{aligned}\mathrm{AF}(t, R, \theta) &= \sum_{m=0}^{M-1} w_m e^{-j2\pi m(f_o t+\frac{\sin(\theta)}{2}-\frac{f_o R}{c})} \\ &= \sum_{m=0}^{M-1} w_m e^{-j2\pi m(f_o t+f_\theta-f_R)}, \end{aligned} \tag{2.2.2}$$

where $f_\theta = \frac{\sin(\theta)}{2}$ and $f_R = \frac{f_o R}{c}$. For the two-dimensional observation section (R, θ), the value of f_θ and f_R is given by

$$-0.5 \leq f_\theta \leq 0.5, \tag{2.2.3}$$

$$\text{and } \frac{f_o R_{min}}{c} \leq f_R \leq \frac{f_o R_{max}}{c}. \tag{2.2.4}$$

The vector form of array factor equation is obtained as

$$\mathrm{AF}(t, R, \theta) = \begin{bmatrix} w_0, w_1, \ldots, w_{M-1} \end{bmatrix} \begin{bmatrix} 1 \\ e^{-j2\pi(f_o t+f_\theta-f_R)} \\ \vdots \\ e^{-j2\pi(M-1)(f_o t+f_\theta-f_R)} \end{bmatrix}, \tag{2.2.5}$$

$$= \mathbf{w}^{\mathsf{H}} \mathbf{a}_T(t, \theta, R), \tag{2.2.6}$$

where the transmit steering vector $\mathbf{a}_T(t, \theta, R)$ is dependent on time, angle and range. Therefore, FDA radar has an angle, time and range-dependent beampat-

tern. The transmit steering vector is given by

$$\mathbf{a}_T(t,\theta,R) = \mathbf{a}_T(t) \odot \mathbf{a}_T(\theta) \odot \mathbf{a}_T(R), \tag{2.2.7}$$

where

$$\mathbf{a}_T(t) = \left[1, e^{-j2\pi f_o t}, \ldots, e^{-j2\pi(M-1)f_o t}\right]^{\mathsf{T}}, \tag{2.2.8}$$

$$\mathbf{a}_T(\theta) = \left[1, e^{-j2\pi f_\theta}, \ldots, e^{-j2\pi(M-1)f_\theta}\right]^{\mathsf{T}}, \tag{2.2.9}$$

$$\mathbf{a}_T(R) = \left[1, e^{j2\pi f_R}, \ldots, e^{j2\pi(M-1)f_R}\right]^{\mathsf{T}}. \tag{2.2.10}$$

The transmit steering vector is given by (2.2.7), the transmit weight is designed by

$$\mathbf{w} = \mathbf{w}_t \odot \mathbf{w}_\theta \odot \mathbf{w}_R. \tag{2.2.11}$$

2.2.1 Angle and time-dependent beampattern

For $f_o = 0$ Hz, the FDA radar acts like a phased array (PA) radar and the equation of FDA array factor reduces to the function of θ only.

$$\begin{aligned} \mathrm{AF}(t,R,\theta)|_{f_o=0} &= \mathbf{w}_\theta^{\mathsf{H}} \mathbf{a}_T(\theta) \\ \mathrm{AF}(\theta) &= \sum_{m=0}^{M-1} w_{\theta_m} e^{-j2\pi m f_\theta} \end{aligned} \tag{2.2.12}$$

The array factor in (2.2.12) is the discrete-Fourier-transform (DFT) of weights applied at transmit antenna elements.

$$\mathrm{AF}(\theta_d) = \mathscr{F}\{w_{\theta_m}\} \tag{2.2.13}$$

where $\mathscr{F}\{\cdot\}$ denotes the Fast-Fourier-transform of a column vector. These weights in angular dimension can be found by taking the IFFT of the desired angle-dependent array factor.

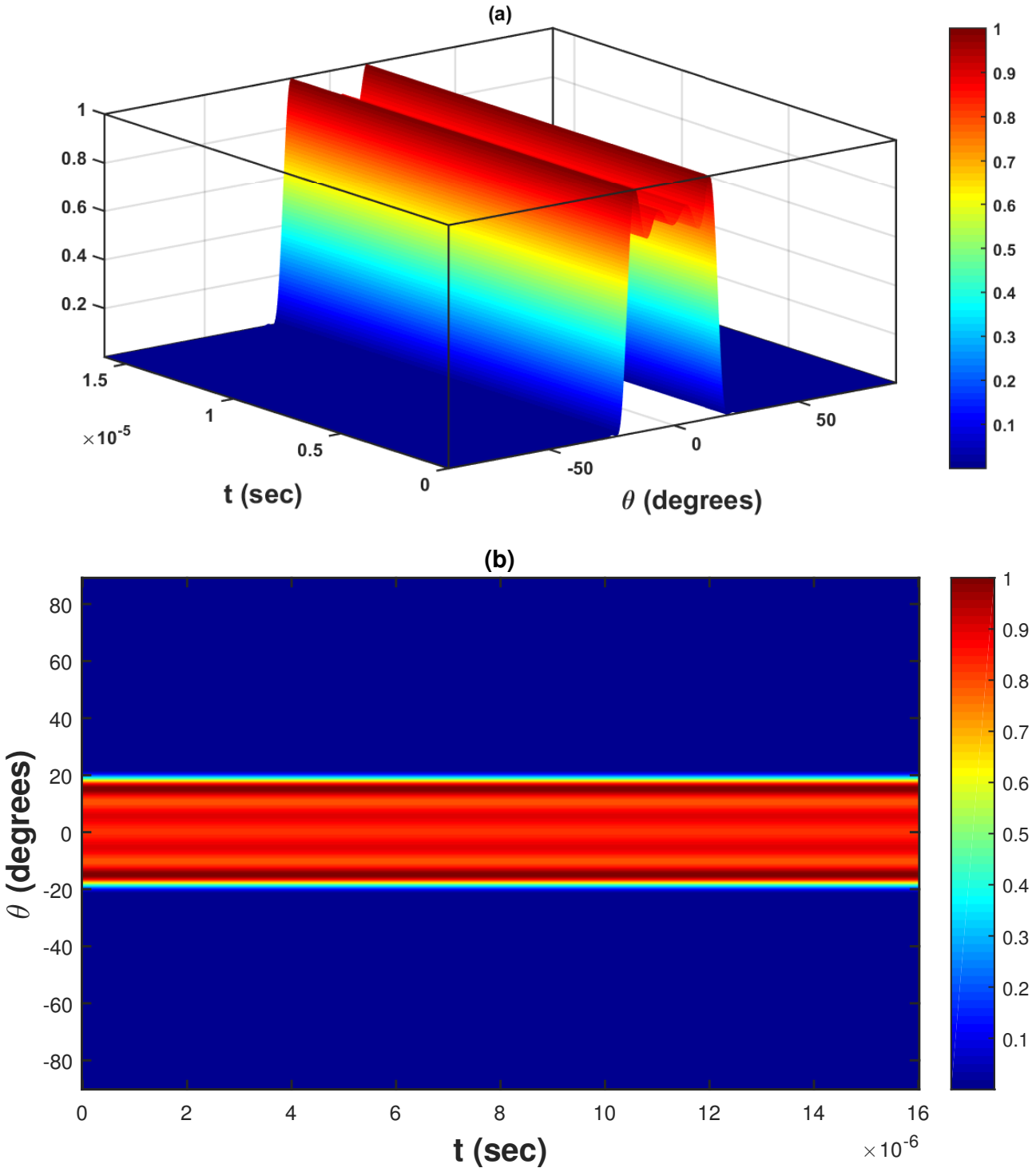

Figure 2.2: FDA beampattern as a function of angle and time for a fixed R at $f_o = 0$ Hz

$$w_{\theta_m} = \sum_{f_\theta=-0.5}^{0.5} \mathrm{AF}(\theta_d) e^{j2\pi m f_\theta} = \mathscr{F}^{-1}\{\mathrm{AF}(\theta_d)\} \tag{2.2.14}$$

As an example, the transmit beampattern of FDA radar is designed for the desired angular region $-20^o \leq \theta_d \leq 20^o$ for $M = 40$, $d = \frac{\lambda}{2}$, $f_c = 5$ GHz and $T = 16\mu$s. The equation (2.2.12) is showing array factor as a function of θ for $f_o = 0$ Hz, hence the designed beampattern is time-invariant in this case as shown in Fig. 2.2. In this case, FDA radar behaves as PA radar and a range-dependent beampattern could not be obtained.

FDA radar has a time-dependent beampattern that can be obtained by $f_o > 0$ Hz, $t > 0$ s. There is a shift in beampattern which is proportional to $f_o t$ and fixed R utilizing the time shifting property of DFT. Hence the spatial beampattern has moved towards negative angular direction for $f_o = 30$ kHz as shown in Fig. 2.3. From (2.2.13), the $\mathrm{AF}(\theta_d)$ is the FFT of w_{θ_m}. Therefore, for a fixed range R_k, the angular shift in $\mathrm{AF}(\theta + \theta_d)$ is given by

$$\mathrm{AF}(\theta + \theta_d) = \mathscr{F}\{e^{-j2\pi m f_o t} w_{\theta_m}\} \tag{2.2.15}$$

The angle-dependent beampattern of FDA radar on a polar plot is shown for different time instances in Fig. 2.4. At $t = 0$ s, the beampattern illuminates the angular region $[-20^o, 20^o]$ only, exactly following the desired beampattern. At $t = 5\mu$s, due to spatial shift in beampattern, the illumination region shifts to $[-7^o, -47^o]$, whereas at $t = 10\mu$s, the angular illumination region is $[-34^o, -74^o]$. At $t = 16\mu$s, the illumination region shifts to $[-67^o, -90^o]$ and $[83^o, 90^o]$. Therefore, the total illumination angle at a particular time instant is 40^o. For $f_o > 0$ Hz, the FDA beampattern scans across the whole angular observation region $[-90^o, 90^o]$ in a clockwise direction.

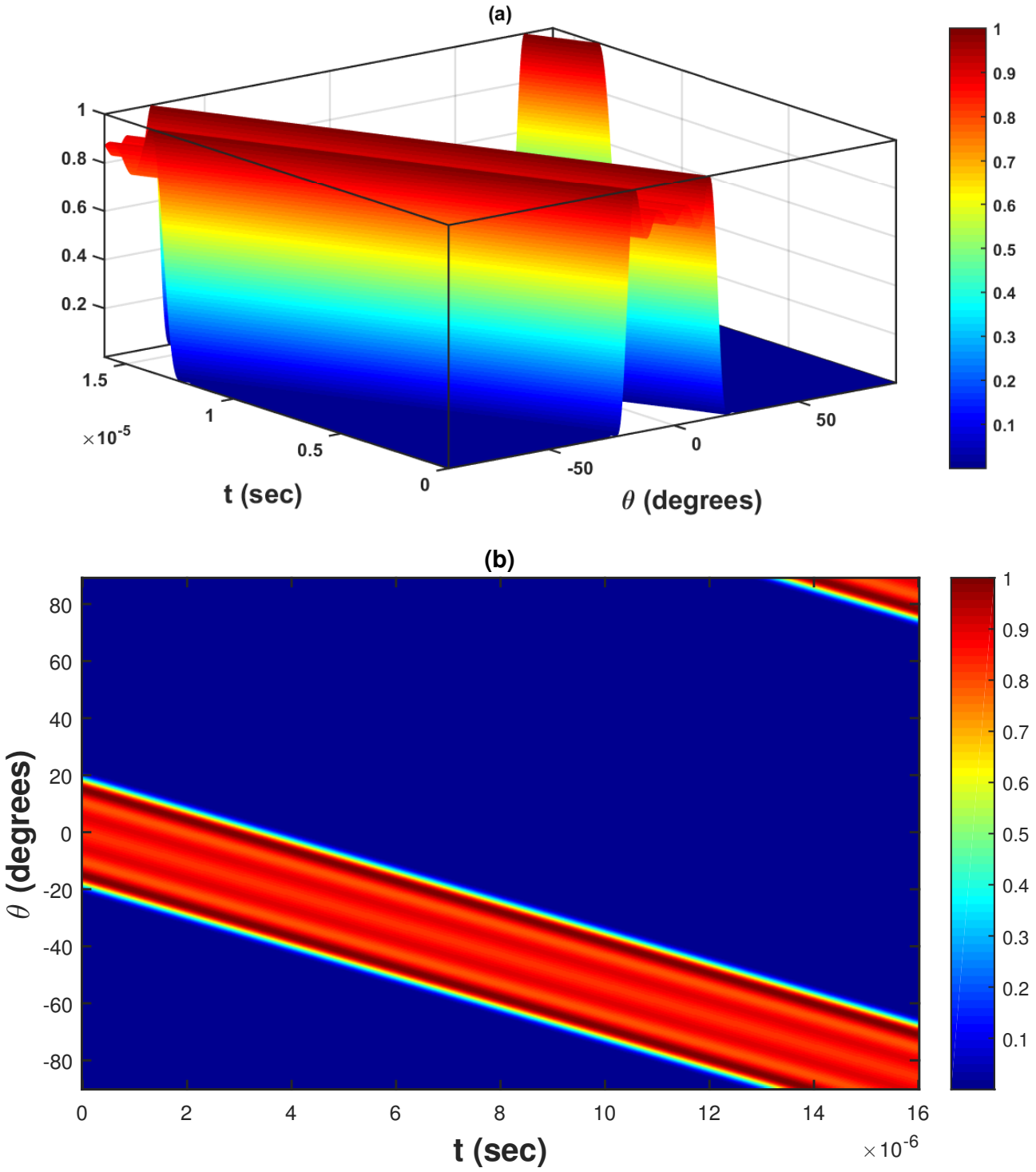

Figure 2.3: FDA beampattern as a function of angle and time for a fixed R at $f_o = 30$ kHz

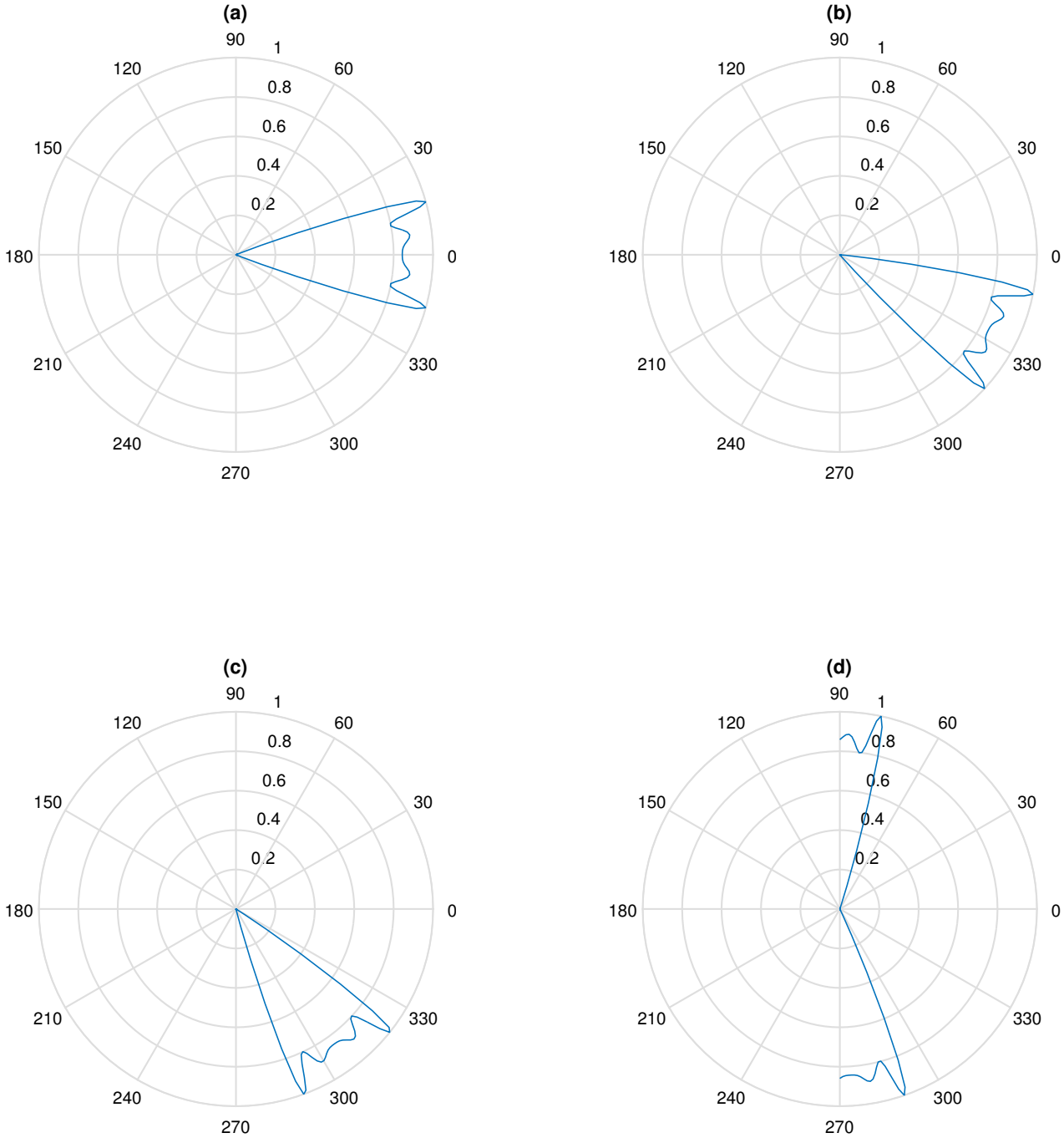

Figure 2.4: FDA beampattern polar plot for $f_o = 30$ kHz at different time instances (a) at $t = 0$s (b) at $t = 5\mu$s (c) at $t = 10\mu$s (d) at $t = 16\mu$s

For $f_o < 0$ Hz, $t > 0$ s and fixed R, there is a shift in beampattern, proportional to $-f_o t$, hence the spatial beam pattern moves towards positive angular direction for $f_o = -30$ kHz as shown in Fig. 2.5.

The angle-dependent beampattern of FDA radar on a polar plot is shown for different time instances in Fig. 2.6. At $t = 0$ s, the beampattern illuminates the angular region $[-20^o, 20^o]$ only, exactly following the desired beampattern. At $t = 5\mu$s, due to spatial shift in beampattern, the illumination region shifts to $[7^o, 47^o]$, whereas at $t = 10\mu$s, the angular illumination region is $[34^o, 74^o]$. At $t = 16\mu$s, the illumination region shifts to $[67^o, 90^o]$ and $[-90^o, -83^o]$. Therefore, the total illumination angle at a particular time instant is 40^o. For $f_o < 0$ Hz, the FDA beampattern scans across the whole angular observation region $[-90^o, 90^o]$ in anticlockwise direction.

2.2.2 Range and time-dependent beampattern

For $\theta = 0$, the value of $f_\theta = 0$ and the equation of array factor reduces to the function of R and t.

$$\begin{aligned} \mathrm{AF}(t, R, \theta = 0) &= \sum_{m=0}^{M-1} w_m e^{-j2\pi m(f_o t - f_R)} \\ &= \sum_{m=0}^{M-1} w_m e^{-j2\pi m f_o (t - \frac{R}{c})} \end{aligned} \tag{2.2.16}$$

For a given R, at $t = \frac{2R}{c}$, then array factor becomes function of R.

$$\begin{aligned} \mathrm{AF}(t = \frac{2R}{c}, R, \theta = 0)|_{\theta=0} &= \mathrm{AF}(R) = \mathbf{w}_R^{\mathsf{H}} \mathbf{a}_T(R) \\ &= \sum_{m=0}^{M-1} w_{R_m} e^{-j2\pi m f_R} \end{aligned} \tag{2.2.17}$$

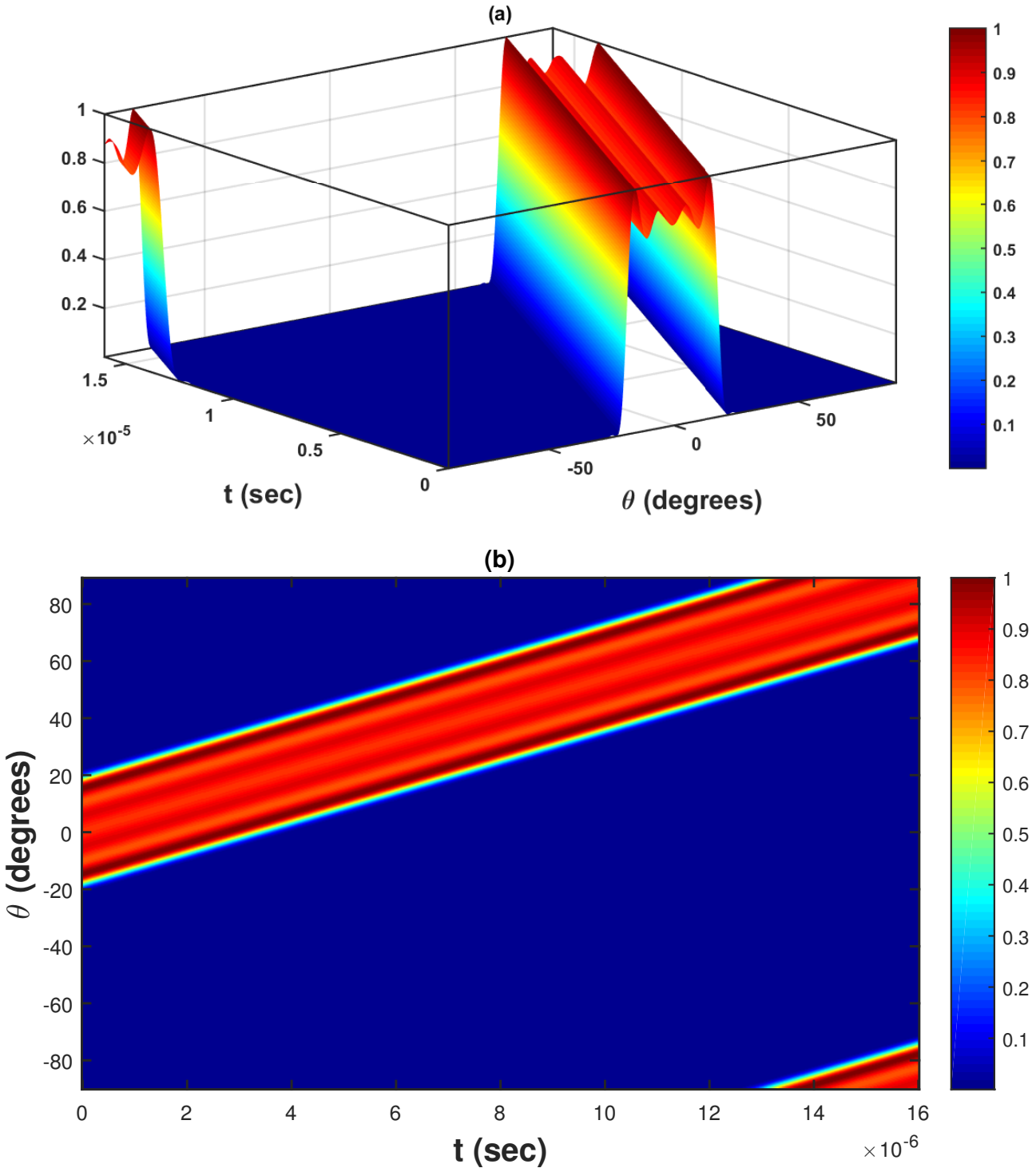

Figure 2.5: FDA beampattern as a function of angle and time for a fixed R at $f_o = -30$ kHz

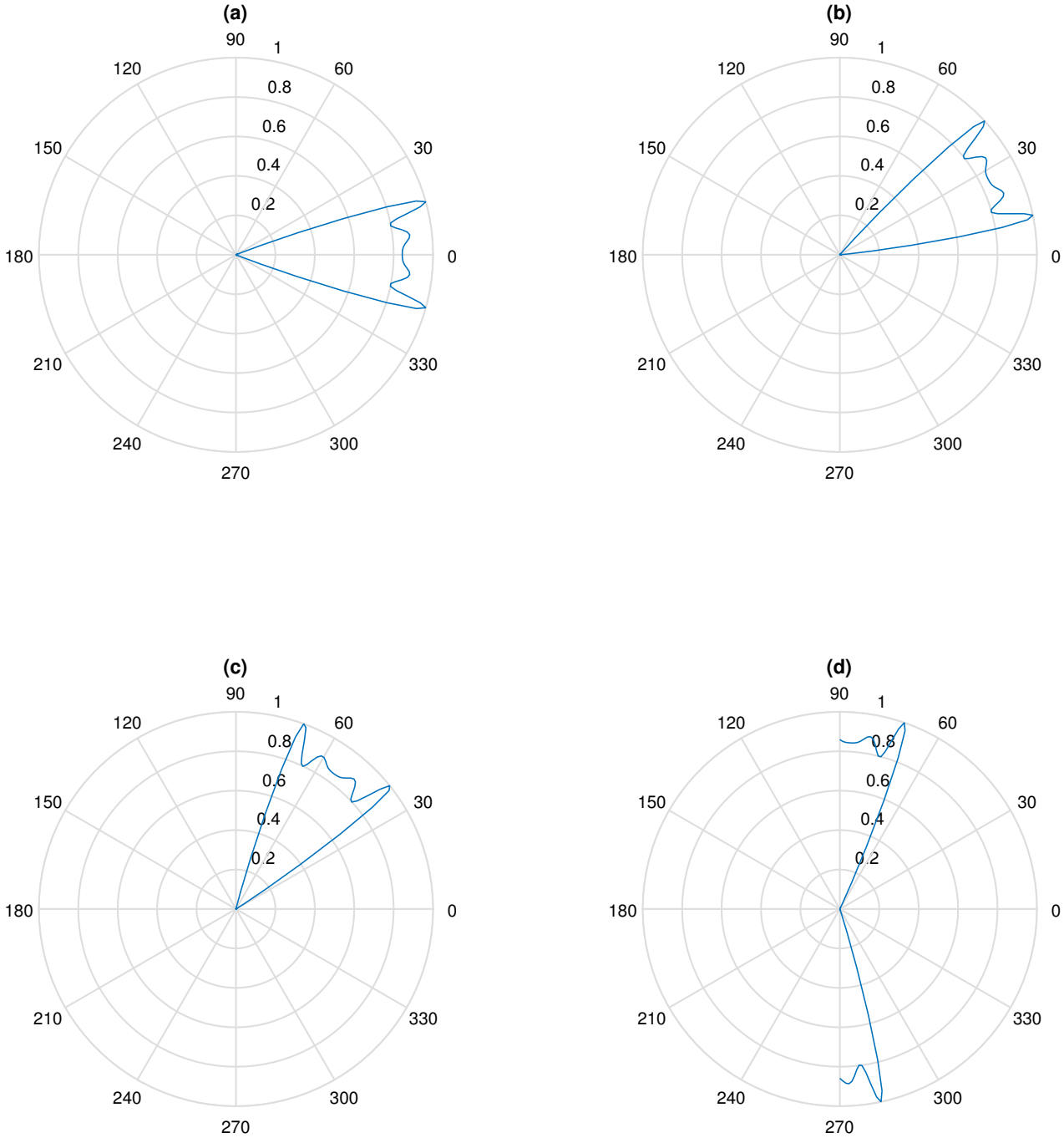

Figure 2.6: FDA beampattern polar plot for $f_o = -30$ kHz at different time instances (a) at $t = 0$s (b) at $t = 5\mu$s (c) at $t = 10\mu$s (d) at $t = 16\mu$s

Therefore, the equation of array factor is the DFT of transmit antenna element weights.

$$\mathrm{AF}(R_d) = \mathscr{F}\{w_{R_m}\} \tag{2.2.18}$$

The weights in range dimension could be found by taking IFFT of the desired range-dependent array factor.

$$\begin{aligned} w_{R_m} &= \sum_{f_R=\frac{f_o R_{min}}{c}}^{\frac{f_o R_{max}}{c}} \mathrm{AF}(R_d) e^{j2\pi m f_R} \\ &= \mathscr{F}^{-1}\{\mathrm{AF}(R_d)\} \end{aligned} \tag{2.2.19}$$

As an example, a range-dependent FDA beampattern is designed for the desired range region 4 km $\leq R_d \leq$ 6 km for $M = 40$, $d = \frac{\lambda}{2}$, $f_c = 5$ GHz and $T = 16\mu$s. At $t = 0$, the leading edge of the transmitted pulse is at $R = 6$ km while the preceding edge is at $R = 4$ km. Therefore, the designed beampattern illumination range region is $[4\text{ km}, 6\text{ km}]$ exactly following the desired beampattern.

FDA radar has a time-dependent beampattern, for either $f_o > 0$ Hz or $f_o < 0$ Hz, the transmitted pulse would illuminate the range region, that is, $R > R_d$. For $t > 0$ s, the shift in beampattern is proportional to $f_o t$, hence the spatial beam pattern is time-variant as shown in Fig. 2.7. The total FDA illumination range region is 2 km at a particular time instant whereas the designed FDA beampattern illuminates the whole range region for $t > 0$ s. Therefore, for a fixed range θ_k, the range shift in $\mathrm{AF}(R + R_d)$ is given by

$$\mathrm{AF}(R + R_d) = \mathscr{F}\{e^{-j2\pi m f_o t} w_{R_m}\}. \tag{2.2.20}$$

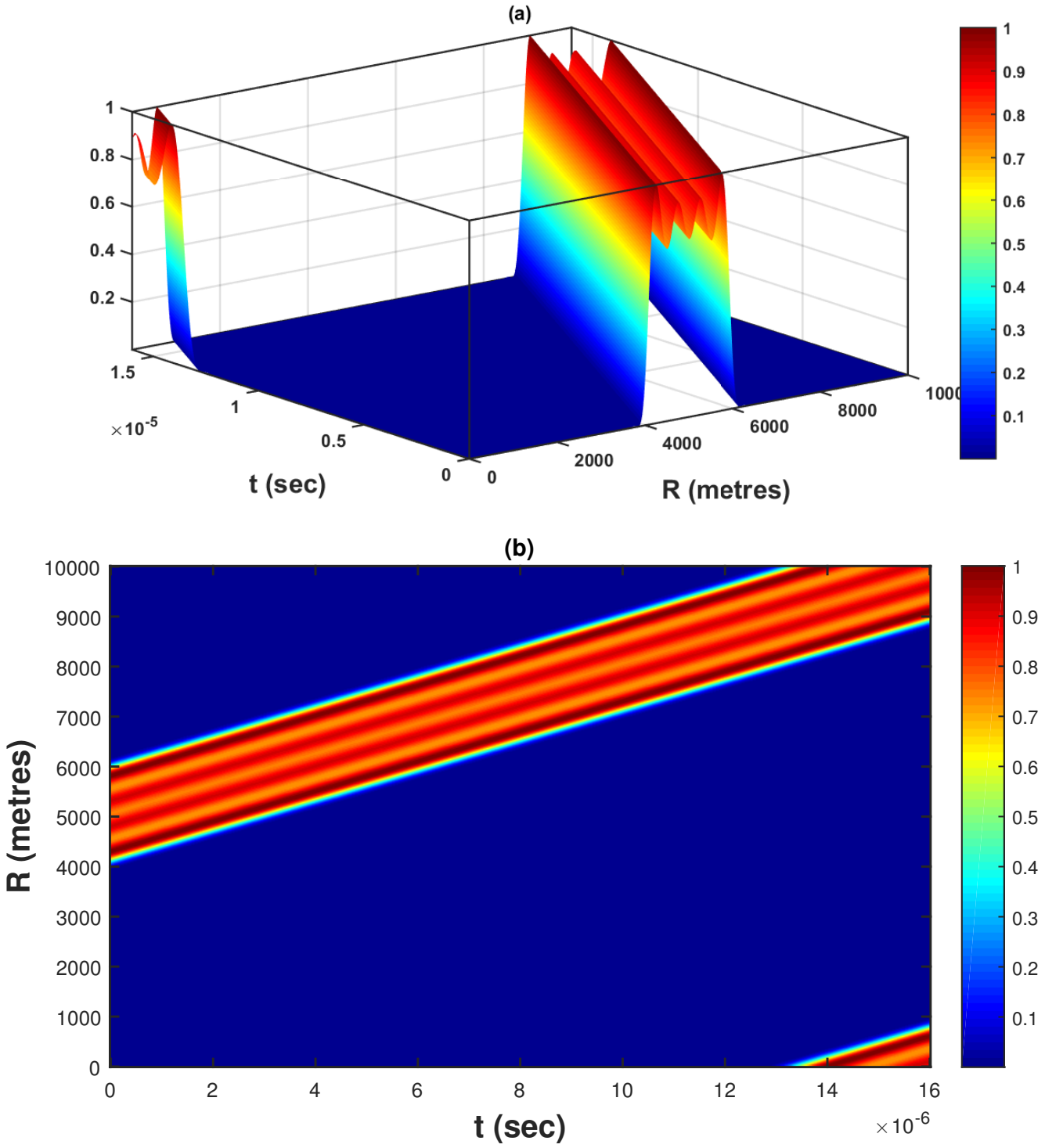

Figure 2.7: FDA beampattern as a function of range and time for a fixed θ at $f_o = 30$ kHz

2.3 Time-variant transmit beampattern

The transmit weight vectors in both angular dimension and range dimension is given by

$$\mathbf{w}_\theta = \left[w^*_{\theta_0}, w^*_{\theta_1}, \ldots, w^*_{\theta_{M-1}}\right]^{\mathsf{T}}, \tag{2.3.1}$$

$$\mathbf{w}_R = \left[w^*_{R_0}, w^*_{R_1}, \ldots, w^*_{R_{M-1}}\right]^{\mathsf{T}}. \tag{2.3.2}$$

The transmit steering vector as a function of angle and range at a given time instant t is given by

$$\mathbf{a}_T(\theta, R) = \left[1, \ldots, e^{-j2\pi(M-1)(f_\theta - f_R)}\right]^{\mathsf{T}}. \tag{2.3.3}$$

The transmit steering vector is given by (2.3.3), the transmit beamspace weight vector $\mathbf{w}$ can be designed as

$$\mathbf{w} = \mathbf{w}_\theta \odot \mathbf{w}_R. \tag{2.3.4}$$

The desired range angle-dependent transmit beampattern is given by

$$\begin{aligned} \mathrm{B}(t, R, \theta) &= |\mathrm{AF}(t, R, \theta)|^2 \\ &= \left|\mathbf{w}^{\mathsf{H}}\mathbf{a}_T(t, \theta, R)\right|^2. \end{aligned} \tag{2.3.5}$$

For designing FDA 2D beampattern, a desired beampattern is formed by dividing the whole observation region in angular and range dimension into number of grid points. To illuminate the desired region, ones are assigned and for the rest of region, zeros are assigned. The proposed transmit weight vector is designed by computing IFFT of the desired array factor. Finally, a desired 2D angle and range dependent beampattern is obtained by (2.3.5). The designed transmit beampattern dwell time is large therefore, it is capable of locating weak targets very easily. The transmit beampattern could also be designed for illuminating multiple directions and ranges.

In order to explain the performance of proposed scheme for designing 2D beampattern for desired spatial section, $\theta_d \in [-20^o, 20^o]$ and $R_d \in [4 \text{ km}, 6 \text{ km}]$. The FDA 2D beampattern designed for $f_o = 30$ kHz is shown in Fig. 2.8–2.9. The FDA transmit beampattern is time-dependent so it illuminates different angular and range regions while scanning over the whole angular and range observation sections at different instances of time. The FDA radar transmit beampattern scans the angular region from $[-90^o, -90^o]$ and range region from $[0 \text{ m}, 10 \text{ km}]$.

For $f_o = -30$ kHz, the beampattern is designed for desired direction $\theta_d \in [-20^o, 20^o]$ and desired range $R_d \in [4 \text{ km}, 6 \text{ km}]$. For frequency decrement, the designed transmit beampattern scans the 2D spatial section in anticlockwise direction. The FDA designed 2D beampattern is shown in Fig. 2.10–2.11 for different time instants. Therefore, the FDA radar transmit beampattern scans the whole angular observation region from $[-90^o, -90^o]$ and range region from $[0 \text{ m}, 10 \text{ km}]$.

The FDA radar beampattern utilizes the time-shifting property of the FFT algorithm. In the case of the frequency increment applied across the transmit antenna elements as time increases, the beampattern moves towards the left side, that is, the negative angular region. Similarly, for frequency decrement, the beampattern moves towards the positive angular region. This is the intrinsic nature of the FDA beampattern because the FDA beampattern is time-dependent.

The proposed designed beampattern moves across the entire observation section over the period of time. The designed beampattern has a larger dwell time but it does not illuminate the desired 2D spatial section for all values of time. The main goal is to design a time-invariant beampattern that illuminates the desired angle and range regions for all values of time.

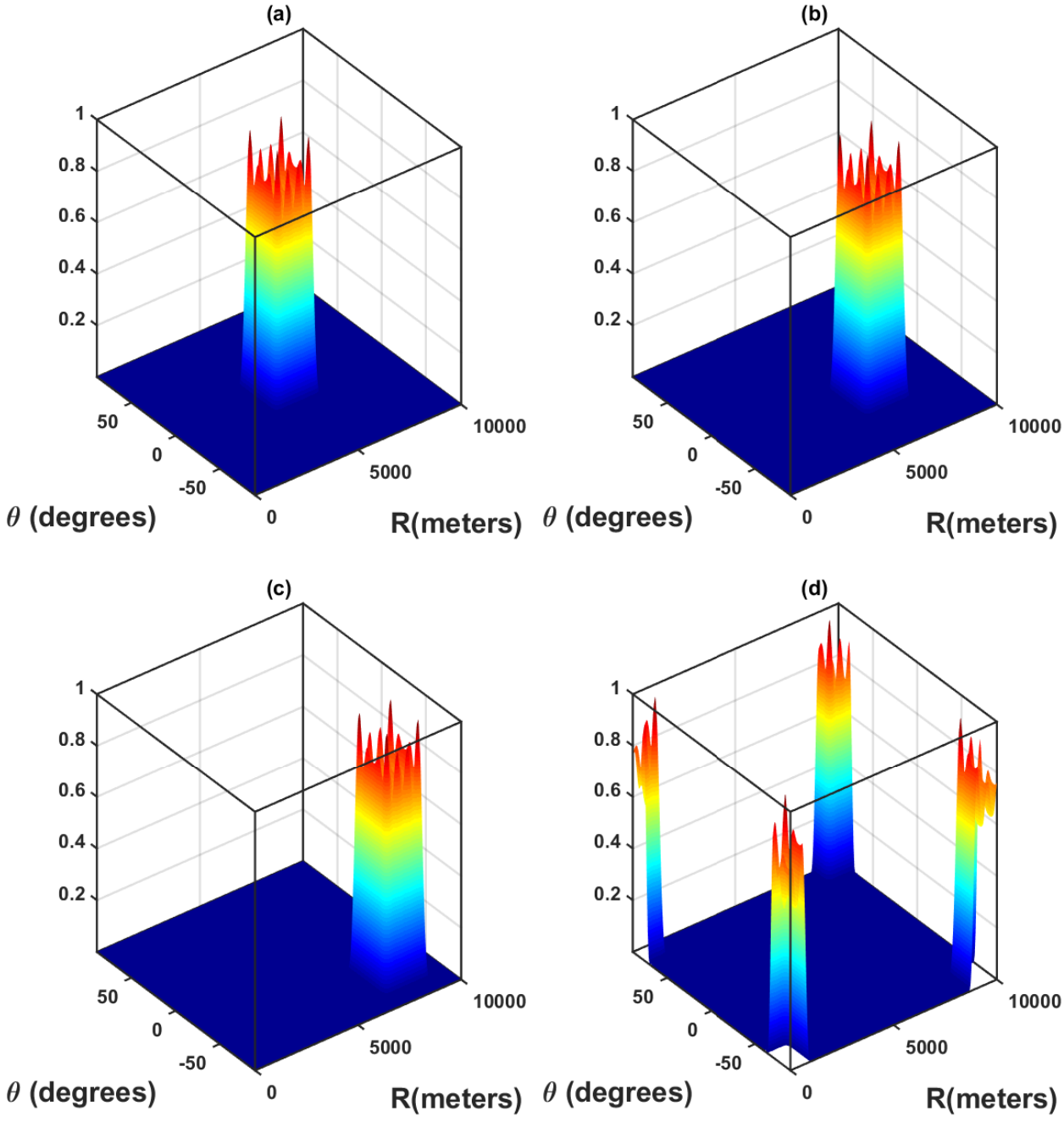

Figure 2.8: 3D view of FDA beampattern as a function of angle and range for $f_o = 30$ kHz at different time instances
(a) at $t = 0$s (b) at $t = 5\mu$s (c) at $t = 10\mu$s (d) at $t = 16\mu$s

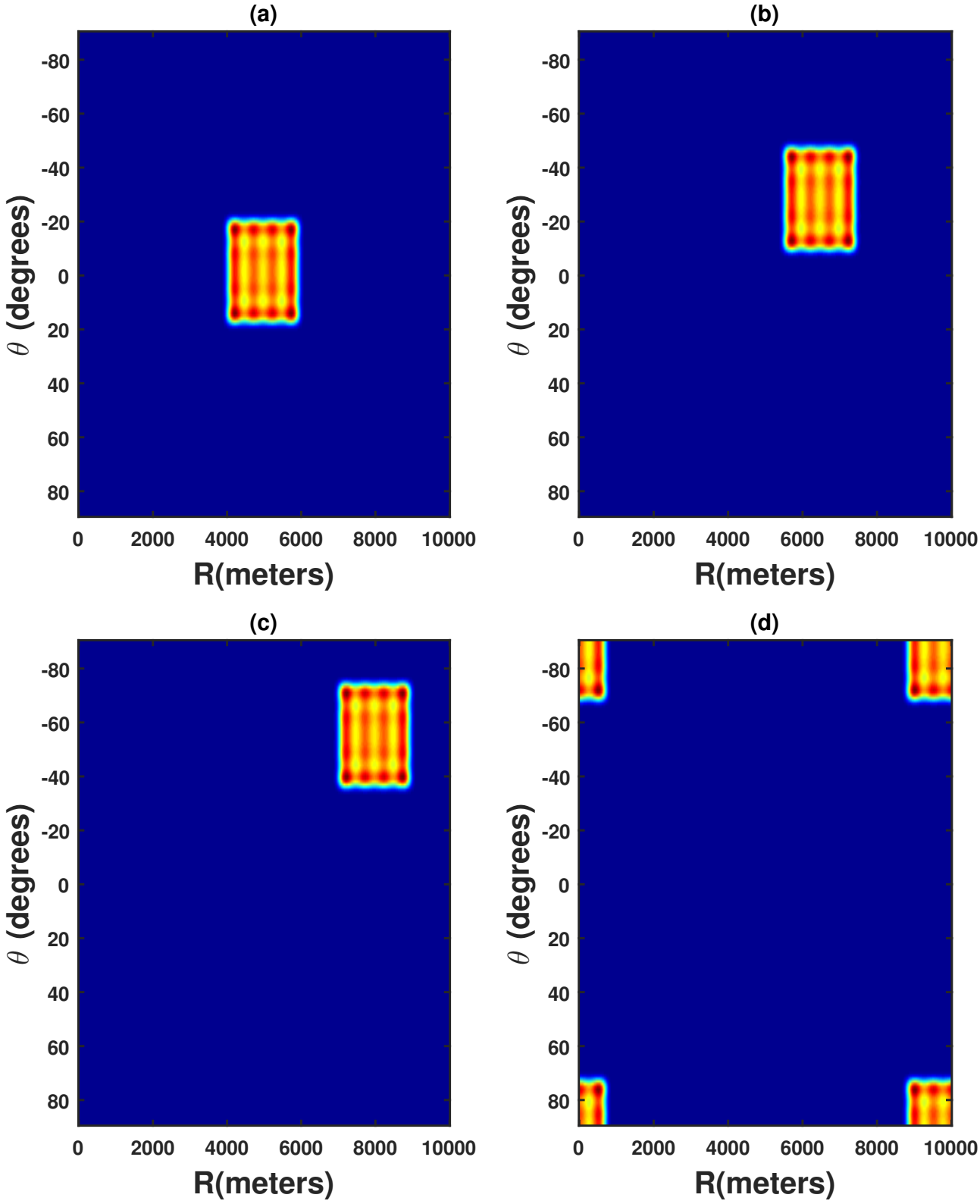

Figure 2.9: 2D view of FDA beampattern as a function of angle and range for $f_o = 30$ kHz at different time instances
(a) at $t = 0$s (b) at $t = 5\mu$s (c) at $t = 10\mu$s (d) at $t = 16\mu$s

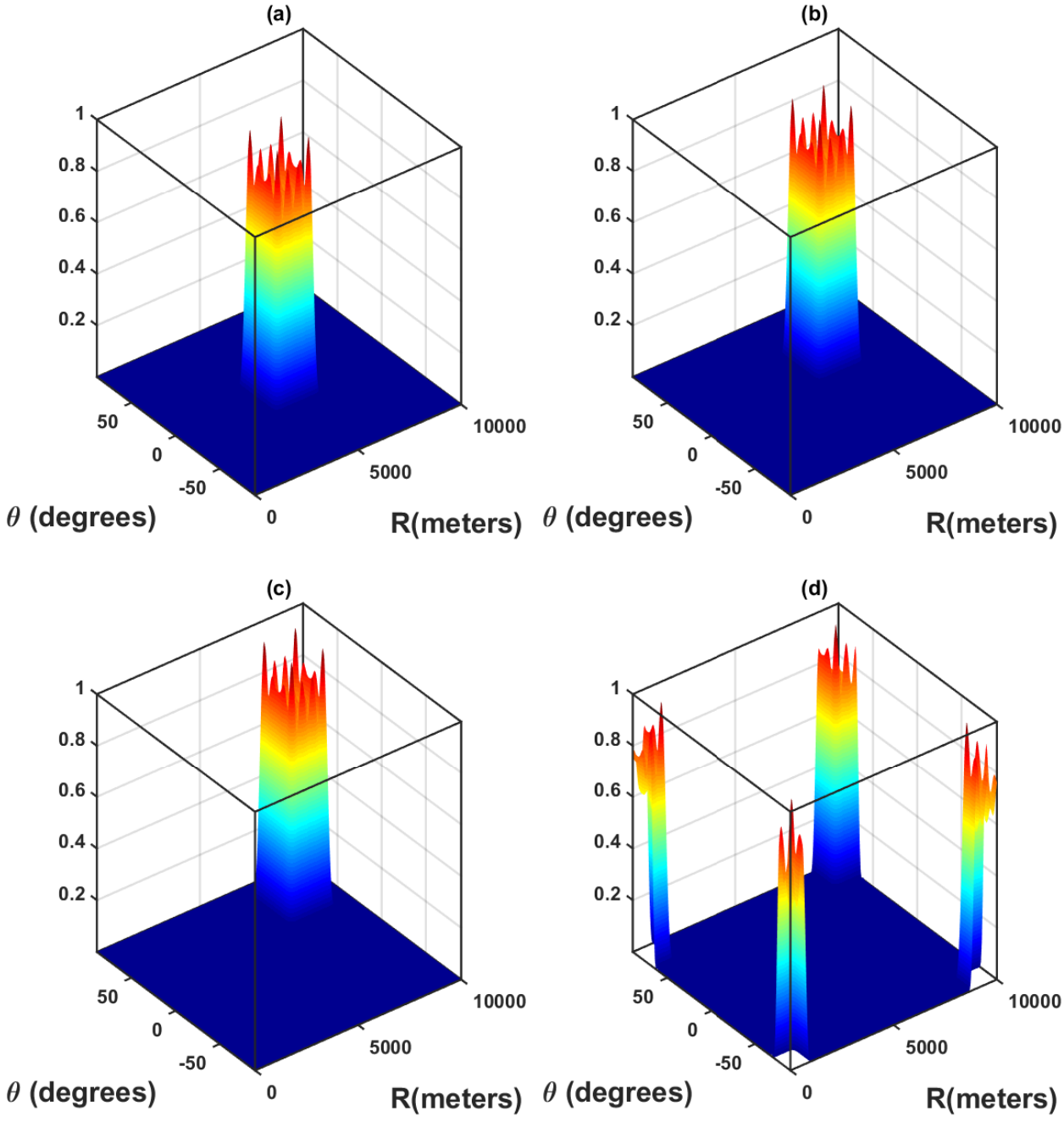

Figure 2.10: 3D view of FDA beampattern as a function of angle and range for $f_o = -30$ kHz at different time instances
(a) at $t = 0$s (b) at $t = 5\mu$s (c) at $t = 10\mu$s (d) at $t = 16\mu$s

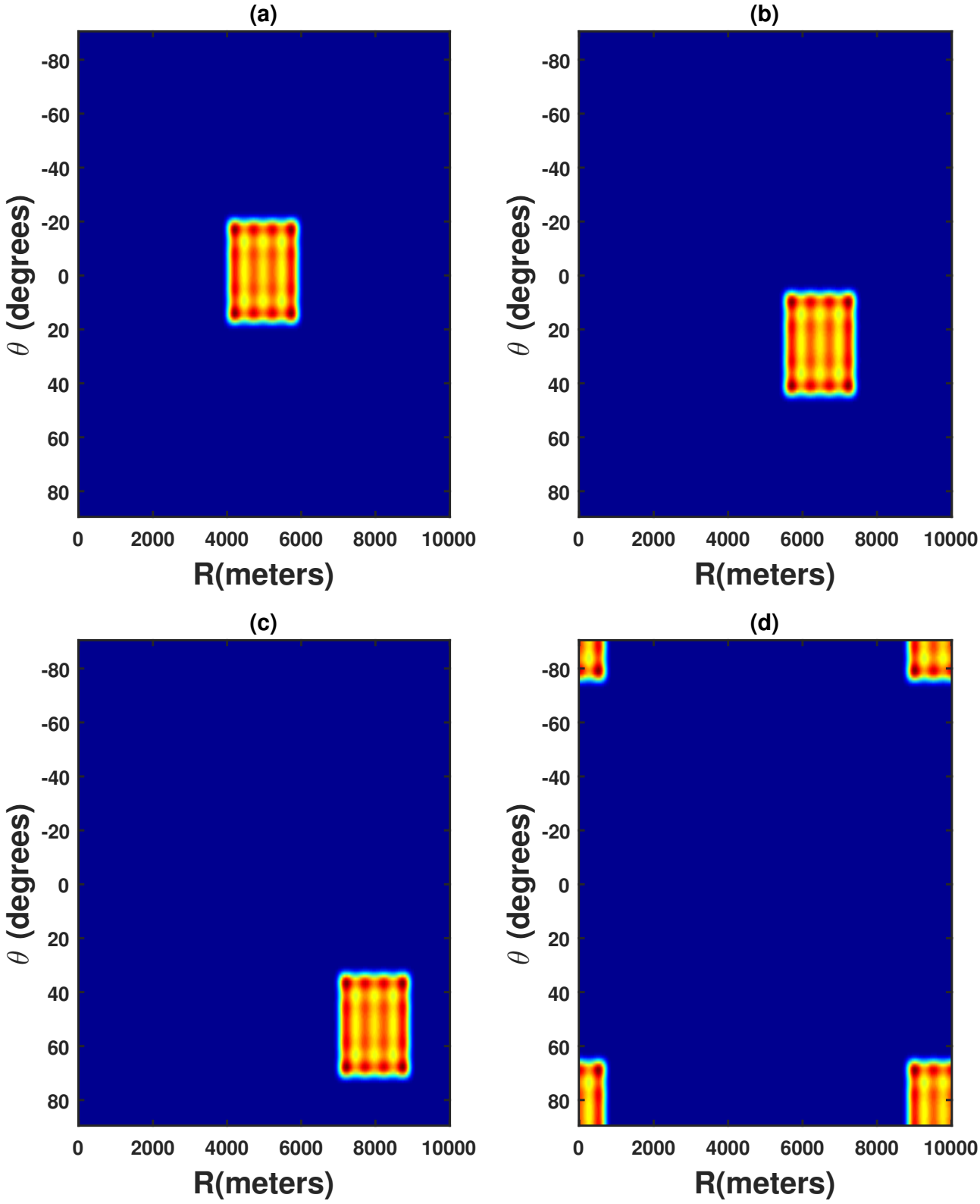

Figure 2.11: 2D view of FDA beampattern as a function of angle and range for $f_o = -30$ kHz at different time instances
(a) at $t = 0$s (b) at $t = 5\mu$s (c) at $t = 10\mu$s (d) at $t = 16\mu$s

2.4 Time-invariant transmit beampattern

The time factor in the transmit steering vector causes FDA transmit beampattern to vary over time. Therefore, we need to design weight vector in time dimension also, that is, $\mathbf{w}_t$ to have a time-invariant transmit beampattern. For $\theta = 0$ and $R = 0$, the equation of array factor becomes the function of t only.

$$\begin{aligned} \mathrm{AF}(t, R = 0, \theta = 0) = \mathrm{AF}(t) &= \sum_{m=0}^{M-1} w_m e^{-j2\pi m(f_o t)} \\ &= \mathbf{w}_t^{\mathsf{H}} \mathbf{a}_T(t) \\ &= \sum_{m=0}^{M-1} w_m e^{-j2\pi m f_o t} \end{aligned} \tag{2.4.1}$$

The time-dependent array factor is the DFT of transmit array weights.

$$\mathrm{AF}(t_d) = \mathscr{F}\{w_{t_m}\} \tag{2.4.2}$$

The weights in range dimension could be found by taking IFFT of the desired range-dependent array factor.

$$\begin{aligned} w_{t_m} &= \sum_{t=0}^{T} \mathrm{AF}(t_d) e^{j2\pi m f_o t} \\ &= \mathscr{F}^{-1}\{\mathrm{AF}(t_d)\} \end{aligned} \tag{2.4.3}$$

The transmit weight vector in time dimension is given by

$$\mathbf{w}_t = \left[w_{t_0}^*, w_{t_1}^*, \ldots, w_{t_{M-1}}^* \right]^{\mathsf{T}}. \tag{2.4.4}$$

The transmit steering vector is given by 2.1.5, therefore the transmit weight vector is therefore designed as given by

$$\mathbf{w} = \mathbf{w}_t \odot \mathbf{w}_\theta \odot \mathbf{w}_R. \tag{2.4.5}$$

The designed transmit beampattern is given by 2.3.5. A time-invariant transmit beampattern is designed for desired direction $\theta_d \in [-20^o, 20^o]$ and desired range $R_d \in [4 \text{ km}, 6 \text{ km}]$ for $f_o = 30$ kHz. The 3D and 2D view of FDA transmit beampattern as a function of angle and time are shown in Fig. 2.12(a) and 2.13(a) respectively . It can be seen from the angle time plot that the transmit beampattern illuminate the desired angular direction $\theta_d \in [-20^o, 20^o]$ for all time instants. The 3D and 2D view of FDA transmit beampattern as a function of range and time are shown in Fig. 2.12(c) and 2.13(c) respectively. It can be seen from the range time plot that the transmit beampattern illuminate the desired range region $R_d \in [4 \text{ km}, 6 \text{ km}]$ for all time instants. The 3D and 2D views of the corresponding range-angle plots are shown in Fig. 2.14(a) and 2.15(a), respectively.

For illuminating two targets present in two different angular directions and at same range, the transmit beampattern is designed for desired direction $\theta_d \in [-40^o, -20^o] \cup [20^o, 40^o]$ and desired range $R_d \in [4 \text{ km}, 6 \text{ km}]$ for $f_o = 30$ kHz. The 3D and 2D view of FDA transmit beampattern as a function of angle and time are shown in Fig. 2.12(b) and 2.13(b) respectively . It can be seen from the angle time plot that the transmit beampattern illuminate the desired angular direction $\theta_d \in [-40^o, -20^o] \cup [20^o, 40^o]$ for all time instants. The 3D and 2D view of FDA transmit beampattern as a function of range and time is shown in Fig. 2.12(c) and 2.13(c) respectively . It can be seen from the range time plot that the transmit beampattern illuminate the desired range region $R_d \in [4 \text{ km}, 6 \text{ km}]$ for all time instants. The 3D and 2D views of the corresponding range-angle plots are shown in Fig. 2.14(b) and 2.15(b), respectively.

For illuminating two targets present in same angular direction and two different range regions, the transmit beampattern is designed for desired direction $\theta_d \in [-20^o, 20^o]$ and desired range $R_d \in [3 \text{ km}, 4 \text{ km}] \cup [6 \text{ km}, 7 \text{ km}]$ for $f_o = 30$ kHz. The 3D and 2D view of FDA transmit beampattern as a function of angle and time is shown in Fig. 2.12(a) and 2.13(a) respectively . It can be seen from the angle time plot that the transmit beampattern illuminate the desired angular direction $\theta_d \in [-20^o, 20^o]$ for all time instants. The 3D and 2D view of FDA transmit beampattern as a function of range and time is shown in Fig. 2.12(d)

and 2.13(d) respectively . It can be seen from the range time plot that the transmit beampattern illuminate the desired range region $R_d \in [3 \text{ km}, 4 \text{ km}] \cup [6 \text{ km}, 7 \text{ km}]$ for all time instants. The 3D and 2D views of the corresponding range-angle plots are shown in Fig. 2.14(c) and 2.15(c), respectively.

For illuminating two targets present in different angular directions and two different range regions, the transmit beampattern is designed for desired direction $\theta_d \in [-40^o, -20^o] \cup [20^o, 40^o]$ and desired range $R_d \in [3 \text{ km}, 4 \text{ km}] \cup [6 \text{ km}, 7 \text{ km}]$ for $f_o = 30$ kHz. The 3D and 2D view of FDA transmit beampattern as a function of angle and time is shown in Fig. 2.12(b) and 2.13(b) respectively . It can be seen from the angle time plot that the transmit beampattern illuminate the desired angular direction $\theta_d \in [-40^o, -20^o] \cup [20^o, 40^o]$ for all time instants. The 3D and 2D view of FDA transmit beampattern as a function of range and time is shown in Fig. 2.12(d) and 2.13(d) respectively . It can be seen from the range time plot that the transmit beampattern illuminate the desired range region $R_d \in [3 \text{ km}, 4 \text{ km}] \cup [6 \text{ km}, 7 \text{ km}]$ for all time instants. The 3D and 2D views of the corresponding range-angle plots are shown in Fig. 2.14(d) and 2.15(d), respectively.

2.5 Conclusion

In this chapter, a time invariant 2D transmit beampattern is designed by designing weights applied at transmit antenna elements. It is concluded that the transmit antenna element weights designed for FDA radar using IFFT algorithm has the capability of illuminating the targets present in multiple directions and ranges. The designed beampattern has a much larger dwell time and it is capable of locating targets present in multiple spatial locations. Therefore, the designed transmit beampattern is very efficient in target localization. For performance evaluation of the designed beampattern, the target parameter estimation is done. For target parameter estimation, the FDA received signal model is derived in the next chapter.

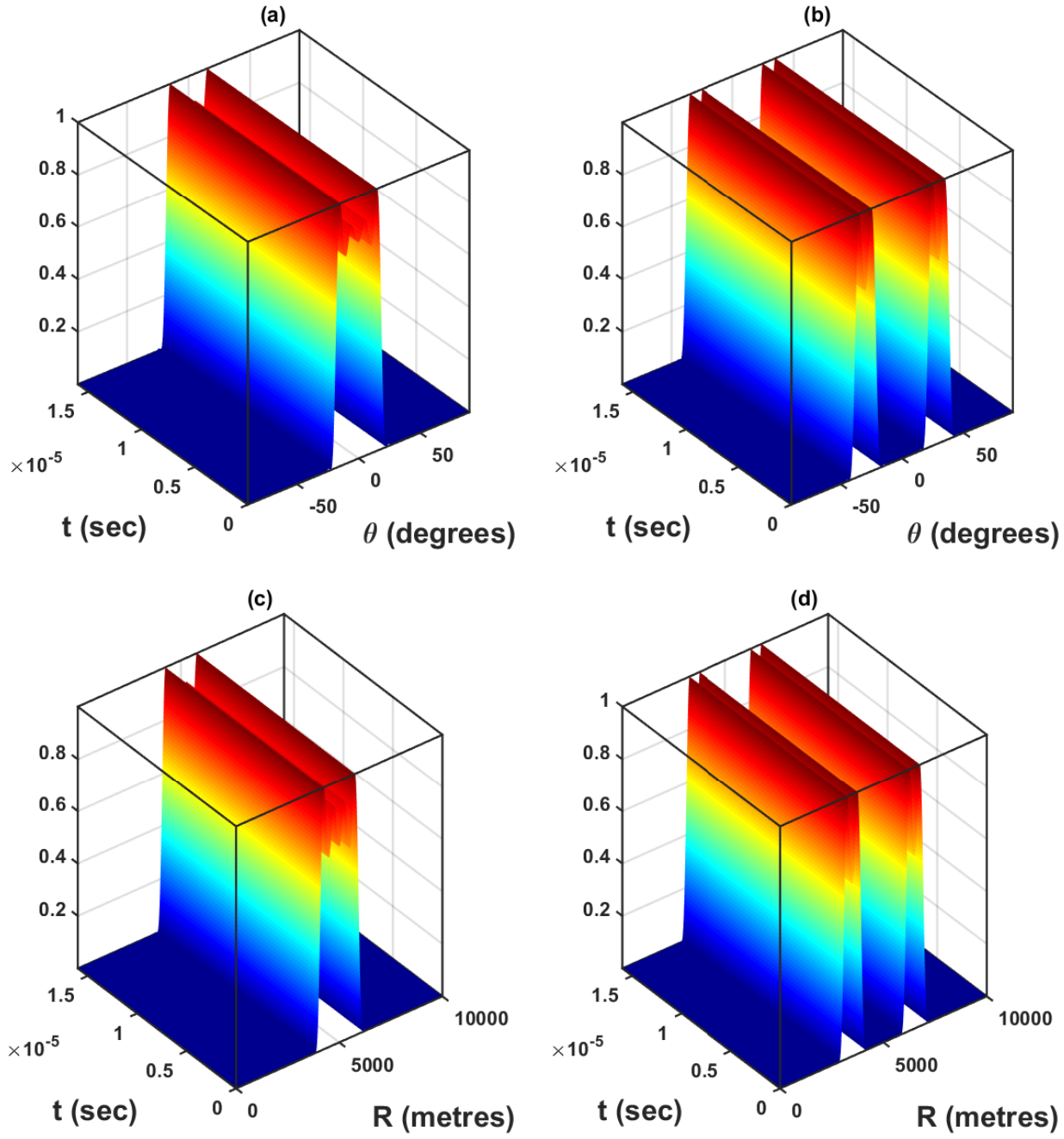

Figure 2.12: 3D view of FDA beampattern
(a) as a function of angle and time for $\theta_d \in [-20^o, 20^o]$
(b) as a function of angle and time for $\theta_d \in [-40^o, -20^o] \cup [20^o, 40^o]$
(c) as a function of range and time for $R_d \in [4 \text{ km}, 6 \text{ km}]$
(d) as a function of range and time for $R_d \in [3 \text{ km}, 4 \text{ km}] \cup [6 \text{ km}, 7 \text{ km}]$

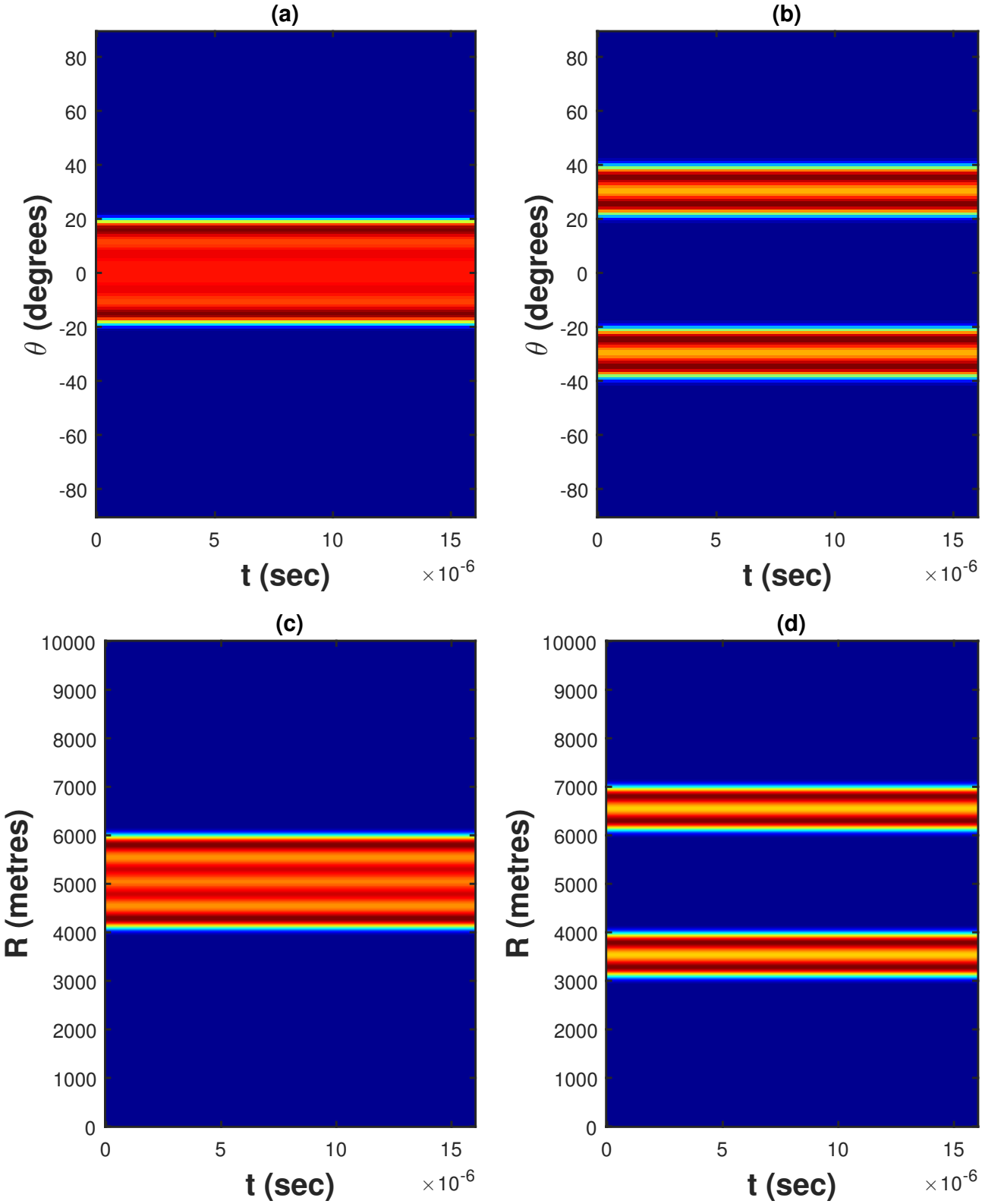

Figure 2.13: 2D view of FDA beampattern
(a) as a function of angle and time for $\theta_d \in [-20^o, 20^o]$
(b) as a function of angle and time for $\theta_d \in [-40^o, -20^o] \cup [20^o, 40^o]$
(c) as a function of range and time for $R_d \in [4 \text{ km}, 6 \text{ km}]$
(d) as a function of range and time for $R_d \in [3 \text{ km}, 4 \text{ km}] \cup [6 \text{ km}, 7 \text{ km}]$

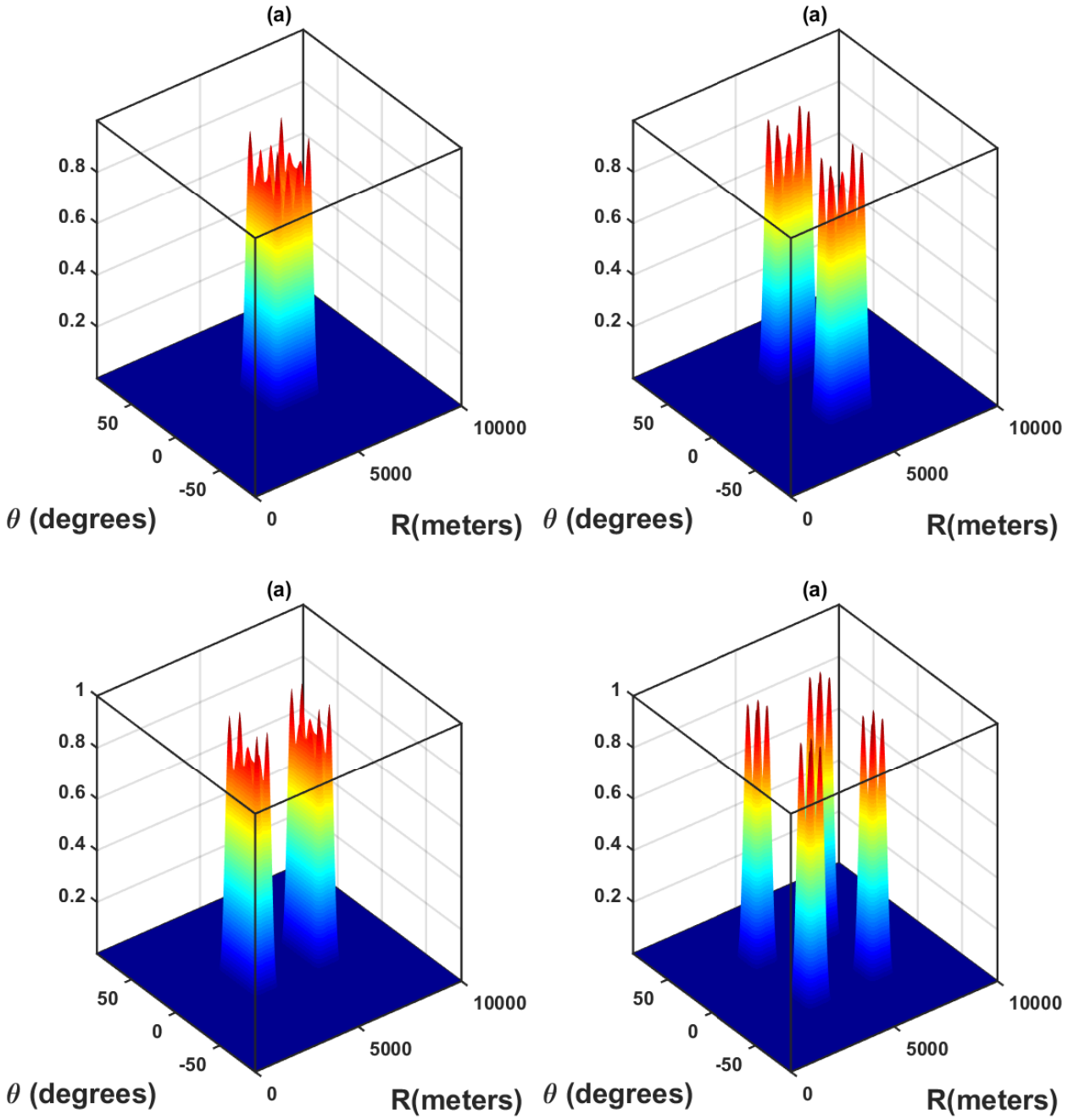

Figure 2.14: 3D view of FDA beampattern as a function of range and angle for
(a) $\theta_d \in [-20^o, 20^o]$ and $R_d \in [4 \text{ km}, 6 \text{ km}]$
(b) $\theta_d \in [-40^o, -20^o] \cup [20^o, 40^o]$ and $R_d \in [4 \text{ km}, 6 \text{ km}]$
(c) $\theta_d \in [-20^o, 20^o]$ and $R_d \in [3 \text{ km}, 4 \text{ km}] \cup [6 \text{ km}, 7 \text{ km}]$
(d) $\theta_d \in [-40^o, -20^o] \cup [20^o, 40^o]$ and $R_d \in [3 \text{ km}, 4 \text{ km}] \cup [6 \text{ km}, 7 \text{ km}]$

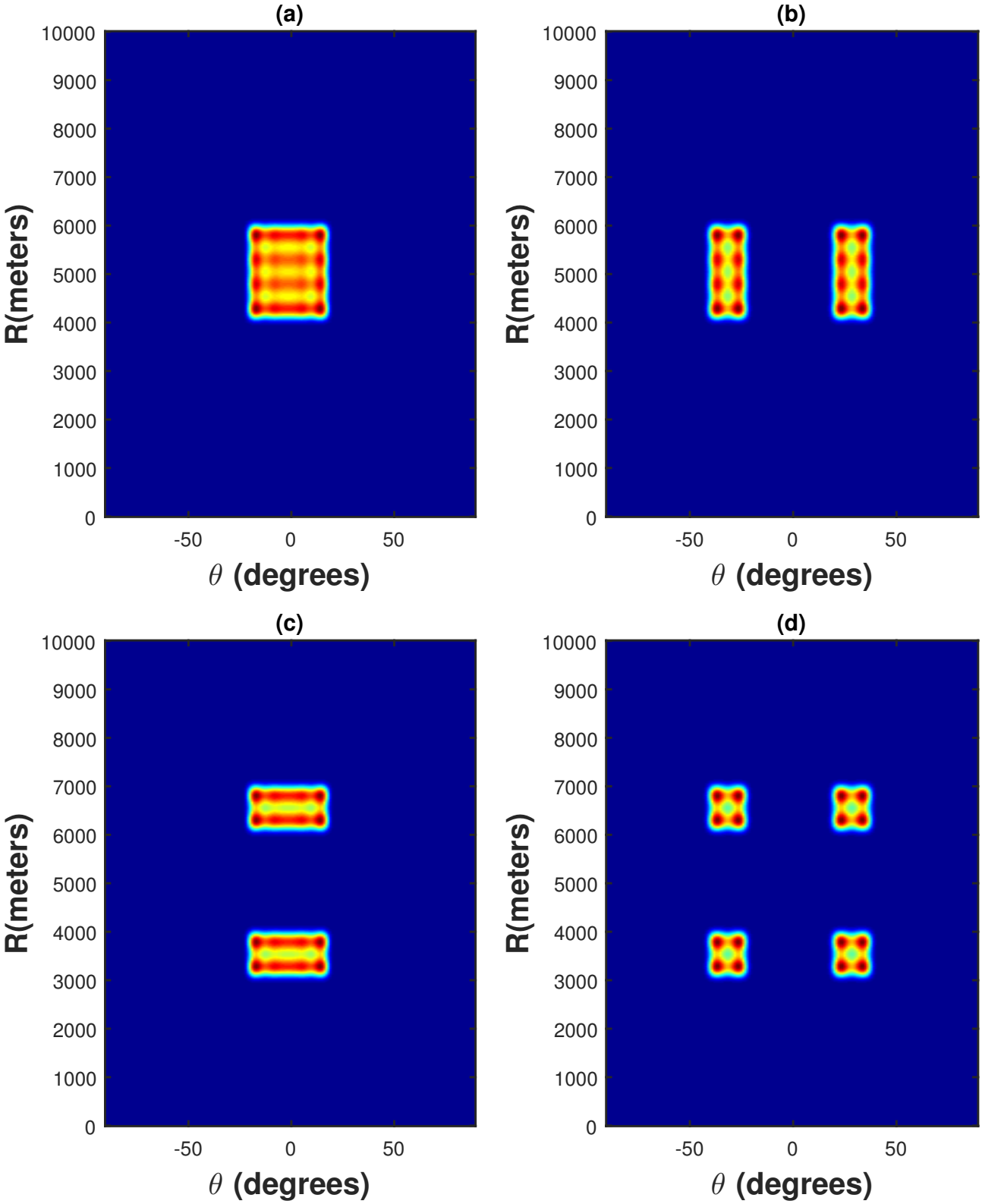

Figure 2.15: 2D view of FDA beampattern as a function of range and angle for
(a) $\theta_d \in [-20^o, 20^o]$ and $R_d \in [4 \text{ km}, 6 \text{ km}]$
(b) $\theta_d \in [-40^o, -20^o] \cup [20^o, 40^o]$ and $R_d \in [4 \text{ km}, 6 \text{ km}]$
(c) $\theta_d \in [-20^o, 20^o]$ and $R_d \in [3 \text{ km}, 4 \text{ km}] \cup [6 \text{ km}, 7 \text{ km}]$
(d) $\theta_d \in [-40^o, -20^o] \cup [20^o, 40^o]$ and $R_d \in [3 \text{ km}, 4 \text{ km}] \cup [6 \text{ km}, 7 \text{ km}]$

Chapter 3

Signal Model

3.1 Received Signal Model

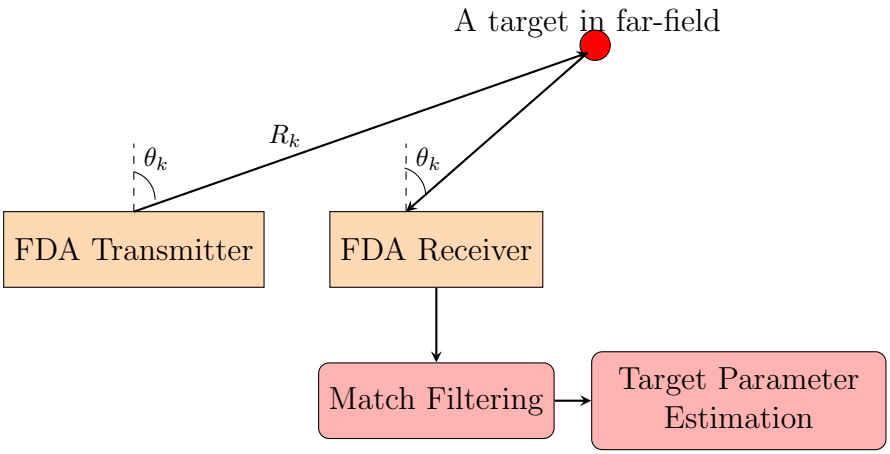

Figure 3.1: Block diagram of FDA radar.

FDA employs small frequency increment f_o along with carrier frequency f_c, which makes the transmit steering vector both angle and range dependent. In order to have a range dependent received steering vector, a frequency diverse array is also employed at the receiver as shown in Fig. 3.1. The FDA transmitter consists of a ULA of M transmit antenna elements and the FDA receiver consists of a ULA of N receiving antenna elements. The vector form of the received signal at the target is obtained from (2.1.4) as given by

$$p(t) = e^{j2\pi f_c \frac{R_k}{c}} \mathbf{a}_T^{\mathsf{T}}(\theta_k, R_k)\mathbf{s}(t) \tag{3.1.1}$$

where $\mathbf{s}(t)$ is the baseband signal vector defined by

$$\mathbf{s}(t) = \Big[s_o(t), s_1(t), \ldots, s_{M-1}(t)\Big]^{\mathsf{T}} = \Big[w_o e^{-j2\pi f_c t}, w_1 e^{-j2\pi f_c t}, \ldots, w_{M-1} e^{-j2\pi f_c t}\Big]^{\mathsf{T}}. \tag{3.1.2}$$

3.1.1 FDA Received Signal with non-zero frequency increment

We have N frequency diverse array receiving antennas each operating at $f_c + nf_o$ frequencies. The phase of signal received at antenna 0 is; $\psi_0 = \frac{2\pi f_c R_k}{c}$
for antenna 1 ; $\psi_1 = \frac{2\pi(f_c+f_o)(R_k - d\sin(\theta_k))}{c}$
$\vdots$
for antenna N-1 ; $\psi_{N-1} = \frac{2\pi(f_c+(N-1)f_o)(R_k-(N-1)d\sin(\theta_k))}{c}$

Taking antenna element 0 as a reference; there is no phase difference among signals arriving at element zero.

$$\Delta\psi_0 = 0 \tag{3.1.3}$$

The phase difference among signals arriving at element zero and element one results in;

$$\begin{aligned}
\Delta\psi_1 &= \psi_1 - \psi_0 \\
&= \frac{2\pi f_o R_k}{c} - \frac{2\pi f_o d\sin(\theta_k)}{c} - \frac{2\pi f_c d\sin(\theta_k)}{c} \\
&\approxeq \frac{2\pi f_o R_k}{c} - \frac{2\pi f_c d\sin(\theta_k)}{c} \\
&\approxeq \frac{2\pi f_o R_k}{c} - \frac{2\pi\sin(\theta_k)}{2}
\end{aligned} \tag{3.1.4}$$

The phase difference among signals arriving at element zero and element N-1 results in;

$$\begin{aligned}
\Delta\psi_{N-1} &= \psi_{N-1} - \psi_0 \\
&= \frac{2\pi(N-1)f_o R}{c} - \frac{2\pi(N-1)^2 f_o d\sin(\theta_k)}{c} - \frac{2\pi(N-1)f_c d\sin(\theta_k)}{c}
\end{aligned}$$

$$\begin{aligned} &\approxeq \frac{2\pi(N-1)f_o R_k}{c} - \frac{2\pi(N-1)f_c d\sin(\theta_k)}{c} \\ &\approxeq \frac{2\pi(N-1)f_o R_k}{c} - \frac{2\pi(N-1)\sin(\theta_k)}{2} \end{aligned} \tag{3.1.5}$$

Therefore, the receive steering vector is given by

$$\mathbf{a}_R(\theta_k, R_k)\begin{bmatrix} e^{j\Delta\psi_0} \\ e^{j\Delta\psi_1} \\ .... \\ e^{j\Delta\psi_{N-1}} \end{bmatrix} = \begin{bmatrix} 1 \\ e^{j(\frac{2\pi f_o R_k}{c} - \frac{2\pi\sin(\theta_k)}{2})} \\ ... \\ e^{j(\frac{2\pi(N-1)f_o R_k}{c} - \frac{2\pi(N-1)\sin(\theta_k)}{2})} \end{bmatrix} \in \mathbb{C}^{N\times 1} \tag{3.1.6}$$

For $t \geq \frac{2R_k}{c}$, a complete snapshot of the target reaches the receiving antennas that is assumed to be corrupted with additive white Gaussian noise (AWGN). The received signal at N receiving antenna elements in vector form is given by

$$\mathbf{r}(t) = e^{\frac{j2\pi f_c R_k}{c}}\mathbf{a}_R(\theta_k, R_k)\mathbf{a}_T^{\mathsf{T}}(\theta_k, R_k)\mathbf{s}(t) + \mathbf{z}(t) \in \mathbb{C}^{N\times 1} \qquad \text{for } t \geq \frac{2R_k}{c} \tag{3.1.7}$$

where $\mathbf{a}_R(\theta_k, R_k) = \mathbf{a}_R(\theta_k) \odot \mathbf{a}_R(R_k)$, $\mathbf{a}_R(\theta_k) = \left[1, e^{-j\pi\sin(\theta_k)}, \ldots, e^{-j\pi(N-1)\sin(\theta_k)}\right]$, $\mathbf{a}_R(R_k) = \left[1, e^{j\frac{2\pi f_o R_k}{c}}, \ldots, e^{j\frac{2\pi(N-1)f_o R_k}{c}}\right]$ and $\mathbf{z}(t) = \left[z_o(t), z_1(t), \ldots, z_{N-1}(t)\right]^{\mathsf{T}}$ is the noise vector. We have assumed $\mathbf{z}(t)$ as uncorrelated noise with zero mean and covariance matrix as; $\mathbf{R}_z = \mathbb{E}[\mathbf{z}\mathbf{z}^{\mathsf{H}}] = \sigma_z^2\mathbb{I}_N$.

To get the baseband signal, match filtering is done at receiver. The output of matched filters denoted by $\mathbf{X}$ is obtained as follows

$$\begin{aligned} \mathbf{X} &= \int_0^T \mathbf{r}(t)\mathbf{s}^{\mathsf{H}}(t)dt \\ &= e^{\frac{j2\pi f_c R_k}{c}}\mathbf{a}_R(\theta_k, R_k)\mathbf{a}_T^{\mathsf{T}}(\theta_k, R_k)\int_0^T \mathbf{s}(t)\mathbf{s}^{\mathsf{H}}(t)dt + \int_0^T \mathbf{z}(t)\mathbf{s}^{\mathsf{H}}(t)dt. \end{aligned} \tag{3.1.8}$$

The result of the involved integration in (3.1.8) is given by

$$\begin{aligned}\int_0^T \mathbf{s}(t)\mathbf{s}^{\mathsf{H}}(t)dt &= \begin{bmatrix} |w_0|^2 & w_0w_1^* & \dots & w_0w_{M-1}^* \\ w_1w_0^* & |w_1|^2 & \dots & w_1w_{M-1}^* \\ \vdots & \ddots & & \vdots \\ w_{M-1}w_0^* & w_{M-1}w_1^* & \dots & |w_{M-1}|^2 \end{bmatrix} \\ &= \mathbf{w}\mathbf{w}^{\mathsf{H}}. \end{aligned} \tag{3.1.9}$$

where $\mathbf{w} = \Big[w_0, w_1, \dots, w_{M-1}\Big]^{\mathsf{T}}$ is the transmit weight vector. The received signal matrix after substituting the results of (3.1.9) in (3.1.8), we get

$$\mathbf{X} = e^{\frac{j2\pi f_c R_k}{c}} \mathbf{a}_R(\theta_k, R_k)\mathbf{a}_T^{\mathsf{T}}(\theta_k, R_k)\mathbf{w}\mathbf{w}^{\mathsf{H}} + \mathbf{Z}' \tag{3.1.10}$$

where $\mathbf{Z}' = \int_0^T \mathbf{z}(t)\mathbf{s}^{\mathsf{H}}(t)dt$. Therefore, the output of the $N \times M$ matched filter is given by

$$\mathbf{X} = e^{\frac{j2\pi f_c R_k}{c}} \mathbf{a}_R(\theta_k, R_k)\mathbf{a}_T^{\mathsf{T}}(\theta_k, R_k)\mathbf{W} + \mathbf{Z}' \tag{3.1.11}$$

where we have defined $\mathbf{W} = \mathbf{w}\mathbf{w}^{\mathsf{H}}$. After applying vec$\{\cdot\}$ operator in order to stack $N \times M$ received signal data into $NM \times 1$ received signal vector data, the lth snapshot of received signal is

$$\begin{aligned}\mathbf{y}(l) &= e^{\frac{j2\pi f_c R_k}{c}} [\mathbf{W}^{\mathsf{T}} \otimes \mathbf{a}_R(\theta_k, R_k)]\mathbf{a}_T(\theta_k, R_k) + \mathbf{v} \\ &= \beta \mathbf{b}(\theta_k, R_k) + \mathbf{v}, \qquad\qquad l = 0, 1, \dots, L-1, \end{aligned} \tag{3.1.12}$$

where $\beta = e^{\frac{j2\pi f_c R_k}{c}}$, $\mathbf{b}(\theta_k, R_k) = [\mathbf{W}^{\mathsf{T}} \otimes \mathbf{a}_R(\theta_k, R_k)]\mathbf{a}_T(\theta_k, R_k)$. The complete model of the received signal, including all L snapshots of the target, is given by

$$\mathbf{Y} = \Big[\mathbf{y}(0), \mathbf{y}(1), \dots, \mathbf{y}(L-1)\Big] \in \mathbb{C}^{NM \times L}. \tag{3.1.13}$$

The received signal obtained in (3.1.12) depends on angle as well as range of the target. Therefore, the angle and the range of the target can be determined. Since the received signal is coupled in both angle and range, therefore they both cannot be jointly estimated. First, we need to have an estimate of angle in order

to estimate the range or vice versa. To independently estimate the angle of the target, the FDA signal model is assumed with zero frequency increment.

3.1.2 FDA Received Signal with zero frequency increment

The FDA received signal with zero frequency increment is independent of range. The vector form of received signal at N receiving antenna elements obtained from (3.1.7) is modified for $f_o = 0$ as given by

$$\mathbf{r}(t) = e^{\frac{j2\pi f_c R_k}{c}} \mathbf{a}_R(\theta_k)\mathbf{a}_T^{\mathsf{T}}(\theta_k)\mathbf{s}(t) + \mathbf{z}(t) \in \mathbb{C}^{N\times 1} \qquad \text{for } t \geq \frac{2R_k}{c} \tag{3.1.14}$$

After demodulation of baseband signal by match filtering at the receiver, the output of the $N \times M$ matched filters is obtained as

$$\mathbf{X} = e^{\frac{j2\pi f_c R_k}{c}} \mathbf{a}_R(\theta_k)\mathbf{a}_T^{\mathsf{T}}(\theta_k)\mathbf{W} + \mathbf{Z}^{'}, \tag{3.1.15}$$

After applying vec$\{\cdot\}$ operator in order to stack $N \times M$ received signal data into $NM \times 1$ received signal vector data, the lth snapshot of received signal is

$$\begin{aligned} \mathbf{y}(l) &= e^{\frac{j2\pi f_c R_k}{c}} [\mathbf{W}^{\mathsf{T}} \otimes \mathbf{a}_R(\theta_k)]\mathbf{a}_T(\theta_k) + \mathbf{v} \\ &= \beta \mathbf{b}(\theta_k) + \mathbf{v}, \qquad\qquad l = 0, 1, \ldots, L-1, \end{aligned} \tag{3.1.16}$$

where $\beta = e^{\frac{j2\pi f_c R_k}{c}}$, $\mathbf{b}(\theta_k) = [\mathbf{W}^{\mathsf{T}} \otimes \mathbf{a}_R(\theta_k)]\mathbf{a}_T(\theta_k)$ and $\mathbf{v} = \text{vec}\{\mathbf{Z}^{'}\}$. The complete model of the received signal, including all L snapshots of the target, is given by

$$\mathbf{Y} = \Big[\mathbf{y}(0), \mathbf{y}(1), \ldots, \mathbf{y}(L-1)\Big] \in \mathbb{C}^{NM\times L}. \tag{3.1.17}$$

$\mathbf{R}_y$ is the covariance matrix of received signal that is

$$\mathbf{R}_y = \frac{1}{L}\sum_{l=0}^{L-1} \mathbf{y}(l)\mathbf{y}^{\mathsf{H}}(l) = \frac{\mathbf{Y}\mathbf{Y}^{\mathsf{H}}}{L} \tag{3.1.18}$$

The received signal in now (3.1.16) is angle-dependent only, therefore the angle of the target can be independently estimated.

3.2 Selection of frequency increment

The transmit weight for for the N_{FFT}-sample points of the array factor $AF(\theta)$ and N_{FFR}-sample points of the array factor $AF(R)$ for FDA radar is given by (2.3.4).

$$w_{\theta_m} = \frac{1}{N_{\text{FFT}}} \sum_{f_\theta=-0.5}^{0.5} \text{AF}(\theta) e^{j2\pi m f_\theta}, \tag{3.2.1}$$

$$w_{R_m} = \frac{1}{N_{\text{FFR}}} \sum_{f_R=\frac{f_o R_{min}}{c}}^{\frac{f_o R_{max}}{c}} \text{AF}(R) e^{\frac{j2\pi m f_o R}{c}} \tag{3.2.2}$$

The above equation (3.2.2) shows that range-dependent weights depends only on f_o. Therefore, for designing a very focused beampattern very close to that of desired beampttern, one must carefully select the f_o. The optimal value of f_o is obtained by minimizing the error between the desired and the actual beampattern for the optimal value of f_o as given by

$$\min_{f_{o_{\text{opt}}}} \Big[\text{AF}(R_d) - \text{AF}(R)\Big]$$

$$\min_{f_{o_{\text{opt}}}} \Big[\text{AF}(R_d) - \sum_{m=0}^{M-1} w_{R_m} e^{-j2\pi m f_R}\Big] \tag{3.2.3}$$

The optimal value of f_o is given by

$$f_{o_{\text{opt}}} = \frac{c}{R_{max}}. \tag{3.2.4}$$

For illuminating a desired 2D spatial section, $\theta_d = [-20^o, 20^o]$ and $R_d = [4 \text{ km}, 6 \text{ km}]$ the optimal value of frequency increment $f_{o_{\text{opt}}}$ must be equal to 30kHz. The effect of choosing the non-optimal frequency increment is shown in Fig. 3.2 where a range-dependent beampattern is designed at $f_o = 10$kHz. The range dependent beampattern has large beamwidth and sidelobes which affects the overall designed

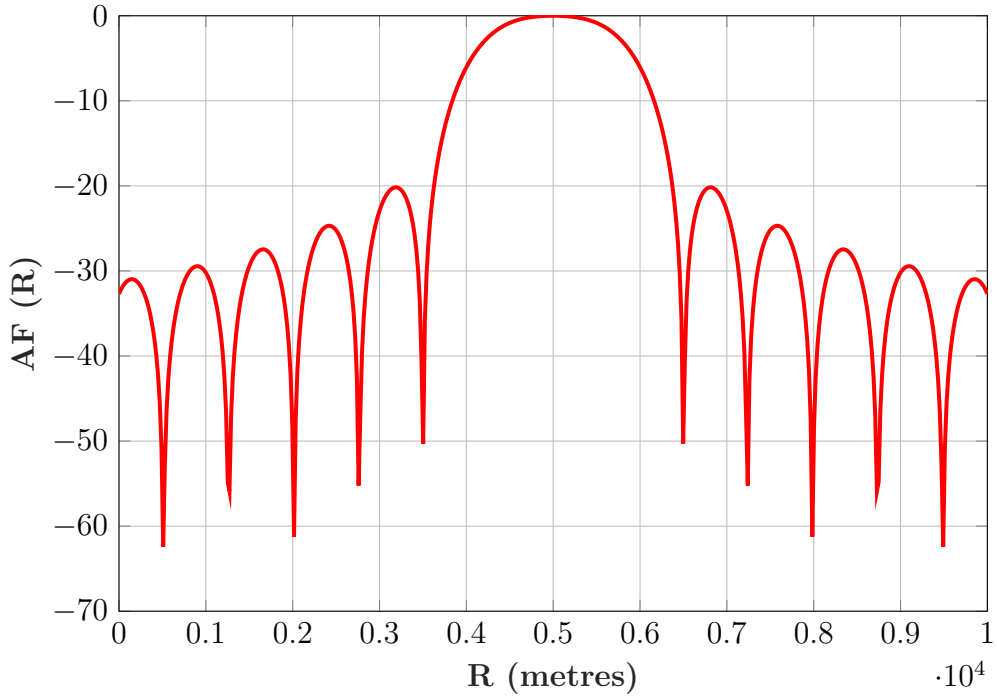

Figure 3.2: FDA range-dependent beampattern for $R_d = [4 \text{ km}, 6 \text{ km}]$ at $f_o = 10$ kHz.

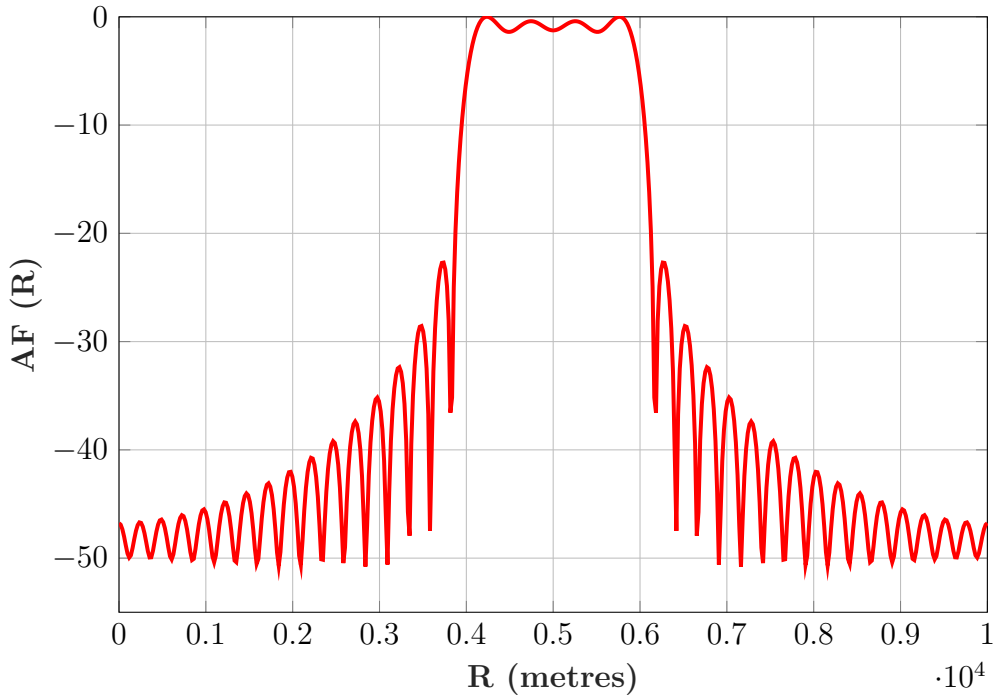

Figure 3.3: FDA range-dependent beampattern for $R_d = [4 \text{ km}, 6 \text{ km}]$ at $f_o = 30$ kHz.

FDA 2D transmit beampattern. The range-dependent beampattern designed at optimal frequency increment $f_o = 30$ kHz is shown in Fig. 3.3. A very focused main lobe beampattern with larger dwell time and smaller sidelobes is obtained for $f_o = 30$kHz as compared to that for $f_o = 10$ kHz, whereas the angle-dependent beampattern is independent of f_o therefore, the same angle-dependent beampattern is obtained for both values of f_o. Therefore, the f_o overall affects the shape of the 2D transmit beampattern hence its optimal selection is important.

Another example of designing a range-dependent beampattern for $R_d = [20 \text{ km}, 25 \text{ km}]$ is shown. The optimal value of f_o must be equal to 10kHz according to the design criteria. The comparison of beampattern designed at non-optimal frequency increment $f_o = 1$ kHz is shown in Fig. 3.4 and at optimal frequency increment $f_o = 10$ kHz is shown in Fig. 3.5. The beampattern designed at $f_o = 1$ kHz has much larger beamwidth than desired. The main lobe illuminates the range region $R_d = [15 \text{ km}, 30 \text{ km}]$ and also it has very large sidelobes as compared to that of previous example. A very focused beampattern with much reduced sidelobes is obtained for $f_o = 10$kHz, which illuminates completely the desired 2D spatial section.

FDA beampattern is range-dependent periodic with a factor of $\frac{c}{f_o}$. Choosing $f_o > \frac{c}{R}$ results in periodic range-dependent beampattern. The beampattern designed for $f_o = 20$kHz is shown in Fig. 3.6. The designed beampattern has although very reduced sidelobes as well as a very focused main lobe beampattern but it has two main lobes. Therefore the designed 2D transmit beampattern illuminates the two range regions $R_d = [5 \text{ km}, 10 \text{ km}]$ U $[20 \text{ km}, 25 \text{ km}]$.

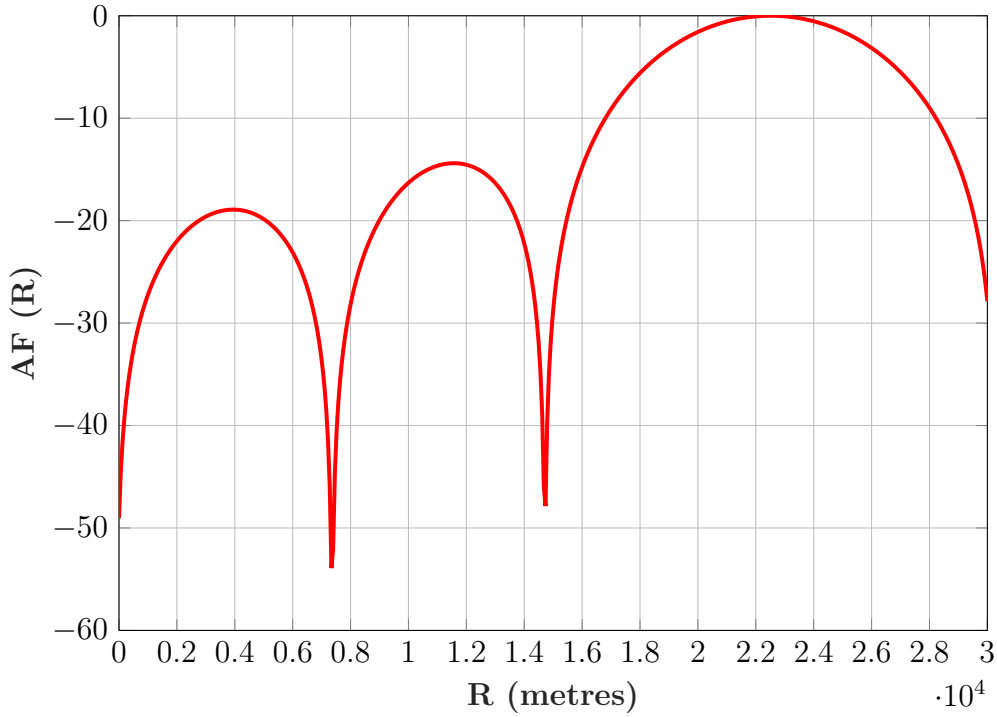

Figure 3.4: FDA range-dependent beampattern for $R_d = [20 \text{ km}, 25 \text{ km}]$ at $f_o = 1$ kHz.

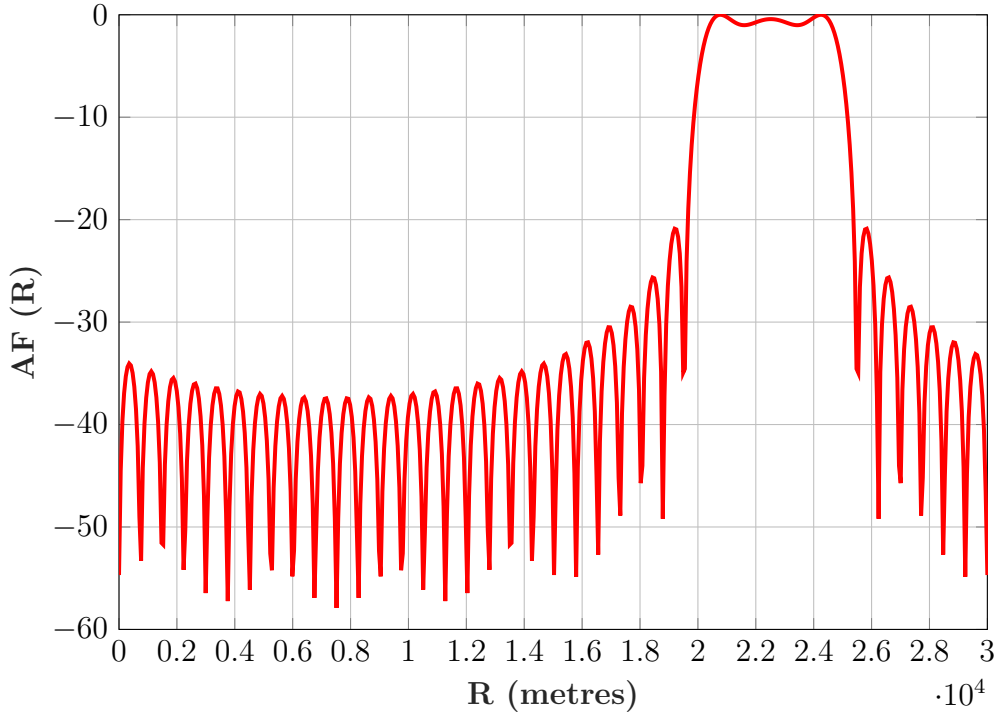

Figure 3.5: FDA range-dependent beampattern for $R_d = [20 \text{ km}, 25 \text{ km}]$ at $f_o = 10$ kHz.

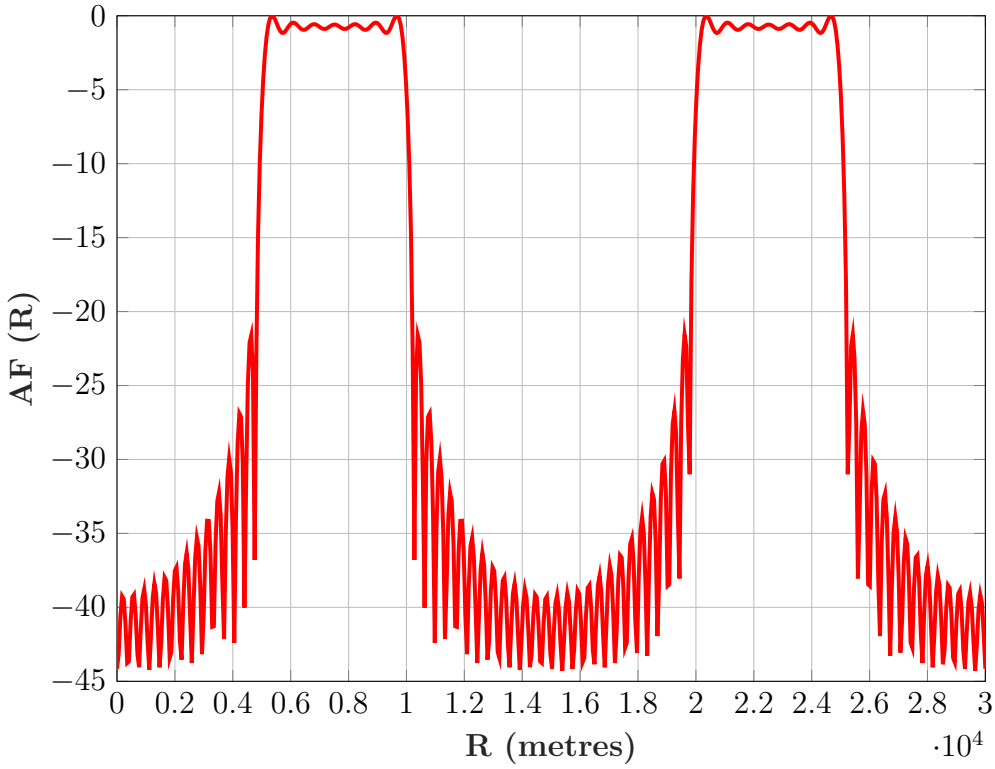

Figure 3.6: FDA range-dependent beampattern for $R_d = [20 \text{ km}, 25 \text{ km}]$ at $f_o = 20$ kHz.

3.3 Selection of Time period of pulse

The bound on choice of f_oT is already derived in [18] by determining the spatial-exploration of FDA radar. The spatial-exploration of FDA radar is given by

$$\begin{aligned} \text{SE} &= \theta_1 - \theta_0 \\ &= \sin^{-1}\left(\frac{\phi_o}{\pi}\right) - \sin^{-1}\left(-2f_oT - \frac{\phi_o}{\pi}\right). \end{aligned} \tag{3.3.1}$$

where θ_0 and θ_1 are the two consecutive zero crossings of average transmit beam-pattern of FDA radar.

$$\theta_0 = \sin^{-1}\left(-2f_oT - \frac{\phi_o}{\pi}\right) \tag{3.3.2}$$

$$\theta_1 = \sin^{-1}\left(\frac{\phi_o}{\pi}\right) \tag{3.3.3}$$

From (3.3.2) with initial phase $\phi_o = 0$, we have

$$\begin{aligned} 2\pi f_o T + 2\pi \frac{\sin(\theta)}{2} &= 0 \\ f_o T &= -\frac{\sin(\theta)}{2} \\ f_o T &\leq \pm 0.5 \end{aligned} \tag{3.3.4}$$

3.4 Bound on Transmit Array Weights

The transmit array weights is the inverse-Fourier-transform of the desired array factor. Here we determine the upper and lower bounds of the absolute value of w_m.

3.4.1 Upper bound

To derive the upper bound on the non-uniform transmit array weights, the desired angular region of illumination is $\theta_d = \theta = [-90^o, 90^o]$ and $R_d = R = [0 \text{ km}, 10 \text{ km}]$. The transmit array weights for the N_{FFT}-sample point of the array factor $AF(\theta)$ and N_{FFR}-sample point of the array factor $AF(R)$ are

$$\begin{aligned} w_{\theta_m} &= \frac{1}{N_{\text{FFT}}} \sum_{f_\theta=-0.5}^{0.5} e^{j2\pi m f_\theta} \\ w_{R_m} &= \frac{1}{N_{\text{FFR}}} \sum_{f_R=\frac{f_o R_{min}}{c}}^{\frac{f_o R_{max}}{c}} e^{j2\pi m f_R} \end{aligned} \tag{3.4.1}$$

which is evaluated to find $|w_m|$ as

$$\begin{aligned} |w_{\theta_m}| &\leq 1 \\ |w_{R_m}| &\leq 1 \end{aligned} \tag{3.4.2}$$

3.4.2 Lower bound

To derive the lower bound on the non-uniform transmit array weights, a single or more angular and range point θ_d and R_d is considered for illumination. The transmit weights in this case are given by

$$\begin{aligned} w_{\theta_m} &= \frac{1}{N_{\text{FFT}}} \sum_{f_{\theta_d}} e^{j2\pi m f_{\theta_d}} \\ w_{R_m} &= \frac{1}{N_{\text{FFR}}} \sum_{f_{R_d}} e^{j2\pi m f_{R_d}} \end{aligned} \tag{3.4.3}$$

which is evaluated to find $|w_m|$ as follows

$$\begin{aligned} |w_{\theta_m}| &\geq \frac{1}{N_{\text{FFT}}}, \\ |w_{R_m}| &\geq \frac{1}{N_{\text{FFR}}} \end{aligned} \tag{3.4.4}$$

where $f_{\theta_d} = \frac{\sin(\theta_d)}{2}$ and $f_{R_d} = \frac{f_o R_d}{c}$. Therefore, to illuminate any desired 2D section, the value of the non-uniform IFFT-based transmit array weights would always be bounded by

$$\frac{1}{N_{\text{FFT}}} \leq |w_{\theta_m}| \leq 1 \tag{3.4.5}$$

$$\frac{1}{N_{\text{FFR}}} \leq |w_{R_m}| \leq 1 \tag{3.4.6}$$

or

$$\frac{M}{N_{\text{FFT}}} \leq \sum_{m=0}^{M-1} |w_{\theta_m}| \leq M \tag{3.4.7}$$

$$\frac{M}{N_{\text{FFR}}} \leq \sum_{m=0}^{M-1} |w_{R_m}| \leq M. \tag{3.4.8}$$

For illuminating the entire 2D observation section $\theta_d = \theta = [-90^o, 90^o]$ and $R_d = R = [0 \text{ km}, 10 \text{ km}]$ for $M = 40$, $N_{\text{FFT}} = 512$ and $N_{\text{FFR}} = 1024$, the transmit weights $|w_{\theta_m}| = 1$ and $|w_{\theta_m}| = 1$ as shown in Fig. 3.7. The desired beampattern is the whole 2D observation section that forms a dc function and the IFFT of a

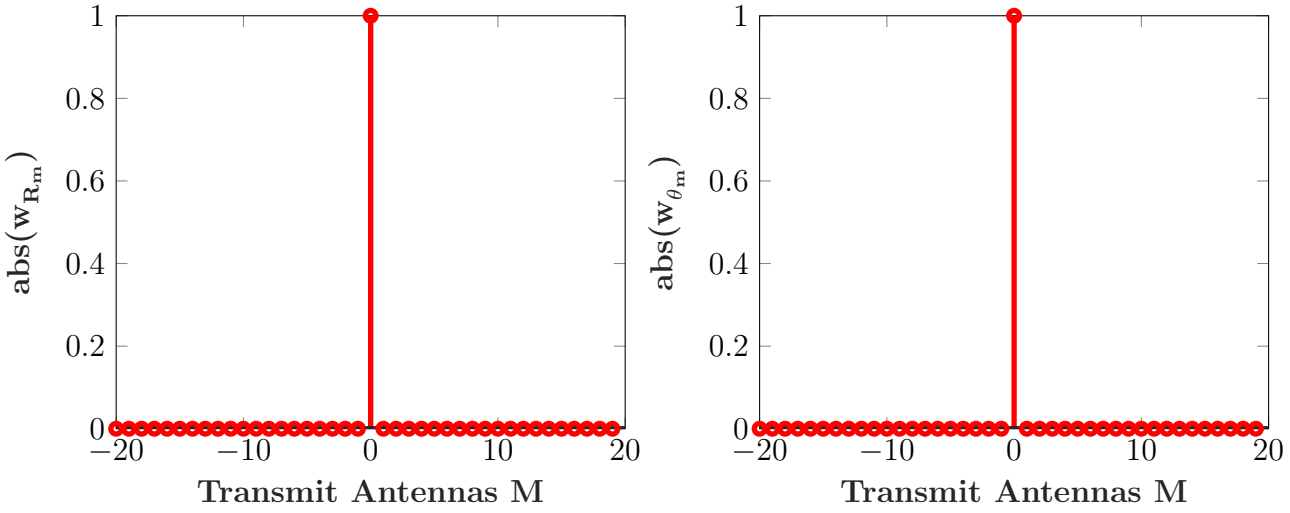

Figure 3.7: FDA transmit weights for $\theta_d = [-90^o, 90^o]$ and $R_d = [0 \text{ km}, 10 \text{ km}]$ at $f_o = 10$ kHz.

dc function is a unit sample function at zero frequency. Therefore, the absolute value of transmit weights is a unit sample at $m = 0$.

For illuminating a target located at $\theta_d = 20^o$ and $R_d = 5$km for $M = 40$, $N_{\text{FFT}} = 512$ and $N_{\text{FFR}} = 1024$, the transmit weights $|w_{\theta_m}| = 1.953 \times 10^{-3}$ and $|w_{\theta_m}| = 0.9766 \times 10^{-3}$ as shown in Fig. 3.8. The desired beampattern is a unit sample function at the angular location and the range of the target and the IFFT of a unit sample function is a constant dc function. Therefore, the absolute value of transmit weights are a constant value as it is shown in the Fig. 3.8.

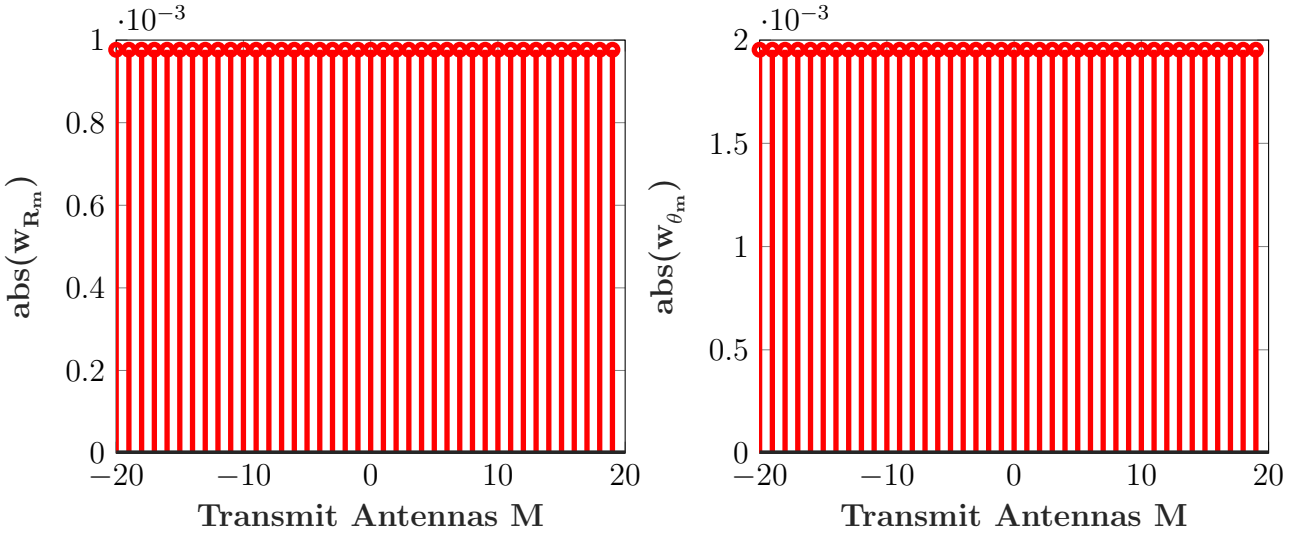

Figure 3.8: FDA transmit weights for $\theta_d = 20^o$ and $R_d = 5$km at $f_o = 10$ kHz.

For illuminating a target located at $\theta_d = [-20^o, 20^o]$ and $R_d = [4\text{ km}, 6\text{ km}]$ for $M = 40$, $N_{\text{FFT}} = 512$ and $N_{\text{FFR}} = 1024$, the transmit weights $|w_{\theta_m}| < 1$ and $|w_{\theta_m}| =< 1$ as shown in Fig. 3.9. The desired beampattern is a rectangular function in this case and the IFFT of a rectangular function is a sinc function. Therefore, the absolute value of transmit weights obtained forms a sinc shape.

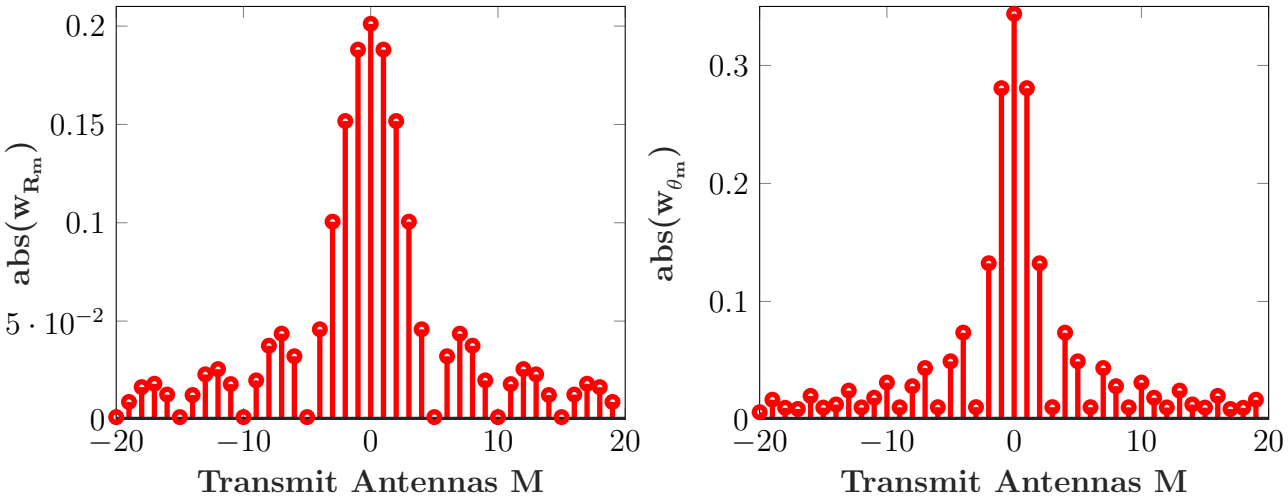

Figure 3.9: FDA transmit weights for $\theta_d = [-20^o, 20^o]$ and $R_d = [4\text{ km}, 6\text{ km}]$ at $f_o = 10$ kHz.

3.5 Selection of Number of Transmit Antenna Elements

The transmit beampattern is designed by properly designing the transmit antenna element weights. A more focused large dwell time pattern with reduced sidelobes could be obtained only for large number of M. The angle and range-dependent transmit beampattern designed for desired region $\theta_d = [-20^o, 20^o]$ and $R_d = [4\text{ km}, 6\text{ km}]$ is shown for different values of M as shown in Fig. 3.10 and 3.11 respectively. The dwell time of designed angle and range-dependent transmit beampattern is very small for $M = 5$, whereas as value of M increases the dwell time of transmit beampattern increases as it is evident from figures. The dwell time is very large for $M = 40$ and the shape of designed transmit beampattern gets very closer to that of desired beampattern.

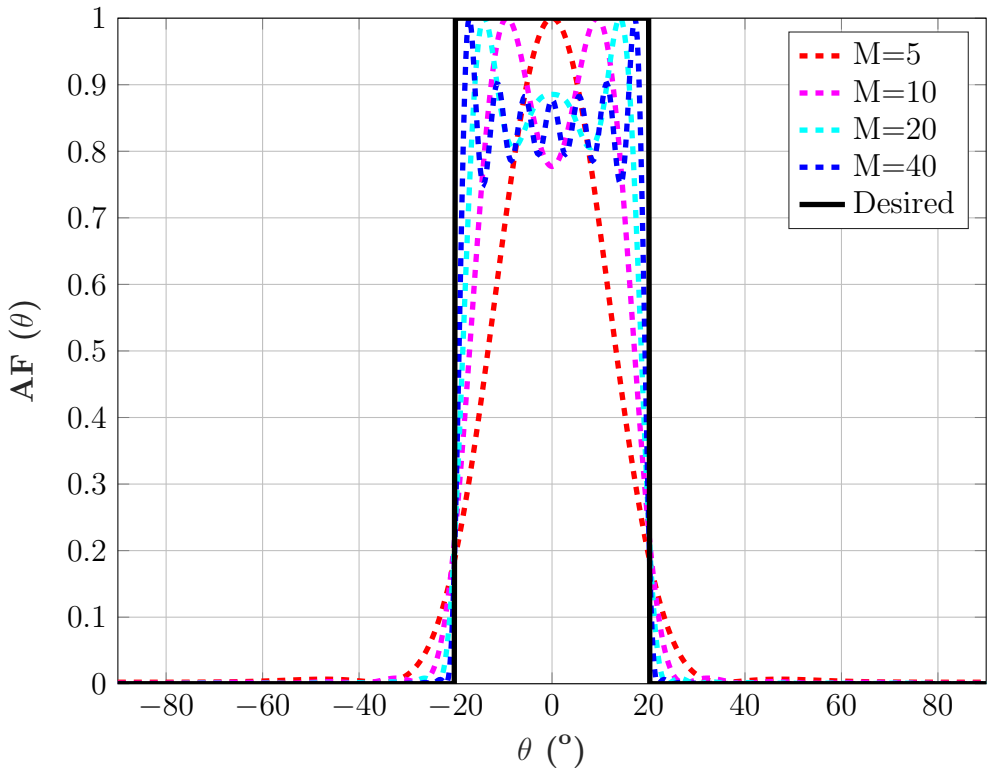

Figure 3.10: FDA angle-dependent beampattern for various values of M.

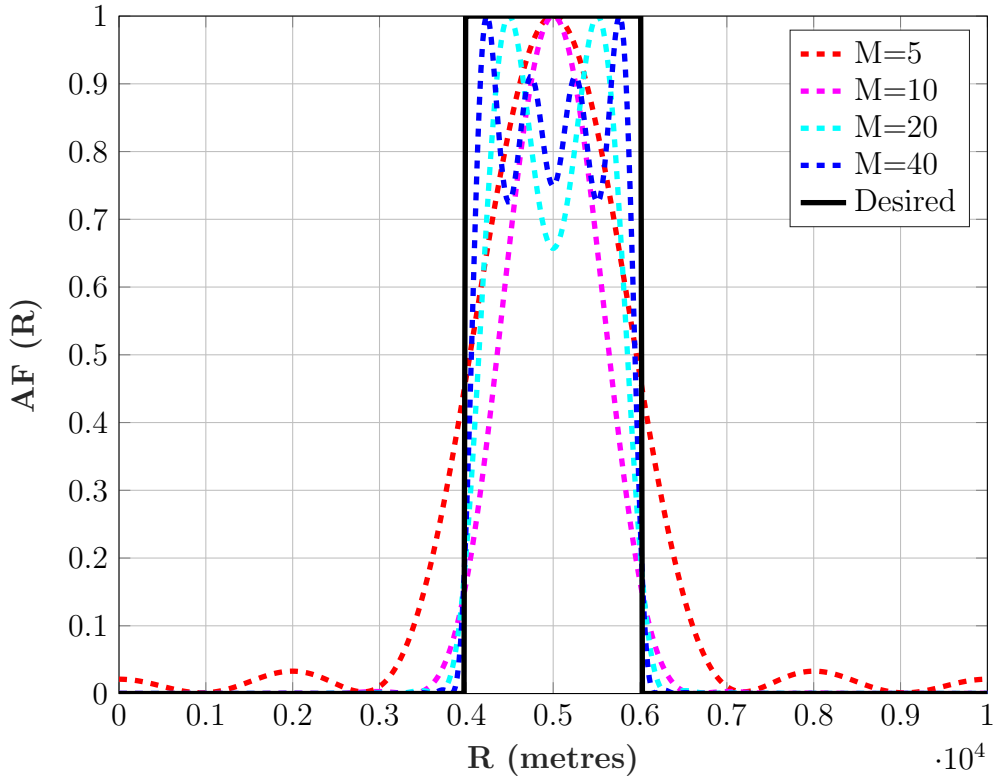

Figure 3.11: FDA range-dependent beampattern for various values of M.

3.6 Conclusion

In this chapter, a complete signal model for FDA radar is derived assuming both zero and non-zero frequency increments at both the transmit and receiving antenna elements. The received signal model is derived by applying $N \times M$ matched filters at the receiver incorporating the concept of a weighted beampattern, which has not yet been proposed in the literature. To design a very focused beampattern close to the desired beampattern, the derivation of optimal frequency offset is proposed. The bounds on the time duration of the transmitted pulse and the transmit antenna element weights have also been derived. It is also verified by simulation results that the application of optimal frequency offset gives only the focused 2D beampattern with reduced sidelobes. Therefore, it is concluded that careful selection of all parameters involved in the beampattern design is very important. The derived received-signal models are utilized for target-parameter estimation in the next chapter.

Chapter 4

Target Parameters Estimation

In this chapter, each target is characterized by its angle and range. For target parameters estimation, the angle and range of the target is estimated.

4.0.1 Angle Estimation

In order to find out location of target, a double pulse method is employed. At first a pulse is transmitted at $f_o = 0$ as well as $f_o = 0$ is used at receiver array so that the received signal model reduced to (3.1.16) and the angular location of target is determined from the received signal. To estimate the angle using a weighted beampattern, the MPDR beamformer is applied to maximize the signal-to-noise ratio (SNR) at the receiver.

$$\min_{\mathbf{k}(\theta)} \mathbf{k}^{\mathsf{H}}(\theta)\mathbf{R}_y\mathbf{k}(\theta) \text{ subject to } \mathbf{k}^{\mathsf{H}}(\theta)\mathbf{b}(\theta) = 1, \tag{4.0.1}$$

where $\mathbf{R}_y$ is the covariance matrix of the received signal $\mathbf{y}(l) = \beta\mathbf{b}(\theta_k) + \mathbf{v}.$, that is

$$\mathbf{R}_y = \frac{1}{L}\sum_{l=0}^{L-1}\mathbf{y}(l)\mathbf{y}^{\mathsf{H}}(l) = \frac{\mathbf{Y}\mathbf{Y}^{\mathsf{H}}}{L}. \tag{4.0.2}$$

The beamformer weight vector obtained by the minimization of above function is obtained as [39]

$$\mathbf{k}(\theta) = \frac{\mathbf{R}_y^{-1}\mathbf{b}(\theta)}{\mathbf{b}^{\mathsf{H}}(\theta)\mathbf{R}_y^{-1}\mathbf{b}(\theta)}. \tag{4.0.3}$$

The power pattern as a function of θ of the beamformer output obtained by using (4.0.3) is given by

$$P(\theta) = \frac{1}{\mathbf{b}^{\mathsf{H}}(\theta)\mathbf{R}_y^{-1}\mathbf{b}(\theta)}. \tag{4.0.4}$$

The peak in this function provides the angle estimate of the target. The algorithm used for the angle estimation is summarized as Algorithm 1.

Algorithm 1 Angle Estimation using weighted FDA

1: **procedure** Angle-estimation
2: Observe $\mathbf{Y}$.
3: Compute $\mathbf{R}_y = \frac{\mathbf{Y}\mathbf{Y}^{\mathsf{H}}}{L}$.
4: Compute $\mathbf{b}(\theta) = [\mathbf{W}^{\mathsf{T}} \otimes \mathbf{a}_R(\theta)]\mathbf{a}_T(\theta)$.
5: Solve (4.0.4).
6: $\hat{\theta}_k \leftarrow$ argmax(4.0.4).
7: **end procedure**

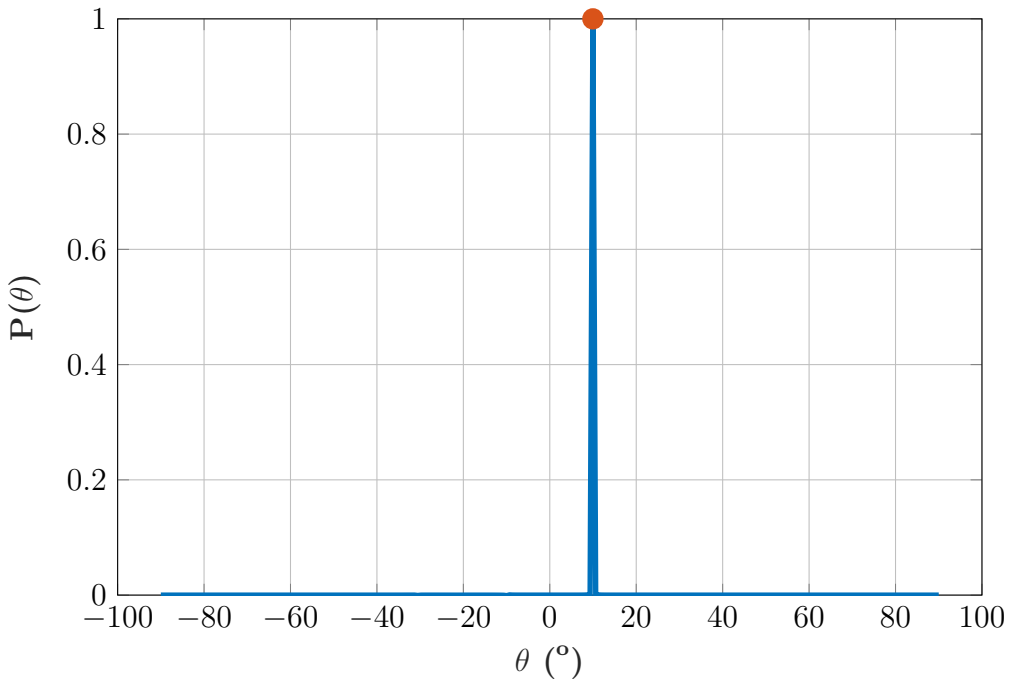

Figure 4.1: FDA received power plot for $\theta_k = 10^o$.

The FDA beampattern is transmitted for desired angular region $\theta_d = [-20^o, 20^o]$, $M = 10$, $N = 10$, $f_c = 5$ GHz and $f_o = 0$ for a target located at $\theta_k = 10^o$. The received power plot is shown in Fig. 4.1.

4.0.2 Range Estimation

Range localization is done after estimating the angular location of the target. To estimate the range using a weighted beampattern, the MPDR beamformer is applied to maximize the signal-to-noise ratio (SNR) at the receiver.

$$\min_{\mathbf{k}(R,\hat{\theta}_k)} \mathbf{k}^{\mathsf{H}}(R,\hat{\theta}_k)\mathbf{R}_y\mathbf{k}(R,\hat{\theta}_k) \text{ subject to } \mathbf{k}^{\mathsf{H}}(R,\hat{\theta}_k)\mathbf{b}(R,\hat{\theta}_k) = 1, \tag{4.0.5}$$

where $\mathbf{R}_y$ is the covariance matrix of the received signal $\mathbf{y}(l) = \beta\mathbf{b}(\theta_k, R_k) + \mathbf{v}$, that is

$$\mathbf{R}_y = \frac{1}{L}\sum_{l=0}^{L-1}\mathbf{y}(l)\mathbf{y}^{\mathsf{H}}(l) = \frac{\mathbf{Y}\mathbf{Y}^{\mathsf{H}}}{L}. \tag{4.0.6}$$

The beamformer weight vector obtained by the minimization of above function is obtained as [39]

$$\mathbf{k}(R,\hat{\theta}_k) = \frac{\mathbf{R}_y^{-1}\mathbf{b}(R,\hat{\theta}_k)}{\mathbf{b}^{\mathsf{H}}(R,\hat{\theta}_k)\mathbf{R}_y^{-1}\mathbf{b}(R,\hat{\theta}_k)}. \tag{4.0.7}$$

The power pattern as a function of R of the beamformer output obtained by using (4.0.7) is given by

$$P(R) = \frac{1}{\mathbf{b}^{\mathsf{H}}(R,\hat{\theta}_k)\mathbf{R}_y^{-1}\mathbf{b}(R,\hat{\theta}_k)}. \tag{4.0.8}$$

The peak in this function provides the range estimate of the target. The algorithm used for the range estimation is summarized as Algorithm 2. The FDA

Algorithm 2 Range Estimation using weighted FDA

1: **procedure** Range-estimation
2: Observe $\mathbf{Y}$.
3: Compute $\mathbf{R}_y = \frac{\mathbf{Y}\mathbf{Y}^{\mathsf{H}}}{L}$.
4: Compute $\mathbf{b}(R,\hat{\theta}_k) = [\mathbf{W}^{\mathsf{T}} \otimes \mathbf{a}_R(R,\hat{\theta}_k)]\mathbf{a}_T(R,\hat{\theta}_k)$.
5: Solve (4.0.8).
6: $\hat{R}_k \leftarrow$ argmax(4.0.8).
7: **end procedure**

beampattern is transmitted for desired angular region $\theta_d = [-20^o, 20^o]$ and range $R_d = [4 \text{ km}, 6 \text{ km}]$, $M = 10$, $N = 10$, $f_c = 5$ GHz and $f_o = 30$ kHz for a target located at $\theta_k = 10^o$ and $R_k = 5$ km. The received power plot is shown in Fig. 4.2.

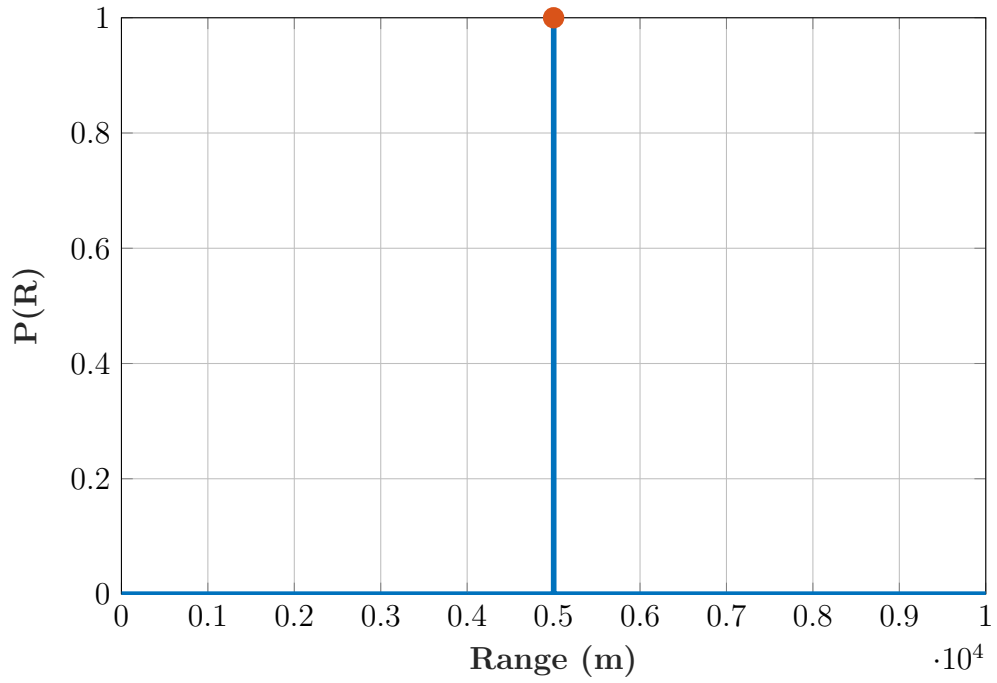

Figure 4.2: FDA received power plot for $R_k = 5$ km.

4.1 Cramer-Rao Lower Bound

To analyze the performance of the FDA radar, CRLB is derived. The Fisherman Information Matrix (FIM) denoted by $\mathbf{F}(\boldsymbol{\eta})$ is given by Slepian-Bang's formula [40]

$$\mathbf{F}(\boldsymbol{\eta}) = 2\mathcal{R}\left[\left(\frac{\partial \boldsymbol{\mu}}{\partial \boldsymbol{\eta}}\right)^{\mathsf{H}} \boldsymbol{\Gamma}^{-1}\left(\frac{\partial \boldsymbol{\mu}}{\partial \boldsymbol{\eta}}\right)\right], \tag{4.1.1}$$

where the parameter vector is $\boldsymbol{\eta} = \left[\theta_k, R_k\right]^{\mathsf{T}}$. The received signal is circularly Gaussian distributed with a mean $\boldsymbol{\mu} = \left[\mathbf{b}(\theta_k), \mathbf{b}(\theta_k, R_k)\right]^{\mathsf{T}}$ and covariance $\boldsymbol{\Gamma} = \sigma_z^2\mathbf{I}$. The FIM with parameter vector is given by

$$\begin{aligned} \mathbf{F}(\eta) &= 2\mathcal{R}\left[\frac{\partial \boldsymbol{\mu}}{\partial \theta_k} \quad \frac{\partial \boldsymbol{\mu}}{\partial R_k}\right]^{H} \boldsymbol{\Gamma}^{-1}\left[\frac{\partial \boldsymbol{\mu}}{\partial \theta_k} \quad \frac{\partial \boldsymbol{\mu}}{\partial R_k}\right] \\ &= 2\boldsymbol{\Gamma}^{-1}\begin{bmatrix} [||\mathbf{q}_\theta||^2 & \mathcal{R}[\mathbf{q}_\theta^{\mathsf{H}}\mathbf{q}_R] \\ \mathcal{R}[\mathbf{q}_R^{\mathsf{H}}\mathbf{q}_\theta] & ||\mathbf{q}_R||^2 \end{bmatrix} \end{aligned} \tag{4.1.2}$$

The elements of FIM is given by

$$\mathbf{q}_\theta = \frac{\partial \boldsymbol{\mu}}{\partial \theta_k} = \frac{\partial [\mathbf{b}(\theta_k), \mathbf{b}(\theta_k, R_k)]^\mathsf{T}}{\partial \theta_k} \tag{4.1.3}$$

$$\mathbf{q}_R = \frac{\partial \boldsymbol{\mu}}{\partial R_k} = \frac{\partial [\mathbf{b}(\theta_k), \mathbf{b}(\theta_k, R_k)]^\mathsf{T}}{\partial R_k} \tag{4.1.4}$$

where

$$\begin{aligned}
\frac{\partial \mathbf{b}(\theta_k)}{\partial \theta_k} &= \frac{\partial}{\partial \theta_k}\Big[((\mathbf{W}^\mathsf{T} \otimes \mathbf{a}_R(\theta_k))\mathbf{a}_T(\theta_k)\Big] \\
&= \Big(\mathbf{W}^\mathsf{T} \otimes (-j\pi\cos(\theta_k))\mathbf{Q}_N\mathbf{a}_R(\theta_k)\Big)\mathbf{a}_T(\theta_k) + \\
&\quad \Big(\mathbf{W}^\mathsf{T} \otimes \mathbf{a}_R(\theta_k)\Big)(-j\pi\cos(\theta_k))\mathbf{P}_M\mathbf{a}_T(\theta_k) \\
&= \mathbf{p_1} \in \mathbb{C}^{NM\times 1}, \qquad (4.1.5) \\
\frac{\partial \mathbf{b}(\theta_k, R_k)}{\partial \theta_k} &= \frac{\partial}{\partial \theta_k}\Big[((\mathbf{W}^\mathsf{T} \otimes \mathbf{a}_R(\theta_k, R_k))\mathbf{a}_T(\theta_k, R_k)\Big]. \\
&= \Big(\mathbf{W}^\mathsf{T} \otimes \Big[(-j\pi\cos(\theta_k))\mathbf{Q}_N\mathbf{a}_R(\theta_k) \odot \mathbf{a}_R(R_k)\Big]\Big)\mathbf{a}_T(\theta_k, R_k) + \\
&\quad \Big(\mathbf{W}^\mathsf{T} \otimes \mathbf{a}_R(\theta_k, R_k)\Big)(-j\pi\cos(\theta_k))\mathbf{P}_M\mathbf{a}_T(\theta_k) \odot \mathbf{a}_R(R_k) \\
&= \mathbf{p_2} \in \mathbb{C}^{NM\times 1}, \qquad (4.1.6) \\
\frac{\partial \mathbf{b}(\theta_k)}{\partial R_k} &= \frac{\partial}{\partial R_k}\Big[((\mathbf{W}^\mathsf{T} \otimes \mathbf{a}_R(\theta_k))\mathbf{a}_T(\theta_k)\Big]. \\
&= \mathbf{0} \in \mathbb{C}^{NM\times 1}, \qquad (4.1.7)
\end{aligned}$$

$$\begin{aligned}
\frac{\partial \mathbf{b}(\theta_k, R_k)}{\partial R_k} &= \frac{\partial}{\partial R_k}\Big[((\mathbf{W}^\mathsf{T} \otimes \mathbf{a}_R(\theta_k, R_k))\mathbf{a}_T(\theta_k, R_k)\Big]. \\
&= \Big(\mathbf{W}^\mathsf{T} \otimes \Big[\mathbf{a}_R(\theta_k) \odot (\frac{j2\pi f_o}{c})\mathbf{Q}_N\mathbf{a}_R(R_k)\Big]\Big)\mathbf{a}_T(\theta_k, R_k) + \\
&\quad \Big(\mathbf{W}^\mathsf{T} \otimes \mathbf{a}_R(\theta_k, R_k)\Big)\mathbf{a}_T(\theta_k) \odot (\frac{j2\pi f_o}{c})\mathbf{P}_M\mathbf{a}_T(R_k) \\
&= \mathbf{p_3} \in \mathbb{C}^{NM\times 1} \qquad (4.1.8)
\end{aligned}$$

The matrices $\mathbf{P}_M$ and $\mathbf{Q}_N$ are given by

$$\mathbf{P}_M = \text{diag } (0, 1, \ldots, M-1),$$
$$\mathbf{Q}_N = \text{diag } (0, 1, \ldots, N-1).$$

The FIM elements obtained after evaluating the partial derivatives results in

$$\begin{aligned} ||\mathbf{q}_\theta||^2 &= \begin{bmatrix} \mathbf{p_1}^{\mathsf{H}} & \mathbf{p_2}^{\mathsf{H}} \end{bmatrix} \begin{bmatrix} \mathbf{p_1} \\ \mathbf{p_2} \end{bmatrix} \\ &= \mathbf{p_1}^{\mathsf{H}}\mathbf{p_1} + \mathbf{p_2}^{\mathsf{H}}\mathbf{p_2} \end{aligned} \tag{4.1.9}$$

$$\begin{aligned} \mathbf{q}_\theta^{\mathsf{H}}\mathbf{q}_R &= \begin{bmatrix} \mathbf{p_1}^{\mathsf{H}} & \mathbf{p_2}^{\mathsf{H}} \end{bmatrix} \begin{bmatrix} \mathbf{0} \\ \mathbf{p_3} \end{bmatrix} \\ &= \mathbf{p_2}^{\mathsf{H}}\mathbf{p_3} \end{aligned} \tag{4.1.10}$$

$$\begin{aligned} \mathbf{q}_R^{\mathsf{H}}\mathbf{q}_\theta &= \begin{bmatrix} \mathbf{0}^{\mathsf{H}} & \mathbf{p_3}^{\mathsf{H}} \end{bmatrix} \begin{bmatrix} \mathbf{p_1} \\ \mathbf{p_2} \end{bmatrix} \\ &= \mathbf{p_3}^{\mathsf{H}}\mathbf{p_2} \end{aligned} \tag{4.1.11}$$

$$\begin{aligned} ||\mathbf{q}_R||^2 &= \begin{bmatrix} \mathbf{0}^{\mathsf{H}} & \mathbf{p_3}^{\mathsf{H}} \end{bmatrix} \begin{bmatrix} \mathbf{0} \\ \mathbf{p_3} \end{bmatrix} \\ &= \mathbf{p_3}^{\mathsf{H}}\mathbf{p_3} \end{aligned} \tag{4.1.12}$$

$$\mathbf{F}(\eta) = 2\mathbf{\Gamma}^{-1} \begin{bmatrix} \mathbf{p_1}^{\mathsf{H}}\mathbf{p_1} + \mathbf{p_2}^{\mathsf{H}}\mathbf{p_2} & \mathcal{R}(\mathbf{p_2}^{\mathsf{H}}\mathbf{p_3}) \\ \mathcal{R}(\mathbf{p_3}^{\mathsf{H}}\mathbf{p_2}) & \mathbf{p_3}^{\mathsf{H}}\mathbf{p_3} \end{bmatrix} \tag{4.1.13}$$

The CRLB obtained by taking the inverse of FIM is given by

$$\begin{aligned} \text{CRLB}(\theta) &= \frac{\sigma_z^2}{2}\frac{||\mathbf{q}_R||^2}{(||\mathbf{q}_\theta||^2||\mathbf{q}_R||^2 - \mathcal{R}[\mathbf{q}_\theta^H\mathbf{q}_R]\mathcal{R}[\mathbf{q}_R^H\mathbf{q}_\theta])} \\ &= \frac{\sigma_z^2}{2}\frac{\mathbf{p_3}^{\mathsf{H}}\mathbf{p_3}}{(\mathbf{p_1}^{\mathsf{H}}\mathbf{p_1} + \mathbf{p_2}^{\mathsf{H}}\mathbf{p_2})(\mathbf{p_3}^{\mathsf{H}}\mathbf{p_3}) - \mathcal{R}(\mathbf{p_2}^{\mathsf{H}}\mathbf{p_3})\mathcal{R}(\mathbf{p_3}^{\mathsf{H}}\mathbf{p_2})} \end{aligned} \tag{4.1.14}$$

$$\begin{aligned} \text{CRLB}(R) &= \frac{\sigma_z^2}{2}\frac{||\mathbf{q}_\theta||^2}{(||\mathbf{q}_\theta||^2||\mathbf{q}_R||^2 - \mathcal{R}[\mathbf{q}_\theta^H\mathbf{q}_R]\mathcal{R}[\mathbf{q}_R^H\mathbf{q}_\theta])} \\ &= \frac{\sigma_z^2}{2}\frac{\mathbf{p_1}^{\mathsf{H}}\mathbf{p_1} + \mathbf{p_2}^{\mathsf{H}}\mathbf{p_2}}{(\mathbf{p_1}^{\mathsf{H}}\mathbf{p_1} + \mathbf{p_2}^{\mathsf{H}}\mathbf{p_2})(\mathbf{p_3}^{\mathsf{H}}\mathbf{p_3}) - \mathcal{R}(\mathbf{p_2}^{\mathsf{H}}\mathbf{p_3})\mathcal{R}(\mathbf{p_3}^{\mathsf{H}}\mathbf{p_2})} \end{aligned} \tag{4.1.15}$$

4.2 Simulation Results and Discussion

For a target located at $\theta_k = 10^o$ and $R_k = 5$ km, a time-invariant transmit beampattern is designed for desired 2D spatial section $\theta_d = [-20^o, 20^o]$ and $R_d = [4 \text{ km}, 6 \text{ km}]$ for $M = 10$, $N = 10$, $f_c = 5$ GHz, $f_o = 30$ kHz, $d = \frac{\lambda}{2}$ and $L = 128$. The performance comparison of non-uniform weighted uniform frequency increment FDA radar was performed with uniform-weighted, transmit weights optimized and non-uniform frequency offset optimized FDA beampatterns. The uniform-weighted FDA radar was proposed in [23]– [24]. For uniform-weighted FDA radar and Hamming window based FDA radar, the dwell time time of transmit beampattern is very small therefore, both are showing large MSE in target parameter estimation.

4.2.1 RMSE Versus SNR

The angle root-mean squared error (RMSE) is plotted for 1000 iterations over a grid size of 0.01^o, as shown in Fig. 4.3. For uniform-weighted FDA radar, the angle RMSE meets the CRLB at SNR= 5 dB because of the shorter dwell time of the beampattern. In Hamming window-based FDA radar, the sidelobes of transmit beampattern are suppressed using Hamming window-based non-uniform

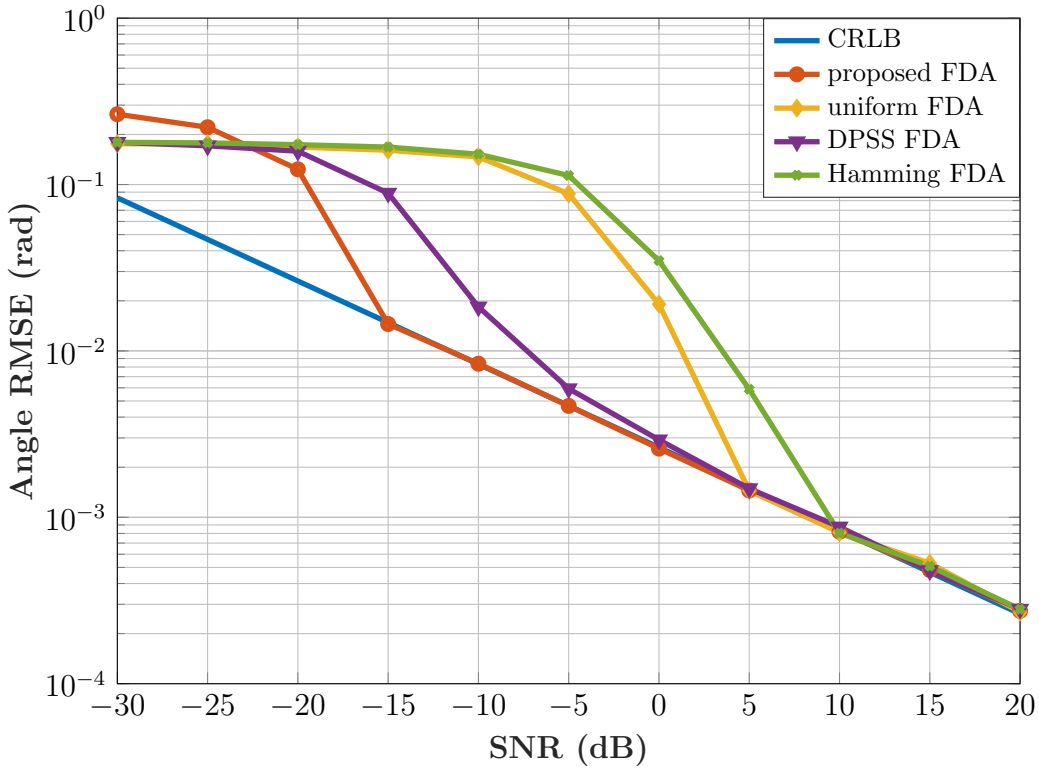

Figure 4.3: Angle Estimation RMSE Versus SNR.

frequency increments; whereas for angle estimation $f_o = 0$ therefore, the transmit beampattern is not optimized for Hamming FDA in this case and it has shown the worst performance than all the compared techniques and therefore meets CRLB at SNR = 10 dB, because of its sharp main lobe and shorter dwell time. For DPSS beampattern, the dwell time of the beampattern is larger therefore, the angle RMSE of the DPSS satisfies the CRLB at SNR = 0 dB but its sidelobes are larger than that of the proposed beampattern. The proposed non-uniform weighted FDA radar meets the CRLB at SNR = −15 dB.

The range RMSE is is plotted for 1000 iterations over a grid size of 1 m, as shown in Fig. 4.4. For range RMSE, the uniform-weighted FDA radar is showing the worst performance and meets the CRLB at 15 dB but in Hamming FDA the beampattern is particularly designed by non-uniform frequency optimization and hence a narrow focused beampattern is directed towards the target therefore it meets the CRLB at 10 dB. This is why it is results in more error in the range estimation of the target. DPSS FDA radar beampattern because of its larger

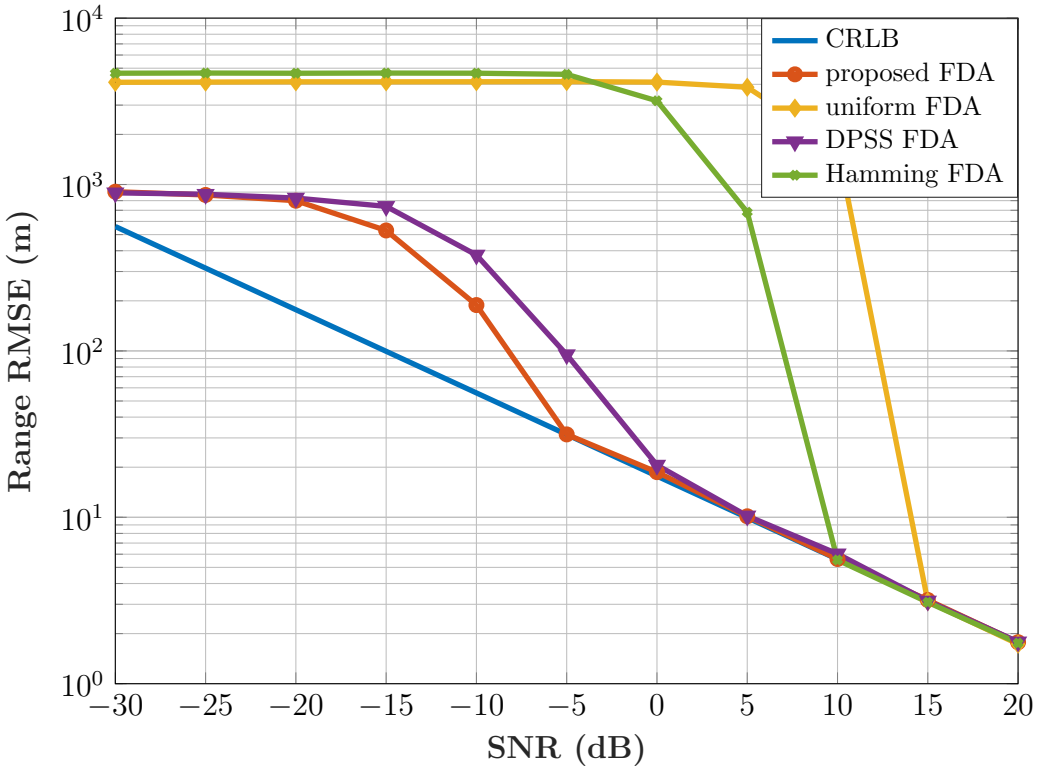

Figure 4.4: Range Estimation RMSE Versus SNR.

dwell shows comparable performance to proposed FDA radar meeting CRLB at SNR = 0 dB but not better than proposed FDA radar, which meets CRLB at SNR= −5dB.

Therefore, the proposed non-uniform weighted FDA radar shows superior performance in target parameter estimation as compared to all the other methods discussed because of the larger beamwidth of the main lobe and hence, larger dwell time.

4.2.2 Computational Complexity

The transmit weights computation complexity comparison of the proposed non-uniform weighted FDA radar has been performed with convex-optimized weighted FDA beampatterns [19]– [21] for solution accuracy $\epsilon = 0.01$ as shown in 4.5.

The computational complexity of the non-uniform weighted FDA radar is $\mathcal{O}(3M \log M)$ as it is using three IFFT algorithms for optimization of transmit antenna el-

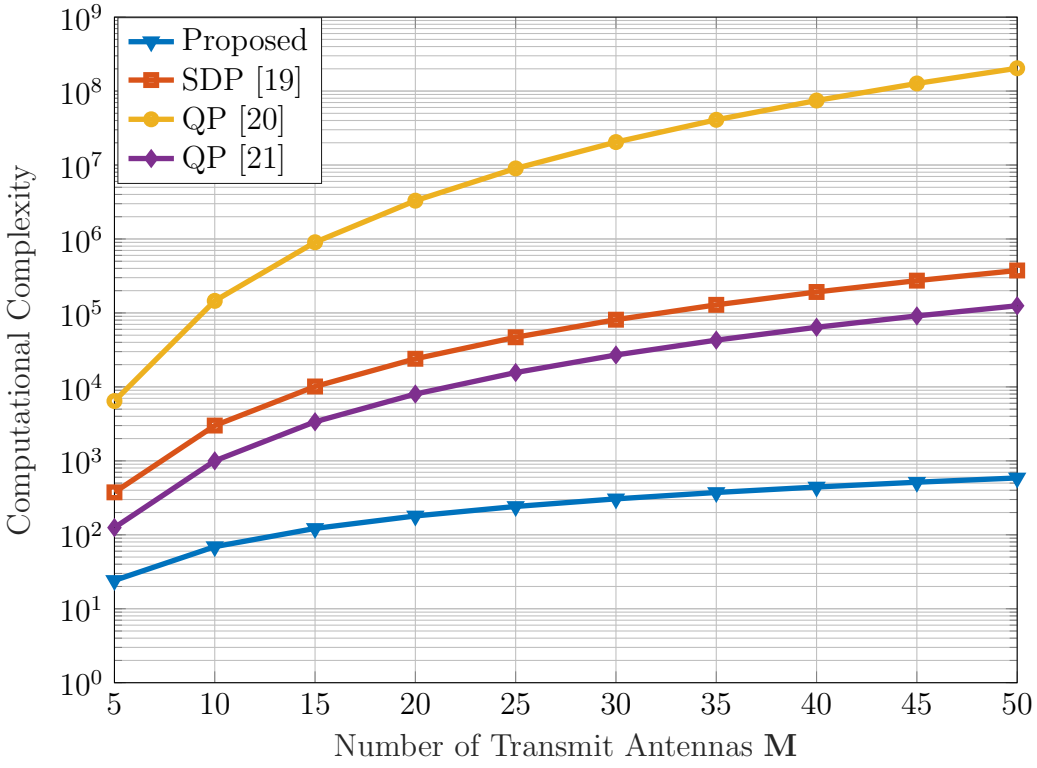

Figure 4.5: Computational Complexity Comparison of Transmit Weights

ement weights, whereas the convex weight optimization techniques in [19] involve semi-definite-programming (SDP). The computational complexity of SDP is $\mathcal{O}(M^{4.5} \log \frac{1}{\epsilon})$. The optimization of transmit antenna element weights in [20] to suppress transmit beamspace sidelobes involve quadratic programming (QP), that costs a computational complexity of $\mathcal{O}(M^3)$. In [21], three different convex optimization problems are solved for optimization of transmit antenna element weights. Therefore, its comutational complexity is $\mathcal{O}(3M^3)$. It is shown in Fig. 4.5 that the proposed non-uniform weighted FDA radar is superior to the other convex optimization techniques in terms of complexity. Therefore, it is more efficient for target localization.

4.3 Conclusion

In this chapter, performance evaluation of the proposed 2D time-invariant transmit beampattern has been done. The proposed received signal model derived has

the capability of providing independent target parameter estimation. The FDA radar with zero frequency increment provides independent angle estimation while the FDA radar with non-zero frequency increment provides range estimation. The proposed weighted beampattern has also proved its efficiency in target parameter estimation and computational complexity as compared to the other literature techniques.

Chapter 5

Conclusion and Future Work

5.1 Summary

Chapter 2: The theory of 2D beampattern design is presented in Chapter 2. First, the array factors AF(θ) and AF(R) were independently represented as the FFT of the corresponding transmit antenna element weights in the angular and range dimensions, respectively. A 2D time-variant beampattern was obtained by applying the designed transmitting antenna element weights. The time variance of the proposed beampattern was shown in the FDA angle, range and time plots. The main goal was to design a 2D beampattern that illuminates the desired two dimensional spatial section for all values of time that was achieved by redesigning transmit antenna weights in the time dimension as well. Finally, the time-invariant transmit beampattern was designed to illuminate multiple spatial sections and the simulation results were presented.

Chapter 3: In Chapter 3, a complete signal model was derived. Complete mathematical calculations of the FDA radar received signal model were presented with both zero and non-zero frequency offsets. The selection of various parameters affecting the shape of the designed beampattern was discussed in detail. The choice of frequency offset, number of transmitting antenna elements and the bounds on the selection of the time duration of the transmitted pulse and transmit antenna element weights were derived.

Chapter 4: In Chapter 4, the angle and range estimation of the target were performed using the MPDR beamformer at the FDA receiver with zero and non-zero frequency offsets, respectively. The performance of the beampattern was monitored for target localization and target parameter estimation was done. The effectiveness of the proposed beampattern was also validated through RMSE versus SNR comparison and computational complexity analysis.

5.2 Conclusion

This thesis presented the novel idea of designing a 2D transmit bempattern for FDA radar to illuminate the desired spatial section. The desired 2D spatial section is illuminated by designing the transmit antenna element weights using IFFT. The idea presented in this thesis is novel from the existing beampattern design techniques using IFFT because the existing techniques exploit IFFT to illuminate the desired angular region only, which is similar to that of the transmit beampattern design for phased array radars. This thesis designs a transmit beampattern for FDA radar to illuminate the desired angular direction as well as the desired range region that is time invariant.

The proposed beampattern design concept has the potential to illuminate any 2D desired spatial section for all values of time. The designed beampattern has larger dwell time due to which it shows efficient performance in target localization even at low SNR. The existing literature uses convex optimization techniques to design a larger dwell time pattern. The IFFT algorithm has less computational complexity in transmitting antenna element weight design compared to other convex optimization techniques. Therefore, the proposed 2D beampattern design outperforms all other existing beampattern design techniques.

5.3 Future Work

This thesis discussed the beampattern design using a uniform frequency offset at the transmit antenna elements for linear arrays. The proposed beampattern has been designed a for static and known targets only. As a future work, this work could be extended for

- Proposed IFFT beampattern design using circular frequency diverse arrays.
- A time-variant beampattern design for tracking moving target.
- Peformance evaluation of time-variant beampattern design.

References

[1] P. Antonik, M. C. Wicks, H. D. Griffiths, and C. J. Baker, "Frequency diverse array radars," *Proc. IEEE Radar Conf.*, Verona, NY, pp. 215–217, Apr. 2006.

[2] P. Antonik, M. C. Wicks, H. D. Griffiths, and C. J. Baker, "Range dependent beamforming using element level waveform diversity," *Proc. Int. Waveform Diversity and Design Conf.*, Las Vegas, NV, USA, pp. 1–4, Jan. 2006.

[3] S. Huang, K. F. Tong, and C. J. Baker, "Frequency diverse array with beam scanning feature," *Proc. IEEE Antennas Propag. Conf.*, San Diego, CA, USA, pp. 1–4, Jul. 2008.

[4] M. C. Wicks and P. Antonik, "Frequency diverse array with independent modulation of frequency, amplitude, and phase," U.S. patent 7,319,427, Jan. 15, 2008.

[5] S. Mustafa, D. Simsek, and H. A. E. Taylan, "Frequency diverse array antenna with periodic time modulated pattern in range and angle," *Proc. IEEE Radar Conf.*, Boston, MA, USA, pp. 427–430, Apr. 2007.

[6] P. Antonik, "An investigation of a frequency diverse array," Ph.D. dissertation, Univ. College London, London, U.K., 2009.

[7] A. Aytun, "Frequency diverse array radar," M.S. thesis, Naval Postgraduate School, Monterey, CA, USA, 2010.

[8] S. Brady, "Frequency diverse array radar: Signal characterization and measurement accuracy," M.S. thesis, Air Force Inst. of Technol., Wright Patterson AFB, OH, USA, 2010.

[9] W. Wang, "Frequency Diverse Array Antenna: New Opportunities," *IEEE Antennas Propag Mag*, vol. 57, no. 2, pp. 145–152, Apr. 2015.

[10] C. Cui, J. Xiong, W. -Q. Wang and W. Wu, "Localization Performance Analysis of FDA Radar Receiver With Two-Stage Estimator," *IEEE Trans Aerosp Electron Syst*, vol. 54, no. 6, pp. 2873–2887, Dec. 2018.

[11] P. Baizert, T.B. Hale, M.A. Temple, M.C. Wicks, "Forward-looking Radar GMTI Benefits Using a Linear Frequency Diverse Array," *Electron. Lett.*, vol. 42, no. 22, pp. 1311–1312, Oct. 26, 2006.

[12] Y. Wang, W. Li, G. Huang and J. Li, "Time-Invariant Range-Angle-Dependent Beampattern Synthesis for FDA Radar Targets Tracking," *IEEE Antennas Wirel. Propag. Lett.*, vol. 16, pp. 2375–2379, 2017.

[13] H. Shao, J. Dai, J. Xiong, H. Chen and W. Wang, "Dot-Shaped Range-Angle Beampattern Synthesis for Frequency Diverse Array," *IEEE Antennas Wirel. Propag. Lett.*, vol. 15, pp. 1703–1706, 2016.

[14] J. Xiong, W. Wang, H. Shao and H. Chen, "Frequency Diverse Array Transmit Beampattern Optimization With Genetic Algorithm," *IEEE Antennas Wirel. Propag. Lett.*, vol. 16, pp. 469–472, 2017.

[15] W. -Q. Wang, "Range-angle dependent transmit beampattern synthesis for linear frequency diverse arrays," *IEEE Trans. Antennas Propag.*,vol. 61, no. 8, pp. 4073–4081, 2013.

[16] W. -Q. Wang, and H. C. So, "Transmit subaperturing for range and angle estimation in frequency diverse array radar," *IEEE Trans. Signal Process.*, vol. 62, no. 8, pp. 2000–2011, 2014.

[17] A. Basit, I. M. Qureshi, W. Khan, S. u. Rehman and M. M. Khan, "Beam Pattern Synthesis for an FDA Radar with Hamming Window-Based Nonuniform Frequency Offset," *IEEE Antennas Wirel. Propag. Lett.*, vol. 16, pp. 2283–2286, 2017.

[18] M. Zubair, S. Ahmed and M. -S. Alouini, "Frequency diverse array radar: New results and discrete Fourier transform based beampattern," *IEEE Trans. Signal Process.*, vol. 68, pp. 2670–2681, Apr. 2020.

[19] S. Gong, S. Wang, S. Chen, C. Xing, and X. Wei, "Time-invariant joint transmit and receive beampattern optimization for polarization-subarray based frequency diverse array radar," *IEEE Trans. Signal Process.*, vol. 66, no. 20, pp. 5364–5379, Sep. 2018.

[20] J. Xiong and W. -Q. Wang, "Sparse reconstruction-based beampattern synthesis for multi-carrier frequency diverse array antenna," *Proc. IEEE Int. Conf. Acoust. Speech Signal Process.*, pp. 3395–3398, Mar. 2017.

[21] K. Gao, W. -Q. Wang, H. Chen and J. Cai , "Transmit Beamspace Design for Multi-Carrier Frequency Diverse Array Sensor," *IEEE Sensors J.*, vol. 16, no. 14, pp. 5709–5714, Jul. 15, 2016.

[22] X. L. Shao, T. Y. Hu, L. Li, Z. L. Xiao and Y. J. Rong, "Sparse Multi-carrier Frequency Diverse Array Transmit Beampattern Optimization," *Proc. Photon. Electromagn. Res. Symp.*, pp. 1620–1625, Nov. 2021.

[23] W. -Q. Wang, "Frequency Diverse Array Auto-Scanning Beam Characteristics and Potential Radar Applications," *IEEE Access*, vol. 10, pp. 85278–85288, 2022.

[24] J. Zhu, S. Zhu, L. Lan and J. Xu, "Adaptive Multi-Target Detection with FDA-MIMO Radar," *Proc. IEEE Sensor Array and Multichannel Signal Process. Workshop*, pp. 370–374, Jun. 2022.

[25] W. LV, K. V. Mishra, S. Chen, "Co-Pulsing FDA Radar," *IEEE Trans. Aerosp. Electron. Syst.*, pp. 1–20, , 2022.

[26] M. Rosamilia, L. Lan, A. Aubry and A. De Maio, "Polarimetric FDA-MIMO Radar Detection," *Proc. IEEE Radar Conf.*, pp. 1–6, Mar. 2022.

[27] C. Zhou, C. Wang, J. Gong, L. Bao, G. Chen and M. Liu, "FDA-MIMO Radar Robust Beamforming Based on Matrix Weighting Method," *IEEE Access*, vol. 10, pp. 58913–58920, 2022.

[28] L. Huang, X. Li, W. Wan, S. Zhang and W. -Q. Wang, "Frequency Diverse Array Introduced Into SAR GMTI to Mitigate Blind Velocity and Doppler Ambiguity," *IEEE Geosci. Remote Sens. Lett.*, vol. 19, pp. 1–5, 2022.

[29] A. Nysaeter, "Adaptive suppression of smart jamming with FDA permutation," *Proc. IEEE Radar Conf.*, 2022, pp. 1–5.

[30] C. Wen, Y. Xie, Z. Qiao, L. Xu and Y. Qian, "A Tensor Generalized Weighted Linear Predictor for FDA-MIMO Radar Parameter Estimation," *IEEE Trans. Veh. Technol.*, vol. 71, no. 6, pp. 6059–6072, 2022.

[31] K. Liao, J. Shen, S. Ouyang and Q. Yu, "A Target Deblurring Method for Frequency Diverse Array Imaging," *IEEE Antennas Wireless Propag. Lett.*, vol. 21, no. 5, pp. 1002–1006, 2022.

[32] Y. Liu, C. Wang, J. Gong and G. Chen, "Discrimination of Mainlobe Deceptive Target With Meter-Wave FDA-MIMO Radar," *IEEE Commun. Lett.*, vol. 26, no. 5, pp. 1131–1135, 2022.

[33] W.-Q. Wang and H. Z. Shao, "Range-angle localization of targets by a double-pulse frequency diverse array radar," *IEEE J. Sel. Topics Signal Process.*, vol. 8, no. 1, pp. 1–9, Feb. 2014.

[34] W. Wang, "Subarray-based frequency diverse array radar for target range-angle estimation," *IEEE Trans Aerosp Electron Syst*, vol. 50, no. 4, pp. 3057–3067, Oct. 2014.

[35] R. Gui, W. -Q. Wang, Y. Pan and J. Xu, "Cognitive Target Tracking via Angle-Range-Doppler Estimation With Transmit Subaperturing FDA Radar," *IEEE J. Sel. Topics Signal Process.*, vol. 12, no. 1, pp. 76–89, 2018.

[36] W. Sun, L. Lan, G. Liao and J. Qi, "Compound Interference Suppression for Bistatic FDA-MIMO Radar Based on Joint Two-Stage Processing," *Proc. IEEE Sensor Array and Multichannel Signal Process. Workshop*, pp. 375–379, Jun. 2022.

[37] L. Wang, W. -Q. Wang and H. C. So, "Covariance Matrix Estimation for FDA-MIMO Adaptive Transmit Power Allocation," *IEEE Trans. Signal Process.*, vol. 70, pp. 3386–3399, 2022.

[38] A. V. Oppenheim, A. S.Willsky, and S. H. Nawab, *Signals & Amp; Systems*, 2nd ed. Upper Saddle River, NJ, USA: Prentice-Hall, 1996.

[39] J. Capon, "High-resolution frequency-wavenumber spectrum analysis," *Proceedings of the IEEE*, vol. 57, no. 8, pp. 1408–1418, 1969.

[40] P. Stoica and R. Moses, *Introduction to Spectral Analysis.* Englewood Cliffs, NJ, USA: Prentice-Hall, 1997.